**Behavior of Bolted Connections During and After a Fire**

**Committee**

_____
**Karl H. Frank, Supervisor**

_____
**Joseph A. Yura**

_____
**Michael D. Engelhardt**

_____
**Eric B. Becker**

_____
**Ofodike A. Ezekoye**

# Behavior of Bolted Connections During and After a Fire

by

## Liang Yu, B.S.; M.S.

## Dissertation

Presented to the faculty of the graduate school of

The University of Texas at Austin

In Partial Fulfillment

Of the requirements

For the degree of

## Doctor of Philosophy

## The University of Texas at Austin

## August 2006

# Dedication

To my beloved family members

# Acknowledgements

I feel I am extremely fortunate to be a graduate student under Dr. Karl H. Frank's supervising. I wish I can express my gratitude to all those who made this dissertation possible. Thanks for Dr. Karl Frank for giving me the opportunity to work under his kind supervision and for giving me such a wonderful learning experience. Thanks to my dissertation committee members, Dr. Joseph A. Yura, Dr. Michael D. Engelhardt, Dr.Eric B. Becker, and Dr. Ofodike A. Ezekoye for their kind advices on my research and my career life.

Special thanks to Eric Schell, Dennis Fillip, Blake Stasney, Mike Wason, Chris Tessler for their precious help to my experiments.

Additionally, thanks to my family, my mother, Ruizeng Zhang, my father, Youmin Yu. They are such wonderful people who are always with me and love me at anytime. Linlin Wang, her endless love and encouragement has been powerful energy to keep studying. It is not me but my family that deserve the entire honor for my accomplishment.

# Behavior of Bolted Connections During and After a Fire

Publication No. _____

Liang Yu, Ph.D.

The University of Texas at Austin, 2006

Supervisor: Karl H. Frank

After the collapse of World Trade Center Buildings, the safety of steel structures in fire and post fire started to draw more and more attention from structural engineer communities and researchers in United States. Efforts are being made on improving fire resistance of steel structures by new design methods, which is an alternative of the traditional passive (spray-on insulation) and active (automatic sprinkler) fire proofing system. In developing the new design methods, the behavior of steel structure at elevated temperature must be understood. Floor beams and bolted connections were studied with both experimental and analytical methods in this research program, which provide useful information on the strength of bolted connection at elevated temperature.

Shear strength of A325 and A490 high strength bolts were studied with double shear tests performed at different temperature levels, from ambient temperature to 1500°F. It was found that both types of bolts reduce their strength significantly between 600°F and 1300°F. Strength reduction factors are recommended for

practical design. Residual strength of A325 and A490 bolts after being exposed to elevated temperature were studied with single shear tests and hardness tests. Strength losses were found on both bolts when they were exposed to a temperature higher than their tempering temperature. Bolt hardness was found to be an accurate method to estimate bolt residual strength and provide an efficient and economical way to assess residual strength of a high strength bolt. Single bolt connections were tested at different temperature. Significant capacity reduction was found on all the connections at elevated temperature. The failure mode changed from a bearing failure to a bolt shear failure when temperature was above 600°F. This phenomenon indicated that a high strength bolt was more sensitive to temperature than structural steel. Two bolts connections were tested to study block shear failure at different temperatures. Residual slip load on slip critical connections was also investigated with slip load tests on connections that had been heated and cooled to ambient temperature. Significant reduction of slip load occurred in connections which had been heated to above 800°F. Material properties of two different heats of Grade 50 structural steel plates used in the connection tests were determined at different temperature levels and strain rates.

Finite Element Analysis was performed on steel beams and composite beams subjected to elevated temperature. Connection forces at different temperatures were obtained. Design recommendations are put forward based on the experimental results on connection strength and connection forces from the analysis.

# Table of Contents

# List of Figures

# List of Tables

# Chapter 1

# Introduction

## 1.1 Background

Fire safety is a major concern with steel structures. Applying Spray applied Fire Resistive Material (SFRM) and installing insulation boards are the popular methods of improving steel structures' fire resistance. Both SFRM and insulation boards prevent the temperature of steel from being increased, or slow down the speed of temperature rise. Therefore the fire resistance of a structure is always expressed with time, such as four hours, which is the time for the temperature of members reach a critical value in the Standard Fire Test (ASTM E119-00a). Until The Broadgate Phase Eight Fire in 1990, steel structures without any fire proofing were considered to be vulnerable to fire attack (Lamont, Lane, Flint and Usmani, 2006). Even though the fire last 4.5 for hours, unprotected steel frame survived without showing any sign of collapse. The big cost of applying fire proofing was questioned after Broadgate Fire. The collapse of the World Trade Center Towers was an example of another extreme case. Plane impact knocked off SFRM and left the structure members unprotected to fire. National Institute of Standards and Technology (NIST) concluded that damage from plane impact and fire caused the collapse of the World Trade Center Towers (NIST NCSTAR 1-6). Similar scenario maybe found in fires post earthquake. Inspired by the Broadgate fire and WTC fires, more efforts are being made on understanding structures' behavior and safety at elevated temperature.

A structure is constructed with separate members, which are jointed together by connections. If these connections fail, the integrity of the structure could be compromised, leading to structural damage and in some cases progressive collapse. Bolted connections are the most widely used connection in

steel structures. These bolts are heat treated high strength bolts, whose strength is sensitive to its temperature. Bolt connection failure has been observed in steel building fires and fire tests on full scale steel structure (Beitel & Iwankiw, 2005; Cardington Fire Test Report, 1998). Currently there are limited research results available about bolt connection behavior and strength at elevated temperature available. It is the purpose of this research program to survey the strength capacity of bolted connections at elevated temperatures.

## 1.2 Research Scope

Experimental study was performed on bolt strength, steel plate bearing strength, and block shear capacity. A high temperature test system and testing procedure for bolted connections was developed. Using this test system, the following tests were performed:

1. Double shear test of A325 and A490 bolts at elevated temperatures ranging from ambient temperature to 1500°F;

2. Post-fire residual shear strength of A325 and A490 bolts after being exposed to elevated temperature;

3. Bolted connection behavior at different elevated temperature levels;

4. Material properties of two different heats of Grade 50 structural steel plates.

Using Finite Element Analysis (FEA) in order to survey the behavior of steel and composite beams at elevated temperatures, we are able to record the reaction force changes in beam connections. Design recommendations were put forward based on experimental results of connection strength and the FEA results on possible connection forces.

## 1.3 Dissertation Overview

Chapter 2 introduces the background of the study. Chapter 3 describes the test methods and equipment to determine the shear capacity of A325 and A490 high strength bolts, the capacity of single bolt connections, and connection slip load. Chapter 4 presents and discusses double shear test results of A325 and A490 bolts at elevated temperatures. Chapter 5 studies the residual strength of A325 and A490 bolts using a direct shear test and hardness tests after exposure to elevated temperatures. Chapter 6 presents the test results of single bolt connections and two bolts connections at elevated temperature levels. Chapter 7 discusses material properties of steel plate. Chapter 8 applies finite element analysis to a case study. Chapter 9 develops the design formulas based on test results of high strength bolts, bolted connections, and plate steel. Chapter 10 provides a summary of the thesis and makes recommendations for future work.

# Chapter 2
# Background

## 2.1 Historical Survey of Steel Building Fires

### 2.1.1 The 1 New York Plaza Fire (Beitel and Iwankiw, 2005)

The 1 New York Plaza (New York, NY) is a 50-story office building constructed out of a steel frame with a reinforced concrete core. It was constructed with Spray applied Fire Resistive Material (SFRM) but no sprinkler system. The fire broke out on August 5, 1970 lasting more than six hours. During the fire attack, bolted connections suffered severe damage. Bolts were found sheared and several steel filler beams had fallen down, resting on the bottom flange of the main girder. In spite of these local failures the building stood through the fire. After investigation, it was concluded that the light spray on fire resistive material peeled off during the early stages of the fire, causing damage to the floor system

### 2.1.2 The First Interstate Bank Fire (FEMA Technical Report, 1988)
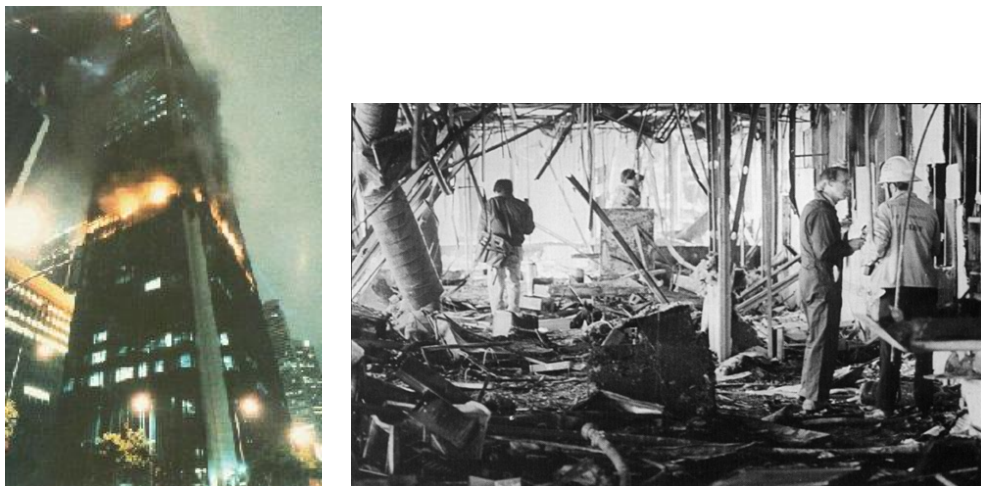


Figure 2-1 The First Interstate Bank Fire and post Fire Damage

The First Interstate Bank (Los Angeles, CA) is a 62-story high rise office building, which has steel column trees surrounding its central concrete core. The fire started on the 12$^{th}$ floor in an open-office area on May 4, 1988. The fire spread quickly, fueled by office furniture, paper documents, and computer terminals. In 3.5 hours, 12 to 16 floors were fully gutted by the fire. The direct property loss was estimated to be $200 million. At the time of fire, a $3.5 million sprinkler system was being installed in the building but was only 90% complete at the time of the fire. Any chance of extinguishing the fire in its early stage was missed. Even though the fire burnt out five floors, no major damage on structure members was found. The building survived the fire. Figure 2-1 shows the building with fire and post fire damage.

**2.1.4 The Broadgate Phase 8 Fire** (Lamont, Lane, Flint, Usmani, 2006)



Figure 2-2 Broadgate Building and local buckled column after Fire (Ivan Burgess, 2002)

The Broadgate building is a 14-story steel frame office building located in London, England. It has a mixed floor with W shape steel beams and steel trusses composite with a concrete slab. The fire broke out in 1990 when the building was fully constructed but not yet fire protected. Construction form works made of timber were the main source of fuel. The fire last about 4.5 hours leaving an entire

story destroyed. Despite the extensive damage to columns, beams and trusses, the building survived without any danger of collapsing. Figure 2-2 shows the damaged story and local buckling of a column in Broadgate Building post fire.

**2.1.4 One Meridian Plaza** (FEMA Technical Report, 1991)

One Meridian Plaza is a 38-floor high rise building in Philadelphia, Pennsylvania. It was constructed with steel framing and a reinforced concrete core. Although the building has sprayed on fire proofing, it does not have a sprinkler system.  A fire started in the building on the 22$^{nd}$ floor on February 23, 1991. In 18 hours the fire spread to eight floors and caused about $100 million in damage. Despite a large amount of fire damage on the exterior of the building, the main structure survived this disaster. No collapse occurred in any part of the building. Figure 2-3 shows the Plaza on fire and post fire scene. A large number of temporary support shores shown in the photo were added to prevent collapsing of the floor.



Figure 2-3 One Meridian Plaza on Fire and post Fire

**2.1.5 The World Trade Center Fire – Building 1 and 2** (NIST NCSTAR 1-6)

The World Trade Center Buildings 1 and 2 were attacked by terrorists with hijacked airplanes on September 11th, 2001. Severe fires were started in both buildings from the fuel carried by the airplanes. WTC 1 collapsed 1.5 hour after jet impact and fire started, and WTC 2 did so 1 hour after impact. According to the investigation report of WTC collapse by NIST, the impact damage to the outer tube structure did not cause the collapse of the building. Instead, gravity load was redistributed into the intact portion of the tube frame and its interior core. In addition, fire increased the temperature of floors, which expanded at an early stage. This expansion pushed the exterior steel columns out. Once the fire fully developed, the floors were heated and weakened further. Significant sag occurred on floors. The catenary forces generated in sagged floor systems pulled the exterior columns in. The floor no longer acted as a brace to the fire-weakened columns and the interior gravity columns were no longer capable of carrying the gravity loads. The loss of the gravity load columns triggered the progressive collapse of whole building. (FEMA 403)

**2.1.6 The World Trade Center Fire – Building 5 and 7** (NIST NCSTAR 1-6)



Figure 2-4 WTC 5 on Fire (FEMA 403);   Figure 2-5 Deformed Floor Beams
post Fire in WTC 5 (FEMA 403)

The reasons for the collapse of WTC 5 and 7 are not for the same reasons as WTC 1 and 2. WTC 5 and 7 were not impacted by any airplane. WTC 5 collapsed due to a combination of fire damage and overload from the debris from WTC 1 and 2. WTC 7 collapsed purely due to fire damage.

WTC 5 was a nine-story steel frame building with a light-weight concrete composite floor. The columns, floor beams, and roof had a fire resistance rating of three hours, two hours and 1.5 hours respectively with sprayed on mineral fiber insulation material. The building was also equipped with an automatic sprinkler system. The debris from WTC 1 and 2 building caused partial collapse and started the fire in WTC 5. Figure 2-4 shows WTC 5 on fire. Figure 2-5 shows the deformed beam in the remaining section of WTC 5 after collapse.
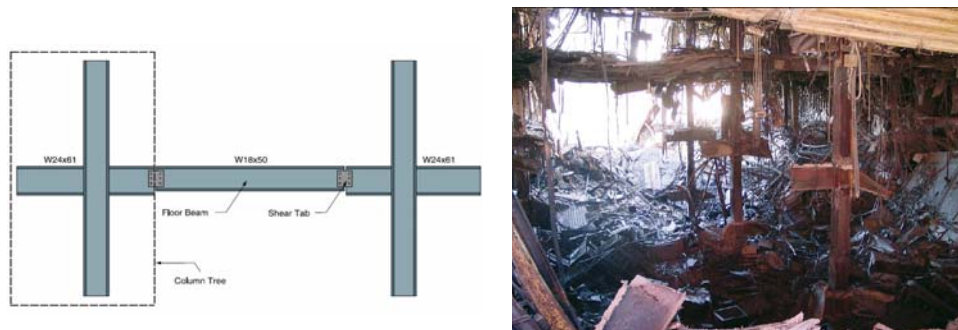


Figure 2-6 Column Tress Design and Internal View after Collapsed in WTC 5 (FEMA 403)



Figure 2-7 Failed Column Tress Connections in WTC 5 (FEMA 403)

Figure 2-8 Failed Bolt Connections from WTC 5 (FEMA 403)

Although the maximum temperature of the fire is unknown, the fire completely burnt out all floors above the fifth in WTC 5. In Figure 2-5, the deformed floor beams confirm the fire damage. Debris from collapse of WTC 1 and 2 overloaded the roof, which had already been weakened by fire. As a result, part of roof progressively collapsed from the eighth floor to the fourth floor. The failure of bolted connections in beam splice, shown in Figure 2-6 and Figure 2-7, played a key role in the collapse of WTC 5. "The structural collapse appeared to be due to a combination of excessive shear loads on bolted connections and unanticipated tensile forces resulting from catenary sagging of the beams." (FEMA 403) Figure 2-8 shows bearing failure in beam splice connections.

WTC 7 was a 47-story office building constructed with a steel frame and a composite floor. Due to a design change, the upper structure design did not comply with the foundation plan. Large scale cantilever beams and trusses were used on the fifth, sixth and seventh stories to transfer gravity loads from upper-story columns to lower-story columns and foundations. The building was equipped with sprayed fire proofing material and sprinkler system. The fire started from the sixth floor and developed through each floors up to the 13th. Due to the diesel oil tanks on the fifth floor for generators, the fire spread quickly out of control. The failure of water supply to the sprinkler system made the situation even worse. After burning for seven hours, the WTC 7 building collapsed entirely

to ground. Fire damage to the load transfer members from the fifth to seventh floors is believed to be the cause of the collapse. (NIST NCSTAR 1-6, September 2005)

### 2.1.7 Caracas Tower Fire (Engineering News Record, 2004)

Caracas Tower is a 56-story office building in Caracas, Venezuela. It is a steel frame building with a composite floor. On October 17, 2004, Caracas Tower suffered from a severe fire, which started on $34^{th}$ and spread to over 26 floors, lasting more than 17 hours. Both sprayed on fire proofing and sprinklers were installed in the building but the sprinkler system malfunctioned during fire. There was a tremendous amount of fire damage on the floors, as shown in Figure 2-9. Even though the whole building barely survived the fire attack, 34 to 49 floors had to be demolished and rebuilt.



Figure 2-9 Caracas Plaza Fire and Fire Damage on Floor

### 2.1.8 The Windsor Building Fire (INTEMAC, 2005)

The Windsor Building is a 32-story office building in Madrid, Spain, which was constructed with a steel-reinforced concrete core and a steel exterior

frame. On the night of February 12, 2005, a fire started on the 21$^{st}$ story.  Due to a lack of water, fire fighters could not stop it and it spread out to floors above the 21$^{st}$.Burning for almost 48 hours, the exterior steel frame from the 21$^{st}$ to 32$^{nd}$ stories collapsed, while the main building survived, as shown in Figure 2-10.



Figure 2-10 Windsor Building on Fire and post Fire

## 2.2 Fire Behavior

The behavior of fire is governed by the balance among its three key components: fuel, oxygen and temperature. A fire starts when fuel temperature is raised above its combustion point and oxygen exists. Combustion of fuel releases more heat, which increase the temperature of its surrounding environment. More and more fuel starts to burn and the fire expands. During a fire, the temperature determines the behavior of the structural members. Figure 2-11 gives the time-temperature curve of a natural fire (Drysdale, 1985). It can be divided into three phases as growth, fully developed and decay. Flashover is defined as the transition of fire from growth to fully developed, which involves a rapid spread from the area of localized burning to all combustible surfaces within the

compartment (Drysdale, 1985). After flashover the heat release rate is greatly increased as long as fuel and oxygen supplies last. The environment temperature and structure temperature reach their maximum during this phase. Generally, when flashover happens in a high rise building fire, it is almost impossible for firefighters to stop it. Structures need to resist fire by itself post flashover. Sprinklers are designed to work only at the growth phase of fire. Sprayed-on fire proofing material is the defense against the fully developed fire. If fire does not remain at its peak phase long, the structure might be safe. Otherwise, long lasting fire will heat up structure members gradually, leading to the failure of the structure members and even to total collapse.
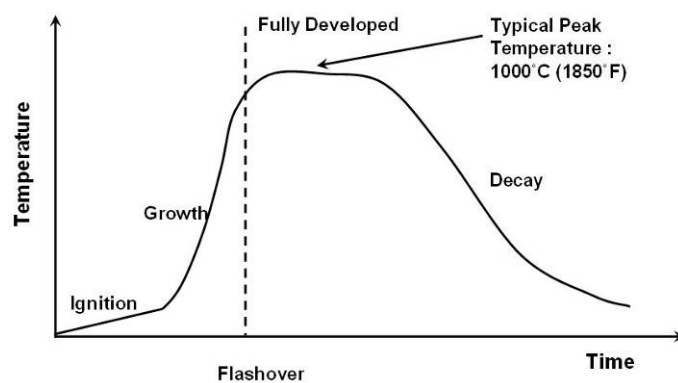


Figure 2-11 Typical Natural Fire Behavior

Real building fires are quite different from case to case depending on fuel and oxygen supplies. A standard fire is defined to perform fire resistant test on structural members. This fire is defined by the time air-temperature curve. The standard test fire time-temperature curves as shown in Figure 2-12. Comparing standard fire with natural fire, standard fire is a simulation of a very severe natural fire post flashover behavior.

## 2.3 Research Work on Steel Structure Fire Safety

### 2.3.1. Structure Behavior in Fire - Cardington Fire Tests

In 1996, Building Research Establishment's Cardington Laboratory of UK carried out a series of fire tests on an eight-story composite steel-framed building, built to represent typical office buildings in full scale. These tests provided valuable information about the behavior of steel framed building in fire. Among the tests, No. 6 was an office demonstration test, in which a 59 ft × 33 ft compartment was built with simulated fire loads in any typical office. All the beams and columns were exposed but connections were fire protected. Figure 2-13 shows the view of fire compartment before and after test. The floor framing system consisted of composite beams intersecting at mid span. Beam A spans 29.6 ft and Beam B spans 19.7 ft between columns. Beam A was connected to Beam B at mid span. The fire lasted 90 minutes with a maximum air temperature of 1200°C (2200°F). Maximum temperature in the steel beams reached 1150°C (2100°F). The maximum beam deflection was 25.2 inches (about 1/9 span), which recovered to 21.3 inches on cooling. No sign of collapse was found.
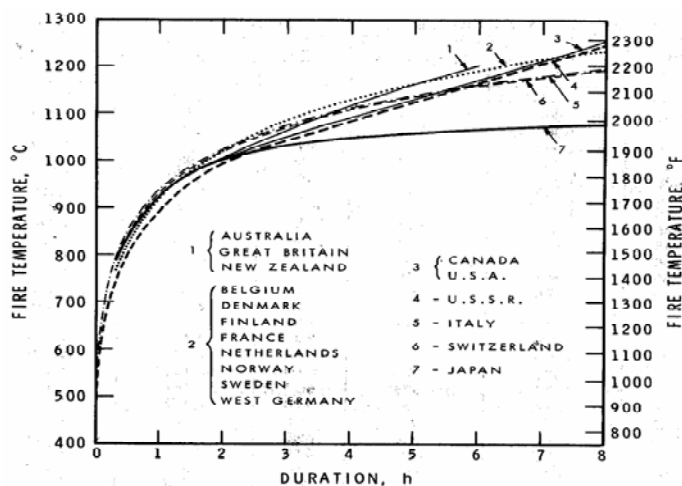


Figure 2-12 Standard Fire Temperature-Time Relations (ASCE No. 78)

Figure 2-13 Office Demonstration Test in Cardington Tests

The Cardington series of fire tests, found that unprotected steel beams have a higher capacity than their design value based on the performance of simply supported beams in a standard fire test. The connection capacity was not tested in most of the experiments because fire protection was applied on connections. Early connection failure might have occurred, followed by floor collapse. In other tests in the Cardington series, fire protected connections were found to fail during the cooling phase due to shrinkage of deformed beams. In test No. 2, unprotected connection failed during the fire. Figure 2-14 shows both failed connections.



Figure 2-14 Connection Failed in Fire (left) and in Cooling Phase (right) (Cardington Fire Test Report, 1998)

Based on observations from Cardington tests, Usmani and Lamont summarized the events of composite steel frame structure response to fire

(Usmani and Lamont, 2004). The first event is compressive membrane action in composite slab beam system, which is not considered in the simplified composite beam design theory used in design. The second is local buckling of the lower flange of steel beams near the end connection. The buckling is due to compressive forces caused by the temperature gradient that creates hogging moments and thermal expansion of the entire section. The buckling allows beam end rotation and releases the rotational restraints from connections. This phenomenon significantly reduces the effects of simple connection's rotational restraint upon the beam behavior at elevated temperature. In the third and final event, the steel section reaches its ultimate axial capacity at about 500˚C, ending the conventional composite flexure mechanism of the composite beam. The reinforced concrete floor starts to carry most of the loads by tensile and compressive membrane mechanism.

Large amount of Finite Element Modeling work have been done in simulating the composite floor system behavior in fire based on Cardington fire tests results. All these simulation work showed reasonable good agreement with the test results. (Elghazouli, Izzuddin, 2001; Martin Gillie, etc, 2001) Base on both experimental and FEM simulation results, analytical methods were also put forward for calculating the ultimate capacity of a concrete slab in fire condition. (Usmani, Cameron, 2004; Huang, Burgess, Plank, 2004; Bailey, 2004)

### 2.3.2 Floor System Fire Resistance - WTC Building Floor Test

After the collapse of WTC 1 and 2 buildings, NIST carried out an experimental study on the fire resistance capacity of the composite floor system in these two building. The floor system was a light weight concrete slab supported by steel trusses spanning between center concrete core and exterior steel column trees. Original design was followed in constructing the specimen.

15

Table 2-1 Summary of WTC Floor Fire Resistance Tests (NIST NCSTAR 1-6B)

| Test No. | Scale | Boundary Condition | SFRM Thickness (in) | Span (ft) | Load | | Test Duration (min) | Temperature Time Stamp (min) | | |
|---|---|---|---|---|---|---|---|---|---|---|
| | | | | | Uniform (psf) | Concentrate (Truss Panel Points, psf) | | $T_{max}$ in Main Truss reached 1300°F (704°C) | $T_{ave}$ in Main Truss reached 1100°F (593°C) | $T$ at unexposed Floor Surface reached 325°F (163°C) |
| 1 | 1:1 | Restraint | 3/4 | 35 | 152 | 0 | 116 | 62 | 66 | 111 |
| 2 | 1:1 | Unrestraint | 3/4 | 35 | 152 | 0 | 146 | 62 | 76 | Not Exceed |
| 3 | 1:2 | Restraint | 3/4 | 17.5 | 341 | 86 | 210 | 80 | 86 | 157 |
| 4 | 1:2 | Unrestraint | 1/4 | 17.5 | 341 | 86 | 120 | 58 | 66 | 58 |

16

Table 2-1 summarizes the condition and results of the four tests. All the tests were performed complying with ASTM E119 standard fire test. The major conclusions from these tests were:

1.  The test assemblies had 3/4 hour to 2 hours fire resistance rating under ASTM standard fire;

2.  Unrestrained assemblies had a longer fire resistance rating than restrained ones;

3.  Reduced scale assemblies gave longer fire ratings than full scale ones.

Areas for future research were pointed out. The first is the behavior of bolted connections in fire, which is not covered in ASTM E119. The second is how to evaluate a reduced scale test result. It is impossible to scale every factor to the same scale. In the reduced scale assemblies, the load was adjusted to maintain the force in major truss chords and diagonals. The cross section dimension of chords and diagonals were not changed in order to preserve the original heat transfer rate. Thus reduced scale truss diagonal in compression did not have the same buckling behavior as the full scale one. The third area of needed research is the effects of boundary conditions. Restraint support generated compression force in the floor system during initial thermal expansion resulted in an earlier compression failure of unexposed concrete surface and spalling of concrete. This phenomenon was not observed in Cardington tests. This indicates that in Cardington testing, the stiffness of restraint against thermal expansion of floor might be lower than that that of the ASTM standard test.

### 2.3.3 Steel Beam Behavior – Catenary Effects

According to ASTM E119, beams are tested as simply supported. Only restraint against thermal expansion can be applied and there is no connection included in the beam test setup. Therefore no catenary reaction effect is revealed in the ASTM fire test on beams. The standard fire test results reveal the ability of

fire proofing material to keep the beam temperature below critical point when the beam moment capacity is lower than the applied moment. This test is more for testing fire proofing material than testing the beam itself. However, beams in real structure are constrained through connection to the surrounding structure. At the beginning of fire, the heated beam is constrained from free thermal expansion and the beam is subject to axial compression plus bending. As the fire develops, the beam loses more bending stiffness and beam deflection grows. Axial tension force increases gradually within beam. This tension force prevents beam deflection from escaping. The phenomenon is called the catenary effect, which is why unprotected steel beams have a much higher fire resistance capacity than what is predicted by standard fire testing. This was found in Cardington fire tests and real fire events in multi-story steel buildings, such as Broadgate Building fire. Theoretically, if the connections and surrounding structure have enough strength, a beam would not collapse until the steel melted. (Yin and Wang, 2005)
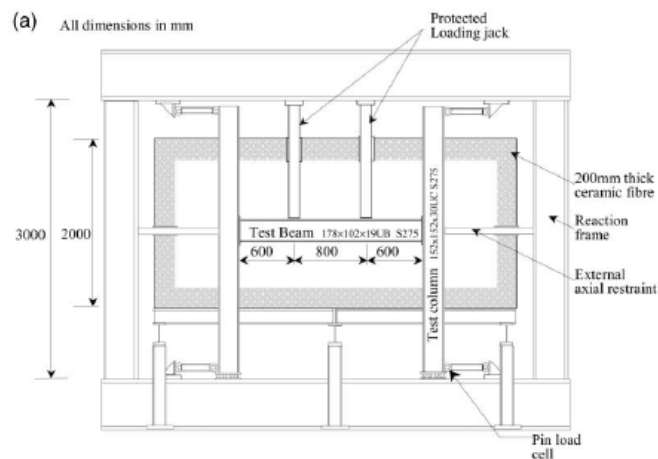


Figure 2-15 Liu's Test Setup (Liu, Fahad, Davies, 2002)

Experimental investigation of behavior of axially restrained steel beam in fire was performed by Liu (Liu, 2002). Figure 2-15 shows the test setup. Specimen beam was loaded with two concentrated loads. Axial restraints were provided by test columns and reaction frame. The effects of different load ratio,

18

axial restraint stiffness and connection type on beam behavior were all studied. Figure 2-16 depicts axial force changes in beam with temperature. The major conclusion is that the higher axial restraint and lower load ratio, the more pronounced the catenary action. However the span to beam height ratio of specimen beam is 11.2, which is much smaller than typical floor beams. The large depth of the beam relative to the span made the specimen beam have a higher percentage of shear deformation in total deflection than general floor beams.  The behavior of specimen beams may not be representative of typical floor beams in real structures. Moreover the bolt connections were all fire protected in tests, with temperatures lower than 200˚C. No connection stiffness and strength were tested.
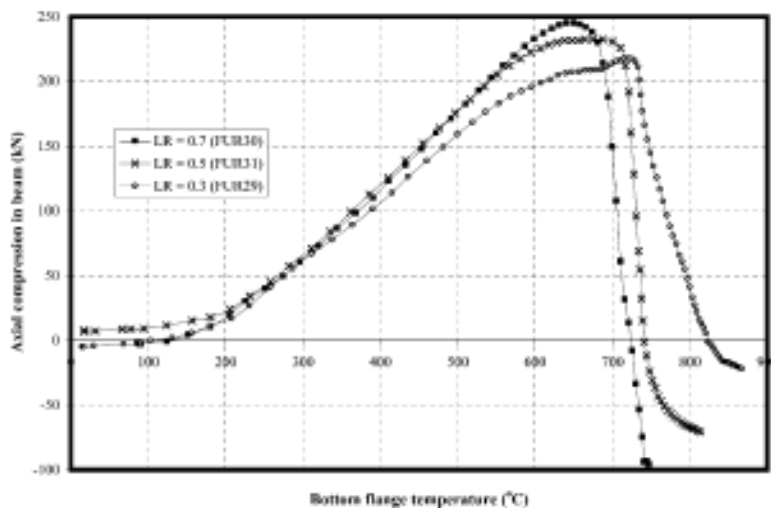


Figure 2-16 Axial Force in Beam Changes with Temperature

A considerable amount of analytical work has been done to investigate catenary effects in beams generated in a fire. Yin and Wang performed numerical study of large deflection behavior of restrained steel beams at elevated temperatures. Beam span, uniform and non-uniform temperature distributions, different load levels, different axial, and rotational restraint stiffness were all studied (Yin and Wang, 2004). Liu's test results were used in validating the Finite Element Model in ABAQUS (Liu and Davies, 2001). It was concluded that

catenary action can enable steel beams to survive very high temperatures without a collapse as long as reliable axial restraints are provided. Among the variables studied, axial restraint stiffness was found to be the most important factor in affecting beam deflection and catenary force. Yin and Wang put forwarded a simplified hand calculation method to determine the catenary tensile force in beams (Yin and Wang, 2005). The temperature is assumed to be uniform across section and along span. A deflection shape of beam is assumed according to load type to determine beam elongation. Combined with thermal expansion, the beam axial force is determined. An incremental approach was used when material becomes plastic. Moss performed analysis to study the effect of support conditions on the fire behavior of steel and composite beams (Moss and etc, 2002). Finite Element software, SAFIR, was used to analyze beams with pin-roller, pin-pin, fixed-slide and fixed-fixed supports. Standard fire from International Organization for Standardization (ISO) was used in analysis. It was found that beam behavior is very different with the changes of support conditions. Stress condition relative to the temperature reduced yield strength is a key variable in beam behavior. Similar sized composite beam and steel beam were found to have similar behavior at elevated temperature.

## 2.3.4 Bolt Connection Behavior at Elevated Temperature

The strength and behavior of bolted beam-to-column or joist-to-beam connections must be considered in determining the behavior of a steel frame structure in a fire. Most of the research in this field was focused on studying the stiffness on bolt connections in fire. Different researchers have put forward component based models to simulate connection stiffness changes in fire (Al-Jabri, 2004; Silva, Santiago, Real, 2001). In addition, Finite Element Modeling was used to analyze connection behavior also (Liu, 1996). Due to high cost, experimental work on this topic is very limited. Al-Jabri performed four transient

state tests on end-plate bolt connection, investigating the stiffness changes with temperature (Al-Jabri, 2004). However at limit state, the connection strength will become more important than stiffness to the safety of the structure. Little work has been done on the strength of the connections.

### 2.3.5 Shear Stud Behavior at Elevated Temperature

Shear connection strength is controlled by the strength of stud and strength of concrete. Both stud steel and concrete suffer strength and stiffness loss as their temperatures rises up during fire. Kruppa and Zhao published their test results of the force slip temperature relation of shear studs; see Figure 2-17 (Kruppa and Zhao, 1995).
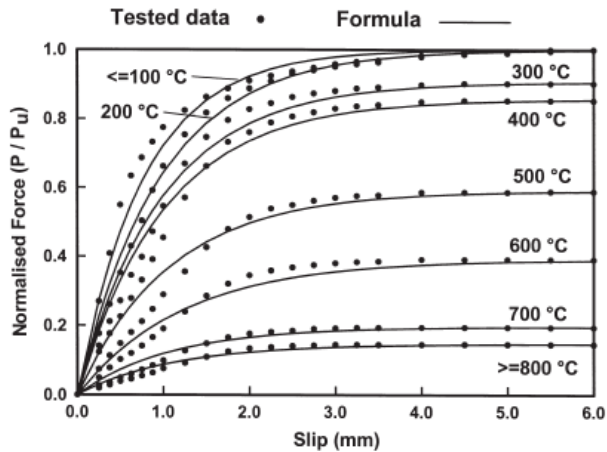


Figure 2-17 Typical Force-Slip-Temperature Curves for Shear Connectors (Huang, Burgess, Plank, 1999)

Huang, Burgess, and Plank fit curves to the test data and put forward an empirical formula for the load-slip relationship of shear connectors.

$$\frac{P}{P_u} = A\left(1.0 - e^{-B\lambda}\right)$$

$P$ = shear force in stud;

21

$P_u$ = shear stud capacity at ambient temperature;

$A, B$ = empirical coefficients (temperature dependent);

$\lambda$ = slip;

Table 2-2 Temperature Dependent Parameters A and B

| Temperature (°C) | A | B | Temperature (°C) | A | B |
|---|---|---|---|---|---|
| ≤100 | 1.0 | 1.2789 | 500 | 0.5909 | 0.9163 |
| 200 | 1.0 | 1.0297 | 600 | 0.3911 | 0.7985 |
| 300 | 0.9063 | 1.0095 | 700 | 0.1964 | 0.9251 |
| 400 | 0.8567 | 0.9781 | ≥800 | 0.1472 | 0.8967 |

This slip-force relationship was used in determining the stiffness of connector in Finite Element Analysis of composite beams in Chapter 8.

## 2.3.6 Material Properties of Steel at Elevated Temperature

Material test can be divided into two types: steady-state test and transient heating test. In a steady-state test, coupon is heated to target temperature level without load and restraint. The coupon is loaded to fracture with the temperature kept constant. In transient heating test, coupon is loaded to target stress level at ambient temperature. Keeping the stress in coupon constant, temperature is raised until fracture occurs. Comparing these two types of test methods, steady-state is easier to carry out, while transient heating test simulates the material's stress and temperature condition in fire more accurately. The results from these two test methods are not exactly the same. The strength results from steady-state test are often higher than those from transient heating tests. One of the reasons for the difference is the creep and relaxation behavior of steel at temperature higher than 500°C. By comparing the results, Kirby concluded that data from steady-state test could be used to model the behavior of steel when only small strains are considered (Kirby, Preston, 1988). However, when dealing with larger strains at "runaway" status, transient heating test results are more accurate.

At ambient temperature, the yielding strength is easily defined by yielding plateau; however when temperature increases, the yielding plateau is replaced by fine serrations until it fully disappears at about 300˚C. Beyond 300˚C, steel enters hardening phase right after its proportional limit. Yielding strength has to be defined by 0.2% rule.

Different structural steels behave quite differently at elevated temperature levels. Chemical composition, crystal structure and manufacture process are the main reasons for the difference. A variety of experimentally determined strength reduction factors are found in the literature. AISC (AISC 13th edition) gives strength reduction factor for structural steels at elevated temperature, which is based on the results of Kirby and Preston (1988). The reduction factor for ultimate strength is given based on yield strength at ambient temperature, which maybe incorrect. ASCE gives reduction factors for yield strength of steel at elevated temperatures (ASCE report No. 78). NIST performed material properties tests on WTC steels (NIST NCSTAR 1-3 and NIST NCSTAR 1-3D, September 2005). S235, S355, S350 GD+Z and S420M are structural steels used in Europe, which were tested by Outinen, Kesti, Makelainen (1997 & 1998) and Outinen, Makelainen (1995). 16Mn is structural steel and 20MnTiB is high-strength bolt steel used in China, which were tested by Li, Jiang, Yin, Chen and Li (2003). The material properties of A514, A588, A992, A572 and A36 steels at elevated temperature were given in the AISC LRFD manual 3rd edition. Figure 2-18 and Figure 2-19 summarize the reduction ratios of yield strength and ultimate strength at elevated temperature. The reduction factors for S235, S355, S350 GD+Z, S420, and AISC were obtained from transient test result; while reduction factors for WTC steel, 16Mn, 20MnTiB, A514, A588, A992, A572, and A36 were obtained from steady state tests. Figure 2-20 gives the Young's Modulus ratio at elevated temperatures.
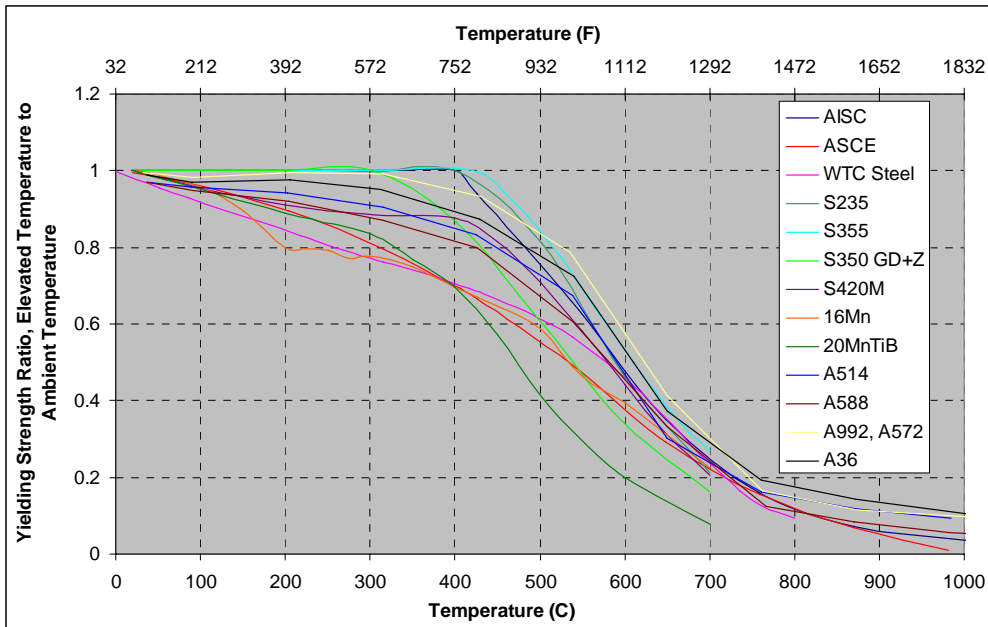
Figure 2-18 Yielding Strength Ratio at Elevated Temperatures of Different Structural Steels
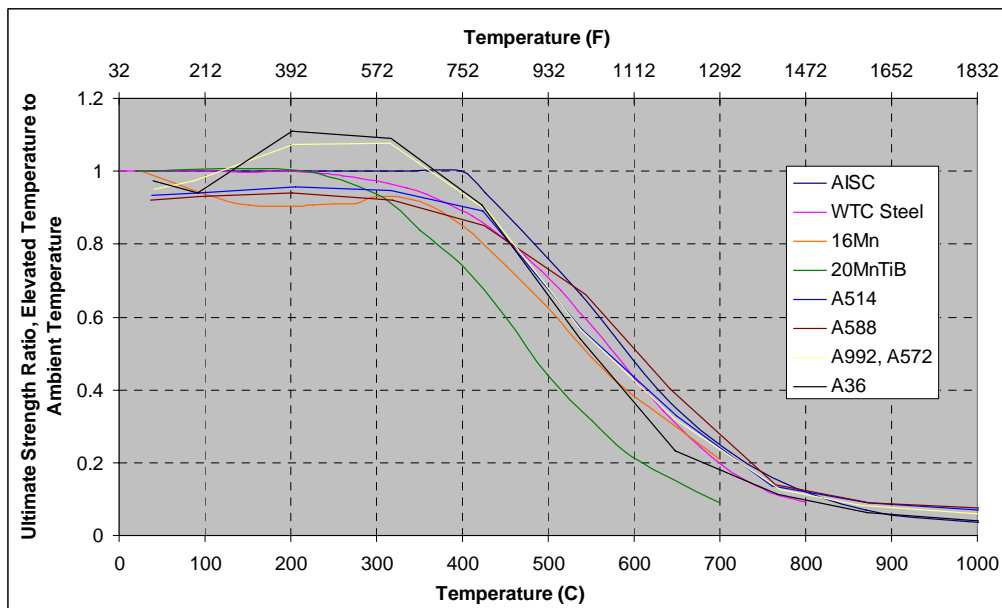


Figure 2-19 Ultimate Strength Ratios at Elevated Temperatures of Different Structural Steels
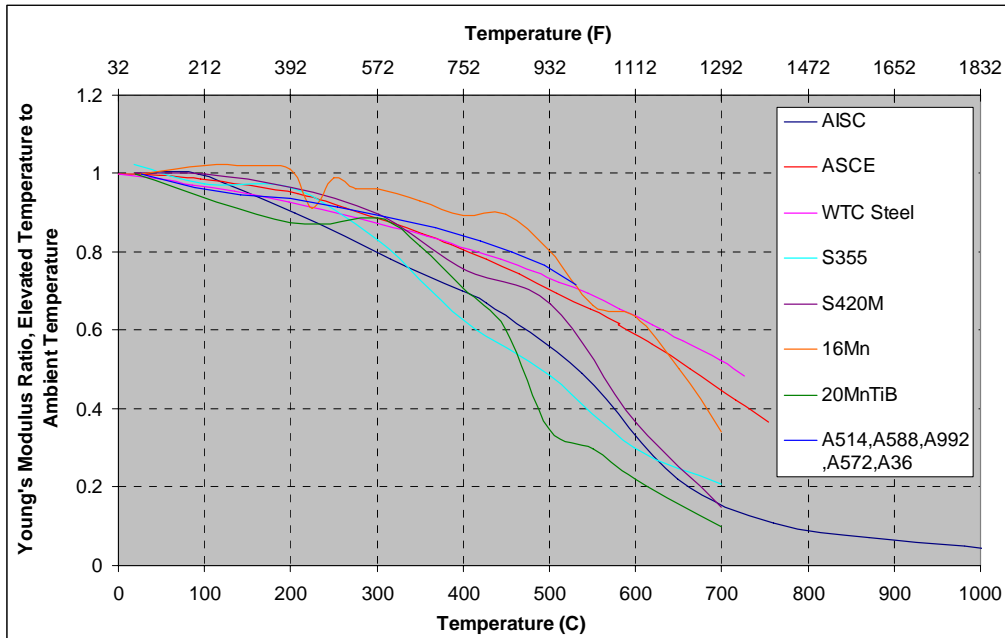
Figure 2-20 Young's Modulus Ratio at Elevated Temperatures of Different Structural Steels

## 2.3.7 Properties of High Strength Bolt at Elevated Temperature

Unlike structural steels, literature about material properties of high strength bolt at elevated temperatures is quite limited. Kirby (Kirby, 1995) performed tensile and shear tests on Grade 8.8 bolts at temperatures up to 800°C. Figure 2-21 shows the tensile capacity and double shear capacity of M20 (20mm diameter, 0.787 inch) Grade 8.8 bolt at elevated temperatures. In tension tests failure of threads stripping on low strength nuts occurred. The residual strength of Grade 8.8 bolts after exposure to elevated temperature was also tested with hardness tests. The results supported the known conclusion that when exposure to a temperature lower than tempering temperature would not damage the strength of the bolt as shown in Figure 2-22.

25
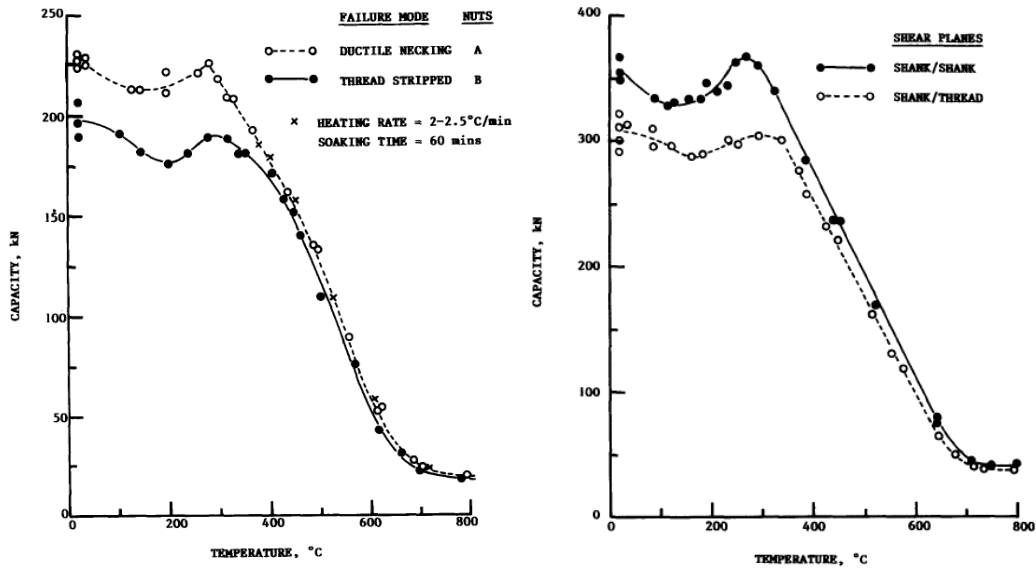
Figure 2-21 Tensile Capacity (left) and Double Shear Capacity (right) of Grade 8.8 Bolts at Elevated Temperatures
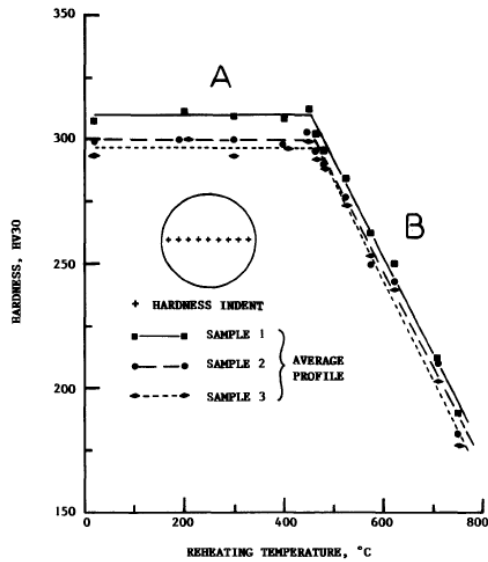


Figure 2-22 Change in Hardness with Maximum Heating Temperature

Based on test results, a tri-linear formula was given to determine both tensile and shear strength reduction factor for Grade 8.8 bolt:

$$SRF = \begin{cases} 1.0, & T \le 300°C \\ 1-(T-300)\times 0.2128\times 10^{-2}, & 300°C < T \le 680°C \\ 0.170-(T-680)\times 0.5312\times 10^{-3}, & 680°C < T \le 1000°C \end{cases}$$

$T$ = Temperature in Celsius.

## 2.4 Research Aims and Outlines

The major findings from observations of real fire events, both experimental and analytical studies follow:

1. Because of the interaction between structure members, unprotected steel beams and composite floor have higher fire resistance capacity than what standard fire tests predicted.

2. Catenary effects play an important role at elevated temperature. It increases the load carrying capacity of floor beams.

3. Catenary forces on beam connections may result in connection failure. Simple connections designed to carry vertical shear force at ambient temperature must be designed to carry both vertical shear force and horizontal catenary force in fire event. Failure of connection may result in partial, and even total, structural collapse.

4. Due to deformation and thermal shrinkage on the beams, connection failure may happen during cooling phase post fire.

The goal of this research study is the development of strength prediction equation for bolted connections in steel buildings during a fire. The main research topics undertaken and reported in this dissertation are:

1. Experimental study of strength reduction of A325 and A490 bolts at elevated temperatures;

2. Experimental study of residual strength of A325 and A490 post exposure to elevated temperatures;

3. Experimental study of connection bearing strength at elevated temperatures;

4. Experimental study of block shear at elevated temperatures;

5. Experimental study of slip load reduction in fully tightened connection post exposure to elevated temperatures;

6. Experimental study of material properties of structural steel at elevated temperatures;

7. Develop design methods for bolt connection at elevated temperatures;

8. Analyzing catenary action of steel beam and composite beam at elevated temperatures and reaction forces on connection.

# Chapter 3
# Test Procedures

This chapter describes the test methods and equipment used to determine the shear capacity of A325 and A490 high strength bolts, the capacity of single bolt connection and double bolts connection, and connection slip load. Double shear tests of A325 and A490 high strength bolts were performed at elevated temperature levels. The residual shear strength of both types of bolts after heating and cooling was measured in single shear fixture and the tensile and shear strength was estimated by Rockwell hardness tests. Single bolt connections were tested at different elevated temperature levels to examine the change in bearing capacity as the connection temperature was increased. A series of two bolt connections that were designed to fail in block shear mode were also tested at elevated temperatures. Slip test connections were tightened at ambient temperatures and heated. Slip tests were performed after the connection was cooled back to ambient temperature.

## 3.1 High Temperature Test System

The high temperature test system consists of an electric furnace, stainless steel clevises, loading frame, hydraulic ram, water cooling system, and data acquisition equipments. Figure 3-1 showed an overview of this test system.

## 3.1.1 Electric Furnace

The test furnace was converted from a MSI Industries D12H electric kiln with inside dimension as $24 \times 24 \times 43$ inches. With upgraded heating elements, the power is about 20 kilowatts. Figure 3-2 shows the furnace heating curve along with ASTM standard fire. ASTM standard fire represents a very severe fire

condition, in which the air temperature reaches 800°C (1500°F) in 20 minutes. The furnace used in this test program does not meet the ASTM standard fire curve. However, because this research program aims to investigate the strength of bolts and bolted connections at elevated temperature, and no fire proofing material is included, the heating rate of the furnace is not an important character. Test results from this slower heating furnace still provide accurate estimates of bolted connections behavior in a fire.
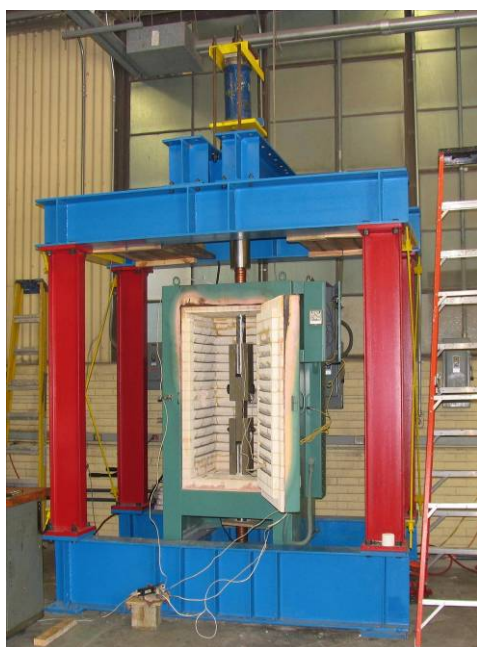


Figure 3-1 High Temperature Test System
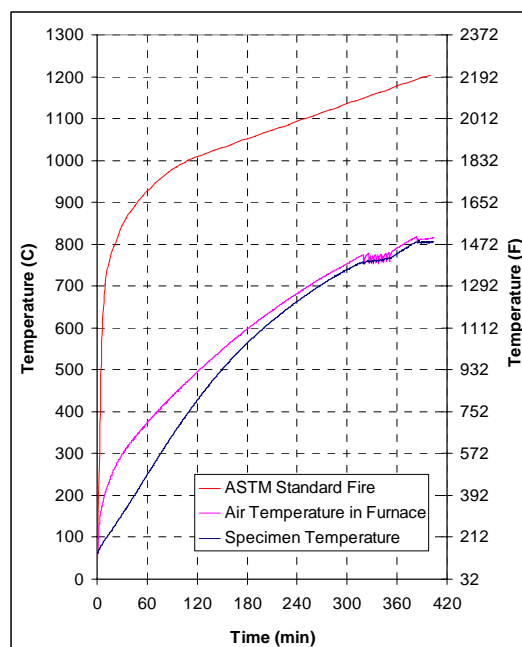


Figure 3-2 Time Temperature Curve

The furnace has a temperature control unit, which reads the air temperature inside the furnace using a thermocouple probe. The accuracy of the air temperature is controlled within ±10°C (±18°F). Because steel has a higher specific heat than air, the specimen temperature stays within ±5°C (±9°F) of a set level, as shown in Figure 3-3. In this case, the desired specimen temperature was 800°C. The specimen temperature stabilized at 803°C, approximately 10°C below

the furnace air temperature. Because there is no forced air circulation in the furnace, a uniform temperature distribution is hard to achieve. A 10˚C temperature difference may exist between the bottom and top of furnace. Because the failure section of high strength bolts and bolted connections is only about a couple of inches, the temperature difference within that range is small enough to be insignificant. Figure 3-4 shows the temperature difference between bottom and other locations along the height of the furnace. As the temperature increases, the temperature difference diminishes.
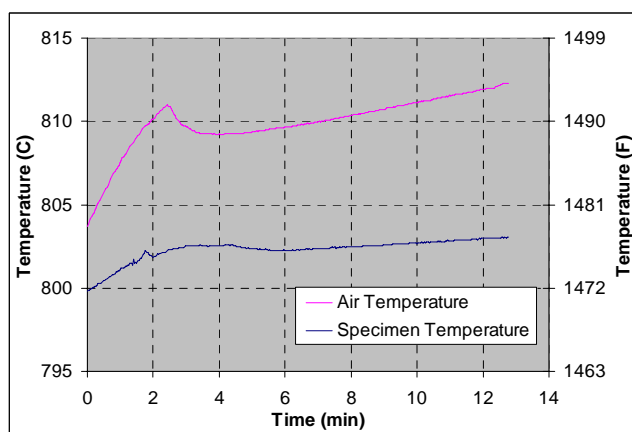


Figure 3-3 Specimen Temperature and Air Temperature during Loading Process
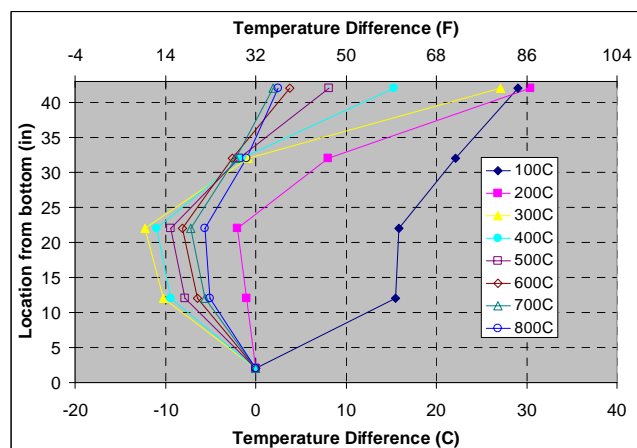


Figure 3-4 Air Temperature Difference between Bottom and other Locations at Different Temperature Level

31

### 3.1.2 Loading clevises and Loading Frame

The loading clevises were made of S321 and S347 stainless steels and were designed to work inside the furnace as hot grips. In order to control the bearing deformation on bolt-hole edge in double shear tests, exchangeable bushings are made, as shown in Figure 3-5. The 4340 steel bushings were found to work better than S321 stainless steel bushings because of their higher strength and hardness.

The loading frame shown in Figure 3-1 was designed and built around the electric furnace to react to loading forces during testing.

### 3.1.3 Hydraulic ram and Pneumatic Pump

The hydraulic ram has a loading capacity of 200kips with a 10.4 inch stroke, as shown in Figure 3-6. As shown in Figure 3-7, a pneumatic pump was used in constant temperature test. Loading speed is controlled to be "slow" in order for the static test condition to be satisfied. In general, specimen failure occurred in 5 to 20 minutes, depending on the total load magnitude. In constant load test, electric pump and load maintainer were used, as shown in Figure 3-8 and Figure 3-9.



Figure 3-5 Bushings          Figure 3-6 Hydraulic Ram

Figure 3-7 Pneumatic Pump



Figure 3-8 Electric Pump;



Figure 3-9 Load Maintainer



Figure 3-10 Water Cooling System

### 3.1.5 Water cooling system

In order to prevent heat from being conducted to the hydraulic ram by the loading steel rod, a water cooling system was designed, manufactured, and installed, as shown in Figure 3-10.

### 3.2 Data acquisition system

### 3.2.1 Temperature measurement

During test, both the air temperature in the furnace and specimen temperature were monitored and recorded. Figure 3-11 shows the type K thermocouple wires that were used during the test.

(a) Bolt Shear Test    (b) Single Bolt Connection    (c) Two Bolt Connection

Figure 3-11 Type K Thermocouple Wires Location in Tests



Figure 3-12 National Instrument SCXI 1000 and SCXI 1328 (left)

Figure 3-13 STRAINSERT FL200U-3SPKT Load Cell (right)

National Instrument (NI) NI SCXI-1000 mainframe and NI SCXI-1328 isothermal terminal block with built-in high-precision cold-junction sensor are used to read temperature from thermal-couple wires, as shown in Figure 3-12. The resolution of temperature readings is ±0.1˚C.

**3.2.2 Load Measurement**

STRAINSERT FL200U-3SPKT load cell is used to measure the load during all the tests, as shown in Figure 3-13. The load cell has a 200 kip capacity and ±0.1% accuracy.

### 3.2.3 Non-contact Displacement Measurement

Machine Vision is the technology of automatic acquisition and analysis of images to obtain desired data. The Machine Vision System used in this research program consists of a digital video camera, frame grabber card, computer, and software. The resolution of this technology is equal to the field of view dimension divided by the number of pixels in each direction on CCD sensor. In bolt double shear tests, single bolt connection tests and two bolts connection tests, the resolution is 0.0048 inch, 0.0071 inch and 0.0065 inch, respectively. Figure 3-14 shows the digital monochrome camera, which takes pictures of specimen through an observation port on the furnace sidewall, as shown in Figure 3-15. National Instrument frame grabber card, PCI-1409 is used to acquire images from the camera.



Figure 3-14 JAI CV M50 monochrome digital video camera (left)
Figure 3-15 TATE-JONES SAF-T-EYE Observation Port (right)

Electronic Engineer at The Ferguson Structural Engineering Laboratory, Eric Schell, created LabVIEW based software, Abel 1.1, for fully automatic data acquisition. The author programmed the Machine Vision module.

## 3.2 Test Setup

There are two types of high temperature tests performed in this research program, which are constant temperature test and constant load test. In constant temperature test, the specimen is heated to the desired temperature without load. Then with the temperature kept constant, the specimen is loaded to fail. The maximum load is taken as the specimen's capacity at this temperature. In constant load test, the specimen is loaded to a certain level at ambient temperature. Then, with the load being kept constant by a load maintainer, see Figure 3-9, the specimen's temperature is raised gradually until failure occurs. The results suggest that the specimen can carry that load until reaching its failure temperature. Constant load testing is a more accurate simulation of structure failure in fire.



Shear Plane
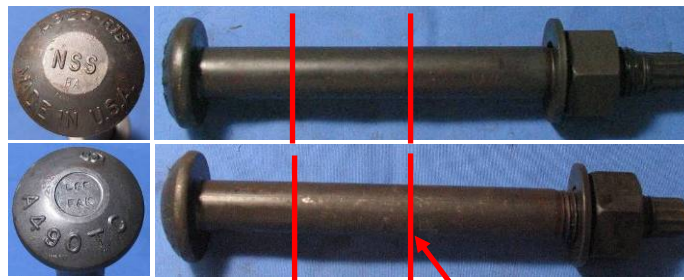
Figure 3-16 A325 and A490 bolts used in this research program

## 3.3.1 Bolt double shear test setup

All the shear tests on bolts were constant temperature tests. Specimen bolts run through the holes in the two plates of bottom clevis and the center plate with bushings. Figure 3-16 shows the A325 and A490 bolts studied.

36

### 3.3.2 Single bolt connection test

All the single bolt connections tests are perform as a constant temperature test. Figure 3-17 shows the dimension of the connection plates. The connection is made with 3/8 inch thick Grade 50 steel plate and 7/8 inch A325 bolt, as shown in Figure 3-18. The bolt was snug tightened only. Figure 3-11(b) shows the specimen connection mounted in furnace before test. The 15/16 inch holes on both plates are for the 7/8 inch A325 bolt. The 1-9/16 inch holes are used to pin test connection to stainless clevises, which transferred load to specimen.
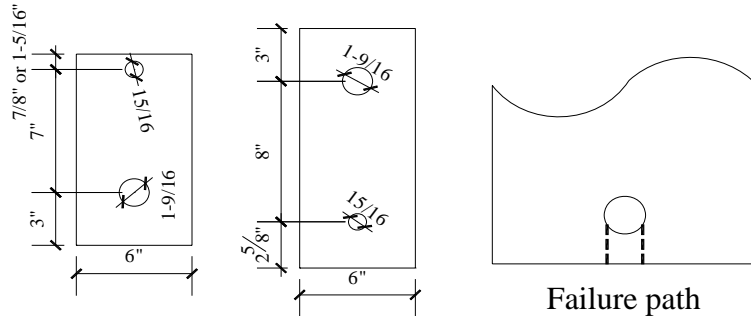


Figure 3-17 Dimensions of connection plates and failure path



Figure 3-18 A325 bolt in single bolt connection test

### 3.3.3 Block shear test

A twin-bolt connection is designed to have block shear failure mode controls, see Figure 3-19. The 15/16 inch holes on both plates are for the 7/8 inch A490 bolts. These 15/16 inch holes were punched instead of drilled. The 1-9/16

inch holes are used to pin test connection to stainless clevises, which transferred load to specimen. The connection is made with ½ inch thick Grade 50 steel plate. Figure 3-11(c) shows a twin bolts connection before test.
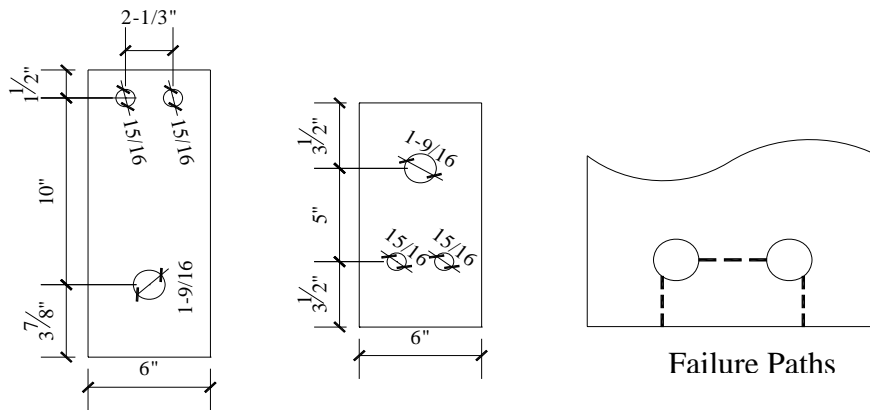


Figure 3-19 Dimension of twin bolts connection and failure paths



Figure 3-20 7 inches long A490 bolt was shortened for block shear tests

     The bolts in these block shear tests are the same A490 bolts, which have been tested for double shear capacity at elevated temperature. The A490 bolt is 7 inches long, which was cut to 3 inches long and tapped threads, see Figure 3-20. Because the bolt is only snug tightened, the threads quality will not affect test result. Seven constant temperature tests and three constant load tests were performed.

### 3.3.4 Slip load test

The AISC Steel Construction Manual provides a standard test method for determining the slip load of bolted connection, which is shown in Figure 3-21, and followed here. 7/8 inch diameter, 3 inches long A490 bolts were tested, see in Figure 3-22. A Skidmore load cell, see in Figure 3-22, was used to determine the tension force in the A490 bolt after tightened with electric twist-off torque wrench, as shown in Figure 3-22. The steel plates are sand blasted on both surfaces first, which creates the same friction coefficient. Figure 3-23 shows the steel plates after being sand blasted. Figure 3-24 shows the slip load test setup.
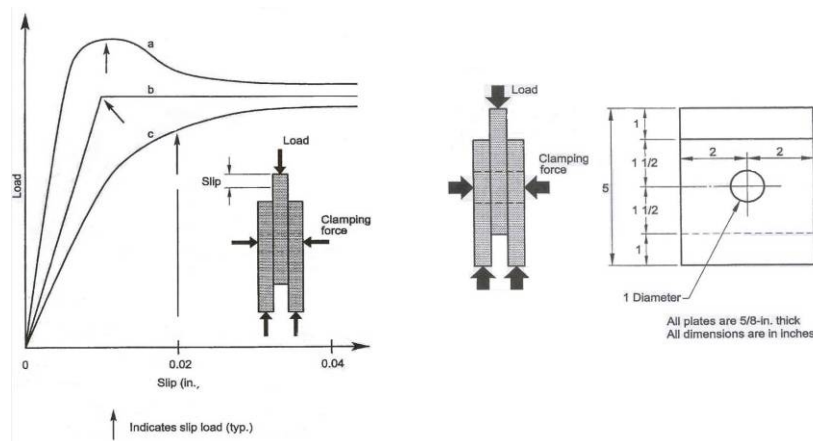


Figure 3-21 Slip Load Test (AISC Steel Construction Manual, 13$^{th}$ edition)



Figure 3-22 Skidmore, Electric Twist-off Torque Wrench and A490 Bolt

Figure 3-23 Steel Plates after Sand Blasted     Figure 3-24 Slip load Test

### 3.3.5 Post fire strength test on A325 and A490 bolt

After the bolt has been tested in double shear at elevated temperature levels, the bolt is tested for its residual strength. Both direct shear tests and hardness tests were performed. Figure 3-25 shows the failure segments for both types of test. There are 13 hardness test points across the bolt section.  The weighted average of the 13 hardness results is used to determine the estimated tensile strength of the bolt.
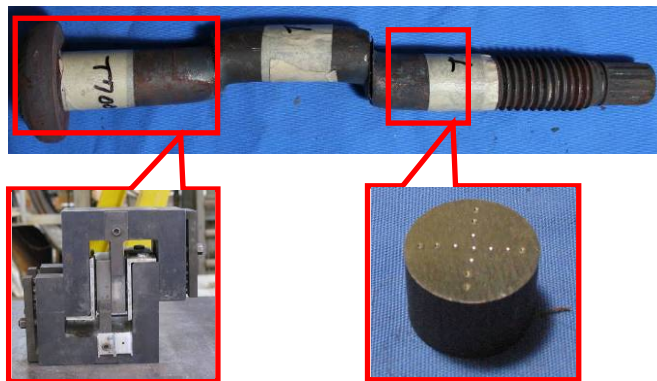


Figure 3-25 Direct Shear Tests and Hardness Tests

### 3.3.6 Material Properties Test of Steel Plate
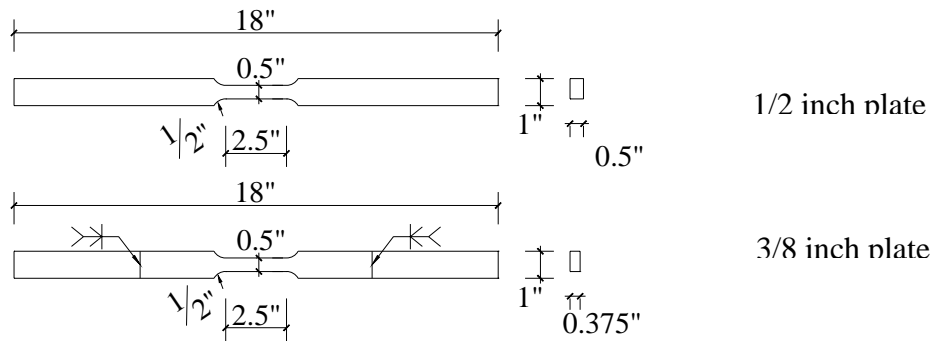


Figure 3-26 Dimensions of Coupons

     The 3/8 inch and 1/2 inch thick Grade 50 steel plates used in bolted connection tests were tested to determine mechanical properties at elevated temperature. The coupons were made from untested plate. The reduced sections of coupons had dimensions in accordance with ASTM E8. However, in order to limit the heat conduction to hydraulic grips through coupon and decrease the temperature gradient in coupon reduced section part, the over all length of coupons were increased, as shown in Figure 3-26. Because the 3/8 inch plate was not long enough to accommodate the required specimen length, extensions were welded.

     Load was applied by MTS 810 material test system and controlled by MTS controller and software. Figure 3-27 shows the overview of test frame. All the tests were run under crosshead displacement control. Two deformation rates, 0.1 inch per minute and 0.01 inch per minute, were used. 30 seconds pauses were performed during tests to determine static strength. The load was measured by MTS 661.20 axial load cell, as shown in Figure 3-27. The resolution of load

41

measurement is 0.007 kip. The crosshead movement was measured by LVDT in actuator. The accuracy of LVDT is 0.0001in. Coupon was gripped by hydraulic grips with water cooled wedges, as shown in Figure 3-28.
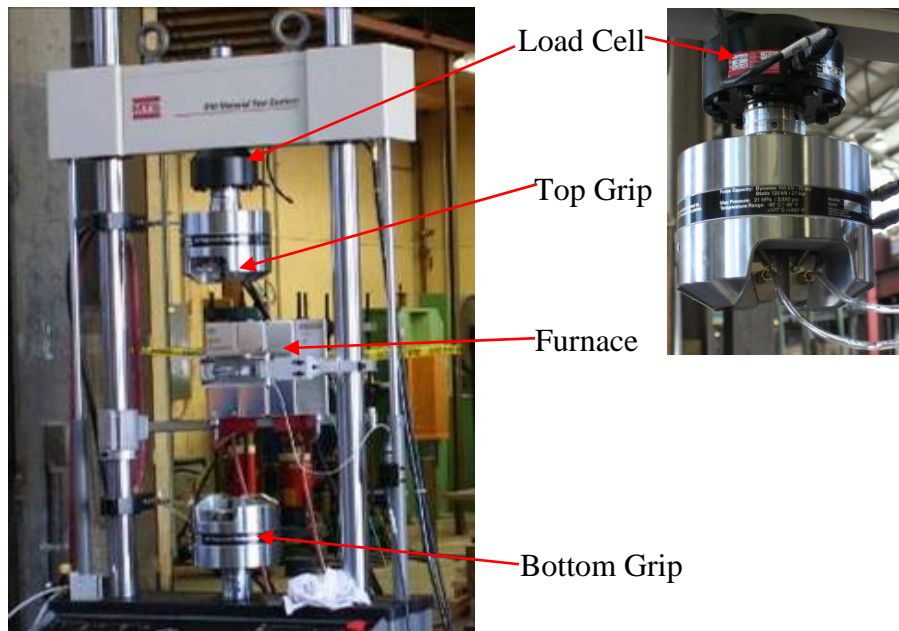


Figure 3-27 Overview of NTS 810 Material Test System

Coupon temperature was controlled by MTS 653 furnace and use of an MTS controller. Its three heating zones work independently, which enable the coupon temperature to be kept at target level in the loading process. Figure 3-29 shows the built-in temperature sensors, which monitor air temperature in furnace. Besides three built-in thermocouples in the 653 furnace, three Omega external type K thermocouple probes were used to monitor coupon temperature, at the top, middle, and bottom of the reduced section part, as shown in Figure 3-30. These thermal probes were connected through an Omega DRF-TCK signal conditioner to the MTS station controller, as shown in Figure 3-31. The thermal probes have stainless steel tube, which were bent to generate spring force to keep them in contact with the coupon surface during test.

Strain was measured with an MTS 632.54 high temperature axial extensometer, as shown in Figure 3-32. The extensometer senses the coupon elongation by two ceramic rods which contact coupon surface and are held against the specimen by a light spring force. An air cooling duct connected to the laboratory air supply was used to cool the extensometer. The extensometer has 1 inch gage length and +10% working range. This extensometer meets the requirements of a $2.5 \times 10^{-4}$ resolution and $5.0 \times 10^{-4}$ accuracy for class B-1in ASTM E83. (ASTM E83)

All coupon tests were performed as constant temperature tests. The coupon was first installed into the top grip. The thermal probes were installed in contact with the specimen and the extensometer was installed. The coupon temperature was raised to the desired level. With the bottom end of the coupon free, thermal expansion during the heating of the specimen did not generate an axial load. Since extensometer gage length was set at ambient temperature, thermal strain was included in results. After coupon temperature was stable, coupon was gripped at the bottom end with load being controlled at zero. Then loading started and continued until fracture. Punched marks with 1 inch gage length were made on coupon for measuring elongation after fracture. All the data acquisition devices were synchronized by the MTS FlexTest GT controller. Load, crosshead displacement, furnace temperature, coupon temperature, and strain were recorded at 1Hz rate.

Figure 3-28 Water Cooled Wedge
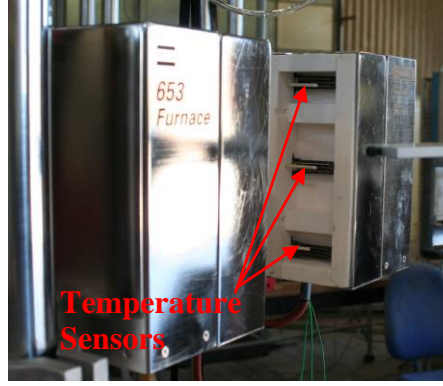


Figure 3-29 MTS 653 Furnace
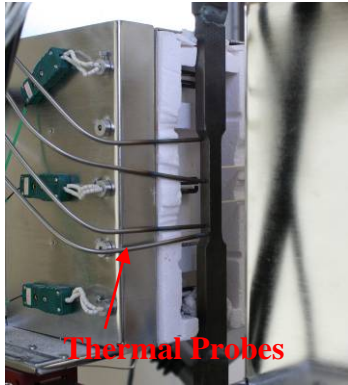


Figure 3-30 Omega Thermal Probes



Figure 3-31 Omega Conditioner Box
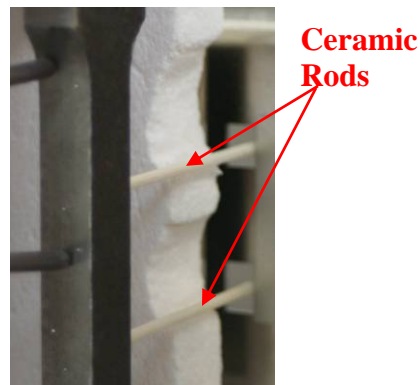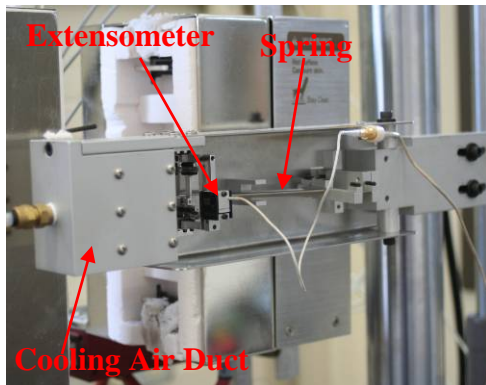


Figure 3-32 Front View and Back View of Extensometer

# Chapter 4

# Shear Strength of A325 and A490 Bolts at Elevated Temperatures

This chapter discusses double shear test results of A325 and A490 bolts at elevated temperatures.

## 4.1 Test Specimen and Test Nomenclature

Figure 4-1 shows the A325 and A490 high strength bolts, which were tested in double shear at elevated temperature. The bolts are twist-off-type, tension-control, with round head. The washer is ASTM F436 and the nut is ASTM A563 Grade DH. In all of the elevated temperature tests, the bolts were snug tightened. Table 4-1 and Table 4-2 give the basic geometry, mechanical, and chemistry information of A325 and A490 bolts that were tested. Table 4-1 also gives the chemical composition of two sets of Grade 8.8 bolts. The Grade 8.8 bolts were tested by B. R. Kirby (B.R. Kirby, 1995), which will be compared to the results of the present study. The ratio of shear to tensile strength of A325 and A490 bolt are 0.625 and 0.653 respectively, which agrees well with the expected value of 0.6 of tensile strength.



Figure 4-1 A325 and A490 high strength bolts

The double shear tests were labeled by the bolt type plus test temperature plus number of tests at this temperature. For example, 325T600-1 is the number 1 double shear test on A325 bolt at temperature T of 600˚C.

Table 4-1 Geometry, Mechanical and Chemistry Information of A325 Bolt

| Mill Report (A325 Bolt) | Mechanical Properties | | | Geometry | | |
|---|---|---|---|---|---|---|
| | Tensile Strength (lbf) | Tensile Strength ($A_n=0.462\text{in}^2$) (ksi) | Hardness (HRC) | Nominal Diameter (in) | Length (in) | Thread Length (in) |
| | 62,285 | 134.8 | 28-32 | 7/8 | 7-1/2 | 1-1/2 |
| | Chemical Composition | | | | | |
| | C | Si | Mn | P | S | Cr | Mo | Ni | B | Cu | N |
| | 0.31 | 0.23 | 0.76 | 0.005 | 0.010 | N/A | N/A | N/A | N/A | N/A | N/A |

| Test Results | Mechanical Properties | | | | | | |
|---|---|---|---|---|---|---|---|
| | Shear Strength, thread excluded (lbf) | Shear Strength ($A=0.601\text{in}^2$) (ksi) | Hardness (HRC) | | | | |
| | 50,660 | 84.3 | 30 | | | | |
| | Chemical Composition | | | | | | |
| | C | Si | Mn | P | S | Cr | Mo | Ni | B | Cu | N |
| | 0.29 | 0.27 | 0.76 | 0.006 | 0.010 | 0.05 | 0.010 | 0.06 | 0.0009 | 0.12 | 0.026 |
| Gr. 8.8 Set A | 0.19 | 0.21 | 1.16 | 0.020 | 0.017 | 0.19 | 0.027 | 0.14 | 0.0051 | 0.22 | 0.0080 |
| Gr. 8.8 Set C | 0.41 | 0.16 | 1.61 | 0.021 | 0.038 | 0.13 | 0.130 | 0.12 | <0.0005 | 0.23 | 0.013 |

Table 4-2 Geometry, Mechanical and Chemistry Information of A490 Bolt

| Mill Report (A490 Bolt) | Mechanical Properties | | | Geometry | | |
|---|---|---|---|---|---|---|
| | Tensile Strength (lbf) | Tensile Strength ($A_n=0.462in^2$) (ksi) | Hardness (HRC) | Nominal Diameter (in) | Length (in) | Thread Length (in) |
| | 75,550 | 163.5 | 35 | 7/8 | 7-1/2 | 1-1/2 |
| | Chemical Composition | | | | | |
| | C | Si | Mn | P | S | |
| | 0.35 | 0.21 | 0.75 | 0.012 | 0.009 | |
| | Cr | Mo | Ni | B | Cu | N |
| | 1.02 | 0.19 | 0.02 | N/A | N/A | N/A |

| Test Results | Mechanical Properties | | |
|---|---|---|---|
| | Shear Strength, thread excluded (lbf) | Shear Strength ($A=0.601in^2$) (ksi) | Hardness (HRC) |
| | 64,133 | 106.7 | 37 |
| | Chemical Composition | | |
| | C | Si | Mn | P | S |
| | 0.36 | 0.24 | 0.76 | 0.015 | 0.009 |
| | Cr | Mo | Ni | B | Cu | N |
| | 1.13 | 0.180 | 0.04 | <0.0005 | 0.03 | 0.023 |

Table 4-3 and Table 4-4 give all the shear test results on A325 and A490 bolts. The single shear capacity and deformation at maximum load are listed for each test. The measured deformation result includes elastic elongation in loading clevises and bearing deformation on bushings. The real shear deformation on bolt should be smaller than measured deformation. All the tests were performed as double shear with both shear planes located in bolt shank and the shear failure sections had the same area. It was found that shear failures on both shear planes happened simultaneously and symmetrically, which indicated the load was

distributed evenly between two shear planes. Therefore half of the maximum load recorded in double shear tests was taken as single shear capacity of bolt. The details of test results will be discussed in section 4.2.

Table 4-3 Summary of test results of A325 bolts

| Test Name | Test Temperature | | Single Shear Capacity | Deformation at |
|-----------|---------|---------|-----------------------|----------------|
|           | ˚F      | ˚C      | (kips)                | Maximum Load (in) |
| 325T25-1  | 77      | 25      | 50.65                 | 0.446          |
| 325T800-1 | 1483    | 806     | 5.05                  | N/A            |
| 325T800-2 | 1472    | 800     | 5.75                  | N/A            |
| 325T700-1 | 1293    | 701     | 6.35                  | 0.158          |
| 325T700-2 | 1307    | 709     | 6.30                  | 0.148          |
| 325T600-1 | 1121    | 605     | 11.45                 | N/A            |
| 325T600-2 | 1107    | 597     | 12.05                 | 0.269          |
| 325T600-3 | 1118    | 603     | 9.80                  | 0.236          |
| 325T500-1 | 935     | 502     | 19.45                 | 0.264          |
| 325T500-2 | 947     | 509     | 19.10                 | 0.245          |
| 325T400-1 | 753     | 401     | 33.00                 | 0.338          |
| 325T400-2 | 761     | 405     | 32.35                 | 0.360          |
| 325T300-1 | 561     | 294     | 55.30                 | 0.578          |
| 325T300-2 | 583     | 306     | 56.78                 | 0.604          |
| 325T200-1 | 394     | 201     | 58.78                 | N/A            |
| 325T200-2 | 395     | 202     | 58.15                 | 0.461          |
| 325T100-1 | 197     | 92      | 50.70                 | 0.398          |
| 325T100-2 | 221     | 105     | 51.80                 | 0.420          |
| 325T25-2  | 77      | 25      | 54.35                 | 0.442          |
| 325T25-3  | 75      | 24      | 54.85                 | 0.451          |

Table 4-4 Summary of test results of A490 bolts

| Test Name | Test Temperature | | Single Shear Capacity | Deformation at |
| --- | --- | --- | --- | --- |
| | ˚F | ˚C | (kips) | Maximum Load (in) |
| 490T25-1 | 88 | 31 | 64.3 | 0.297 |
| 490T25-2 | 90 | 32 | 64.0 | 0.317 |
| 490T100-1 | 212 | 100 | 51.5 | N/A |
| 490T100-2 | 216 | 102 | 60.0 | N/A |
| 490T100-3 | 213 | 101 | 64.2 | 0.335 |
| 490T100-4 | 216 | 103 | 57.2 | 0.308 |
| 490T200-1 | 391 | 199 | 61.7 | 0.340 |
| 490T200-2 | 394 | 201 | 59.6 | 0.313 |
| 490T300-1 | 574 | 301 | 65.0 | 0.271 |
| 490T300-2 | 573 | 300 | 64.0 | 0.379 |
| 490T400-1 | 755 | 402 | 53.8 | 0.377 |
| 490T400-2 | 749 | 398 | 52.9 | 0.360 |
| 490T500-1 | 935 | 501 | 38.3 | 0.313 |
| 490T500-2 | 936 | 502 | 38.2 | 0.358 |
| 490T600-1 | 1115 | 601 | 21.4 | 0.275 |
| 490T600-2 | 1108 | 598 | 22.0 | 0.285 |
| 490T700-1 | 1295 | 702 | 10.2 | 0.319 |
| 490T700-2 | 1295 | 702 | 9.9 | 0.291 |
| 490T800-1 | 1476 | 802 | 8.0 | N/A |
| 490T800-2 | 1473 | 801 | 9.8 | 0.398 |

## 4.2 Evaluation of Test Results

Double shear tests on A325 and A490 bolts were performed from room temperature to 800˚C (1472˚F) at 100˚C (180˚F) increments. At each temperature level, a minimum of two tests were performed. If the results were scattered, a

third test was performed to confirm the test results. All the tests were constant temperature tests with quasi static loading until failure occurred.

Two thermal couple wires were put under washer and bolt head separately and affixed by snug tightening the specimen bolt, as shown in Figure 4-2. Both thermal couple wires had good contact with specimen bolt, which ensured they measured the specimen temperature. Their average reading was taken as the specimen temperature. A third thermal couple wire was used to monitor the air temperature in the furnace during testing, shown Figure 4-2.



(a) On Ends of Specimen       (b) In the Air near Furnace Wall
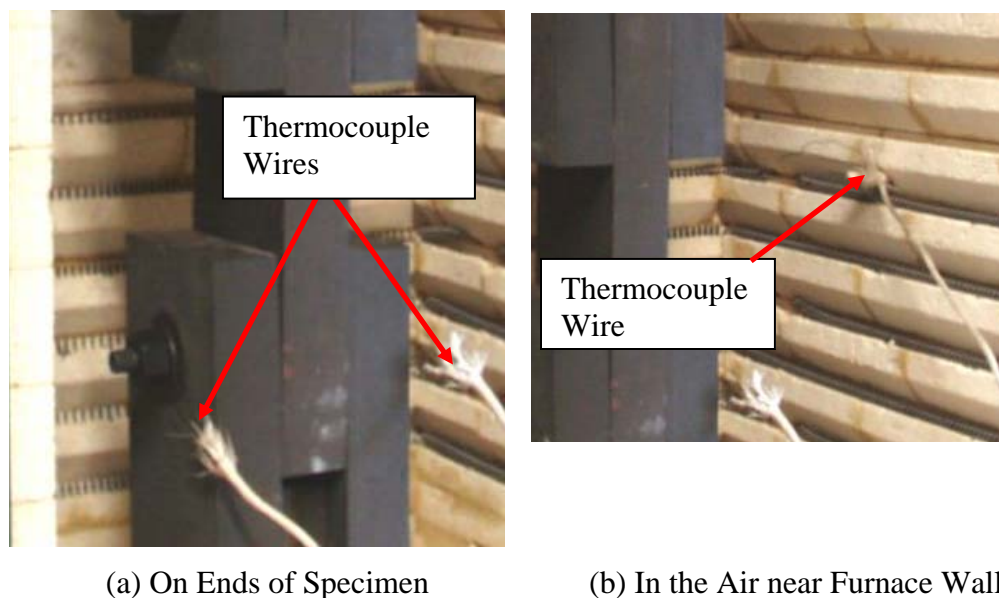
Figure 4-2 Thermal couple wires location in test

Figure 4-3 shows the specimen temperature and air temperature during test 490T800-2 as an example of typical time temperature history of a bolt shear test. The specimen temperature was raised to 800°C in about 6.5 hours and was kept at this temperature during loading phase. In most of tests, the temperature fluctuation during loading phase was less than ±5°C.
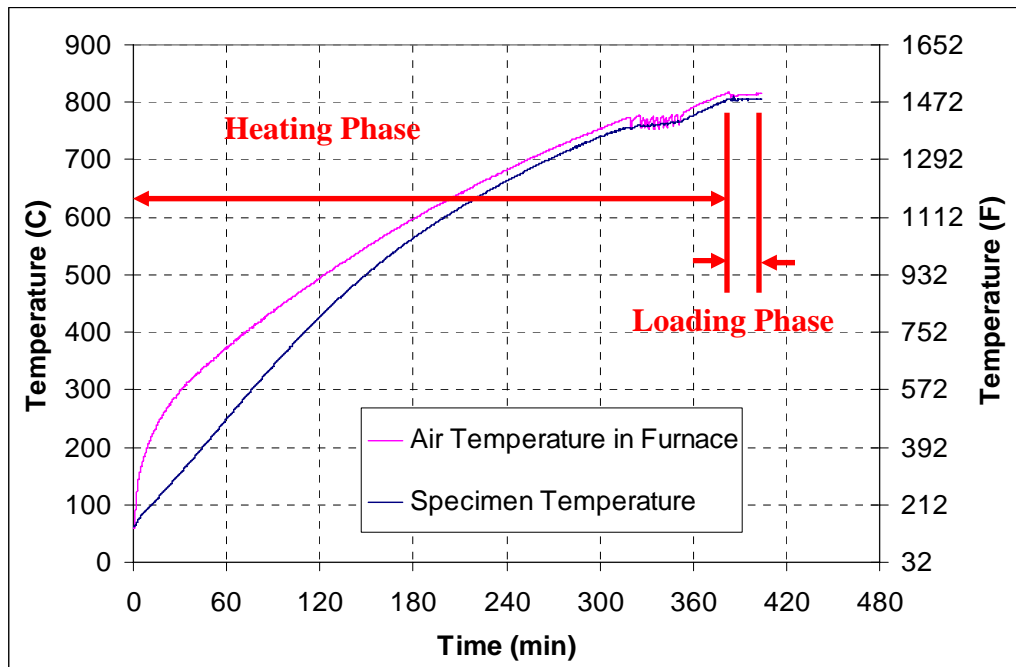
Figure 4-3 Time Temperature Curve of 490T800-2
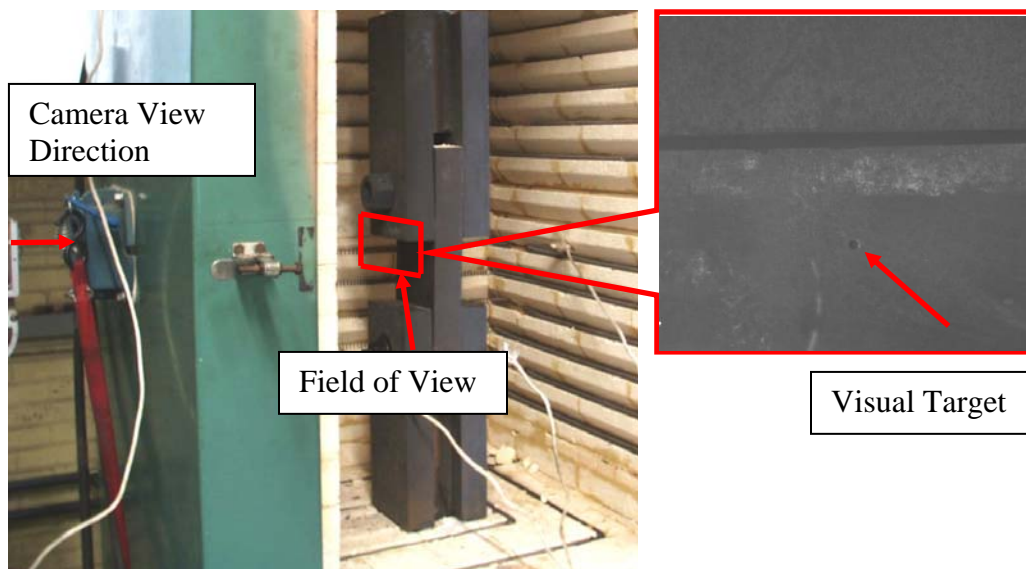


Figure 4-4 Visual Target on Center Loading Plate

The specimen deformation during loading phase is measured by tracking the movement of visual target on center loading plate, shown in Figure 4-4. Because the loading plate had a 2 by 6 inch cross section, its elastic deformation during loading is negligible. However the bearing deformation of bushings was not small. Therefore, movement of the visual target was larger than the real shear deformation of the specimen bolt. The maximum load was taken as the double shear capacity of specimen bolt. The displacement at maximum load was calculated by subtracting the initial take up of the loading system from the displacement at maximum load as shown in Figure 4-4.
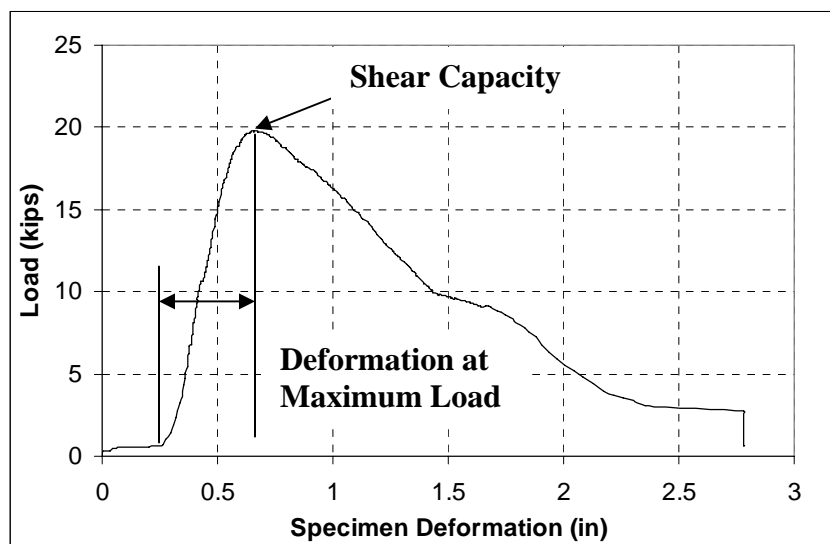
Figure 4-5 Load Deformation Curve of A490T800-2

## 4.3 A325 High Strength Bolts

Figure 4-6 shows all the sheared failure sections of A325 bolts at different temperature levels. At ambient temperature and 100°C, the shear failure sections are grey and shiny. The failure sections are flat but not smooth. The failures of the

bolt within this temperature range are very abrupt with little evidence of ductility. Because the test system is an open loop system, there was no control on the unloading rate; failure of specimen happens very fast (shorter than milliseconds) after reaching its maximum load capacity. In Figure 4-7 (a), load displacement curves of double shear tests on A325 bolts are shown. There is almost no unloading part on the load-displacement curves of tests at 25°C and 100°C. At 200°C, the failure section is very smooth and shiny, but not flat. The failure surface concaves on one segment and convexes on the other segment. The shear capacity of A325 bolt increases by about 10% at 200°C, compared with its shear capacity at 25°C. At 300°C, the failure surface of the bolt shows blue color. This is due to the oxidization of the steel at this temperature. Steel becomes more brittle but also stronger at this temperature, which is often called the blue brittle range. Comparing the load-displacement curves of double shear test at 25°C, 100°C, 200°C, and 300°C, bolt stiffness does not change much within this temperature range. At 400°C, the failure surface shows a combination of smooth part and rough texture. The load capacity and stiffness of A325 bolt both drops significantly at 400°C. Therefore 300°C (570°F) is a key temperature for A325 bolt. Below 300°C, there is no strength loss; while above 300°C, significant strength loss occurs. At temperatures from 500°C to 700°C, the strength and stiffness of A325 bolts decreases with increasing temperature, as shown in Figure 4-7 (b). As the temperature goes up, the steel becomes softer. Parallel abrasion marks are visible on the failure surfaces, which is an indication of the tearing failure that occurred and the high ductility of steel at these temperature levels. The large elongation and the unloading before failure provided large ductility at elevated temperature.

Shear strengths of A325 bolts at all temperature are shown in Figure 4-8. It is found that shear capacity of A325 bolts changed slightly under 300°C with

maximum value at 200˚C. Between 300˚C and 700˚C, shear capacity dropped dramatically with temperature. At 800˚C, the load capacity does not drop any more compared with the capacity of at 700˚C.

The test results are very consistent at most temperature levels except for room temperature. The first room temperature test had capacity of 50.65 kips, while the second test and third test produced higher strengths of 54.35 kips and 54.85 kips. The difference is explained by the accumulated plastic deformation of bushings used between the bolts and the loading clevises. The first room temperature test was performed when the bushings were brand new without any residual deformation, which produced a well defined set of shear planes. The second test and third test were performed after all the tests at elevated temperatures. The bushings had been softened by heat and deformed by load. The deformed bushings allowed the bolt to bend during the test. Figure 4-9 shows the middle failure segment of A325 bolts that were tested at room temperature. The small tails on the middle segment from Test 325T25-2 and Test 325T25-3 were signs of combined shear and tension. Figure 4-10 illustrates these bending effects. Using an un-deformed fixture, shear deformation is concentrated at the very short part of bolt shank, as shown in Figure 4-11 (a). Using a deformed fixture, the bolt is bent at beginning of loading until it conforms to the deformation of the bushings.  At this point shear deformation starts on the bent bolt shank. The final failure of the bolt is a combination of shear and tension failure. Because the shear strength of steel is only 60% of tensile strength, "shear" tests with deformed bushings produced higher apparent shear strengths.

54

(a) T=25°C (77°F)  (b) T=100°C (212°F)  (c) T=200°C (392°F)

(d) T=300°C (572°F)  (e) T=400°C (752°F)  (f) T=500°C (932°F)

(g) T=600°C (1112°F)  (h) T=700°C (1292°F)  (i) T=800°C (1472°F)
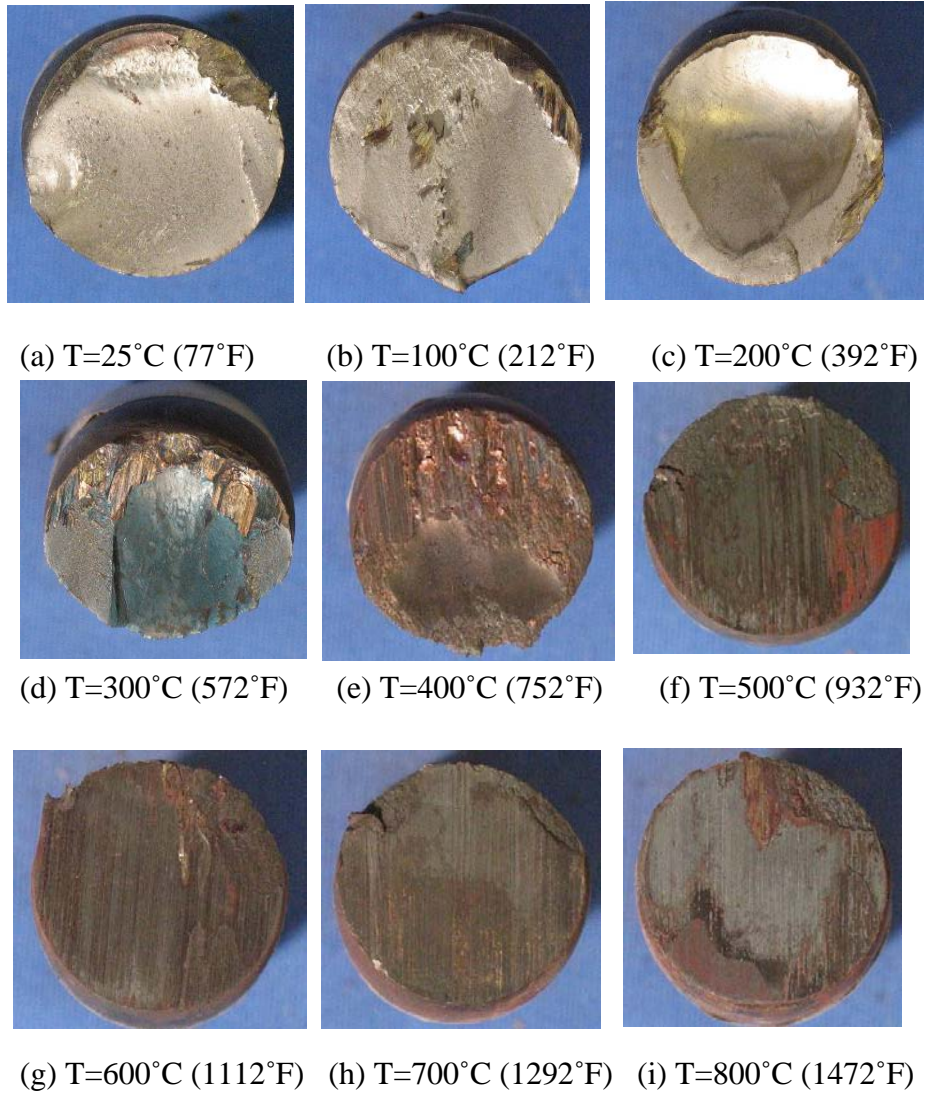
Figure 4-6 Failure Sections of A325 at Different Temperature Levels
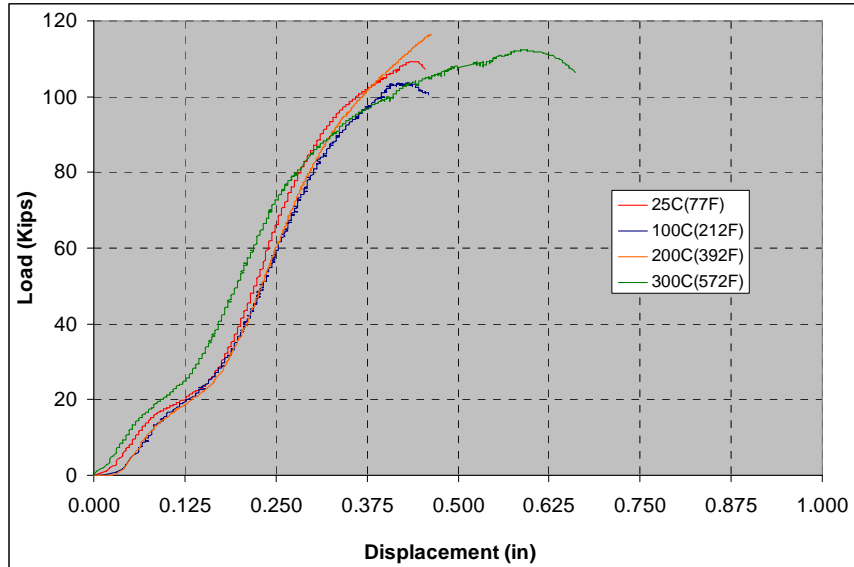
(a) 25°C to 300°C
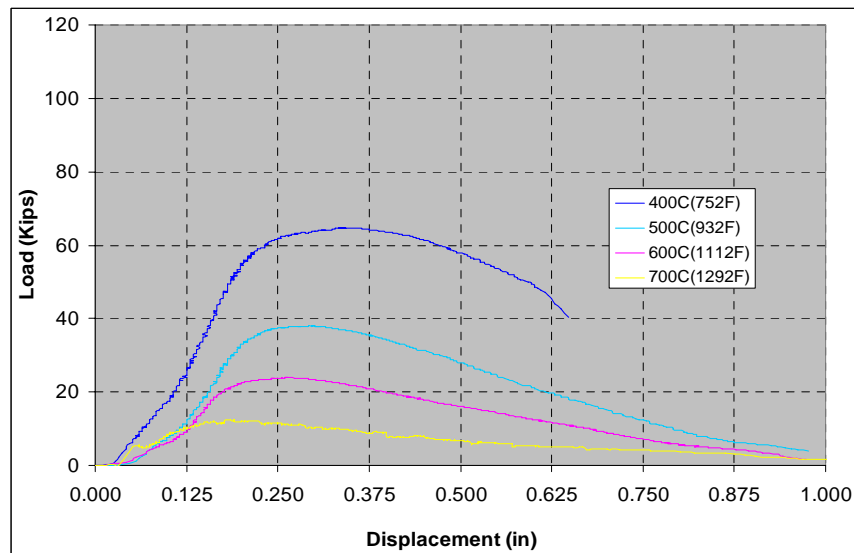


(b) 400°C to 700°C

Figure 4-7 Load Displacement Curves of Double Shear Tests on A325 Bolts

56
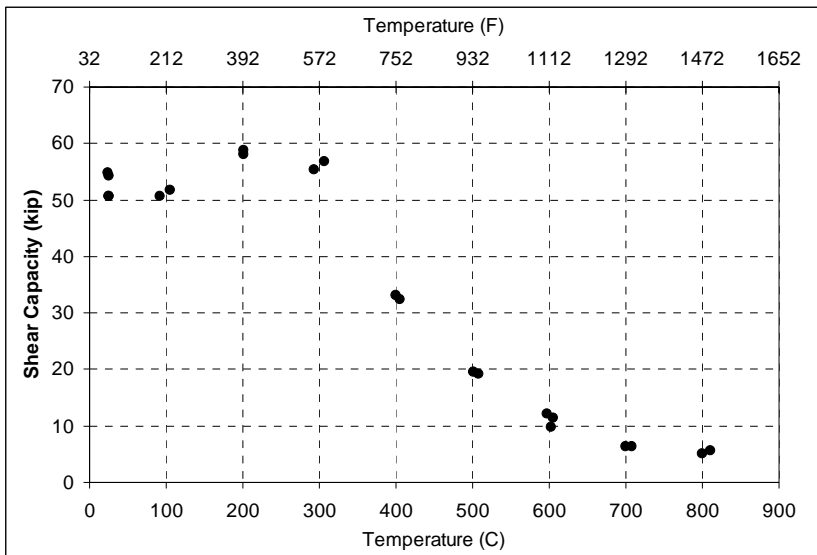
Figure 4-8 Shear Capacity of A325 Bolts at Different Temperature Levels



(a) Test 325T25-1



(b) Test 325T25-2



(c) Test 325T25-3
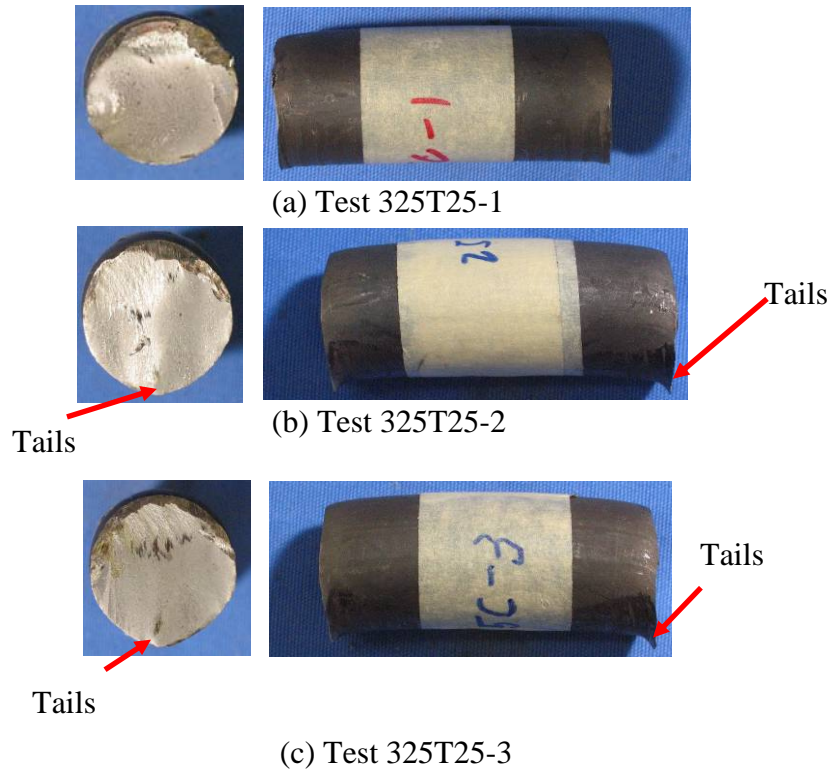
Figure 4-9 Middle Failure Segments of A325 Bolt Tested at 25˚C

57

(a)                                           (b)
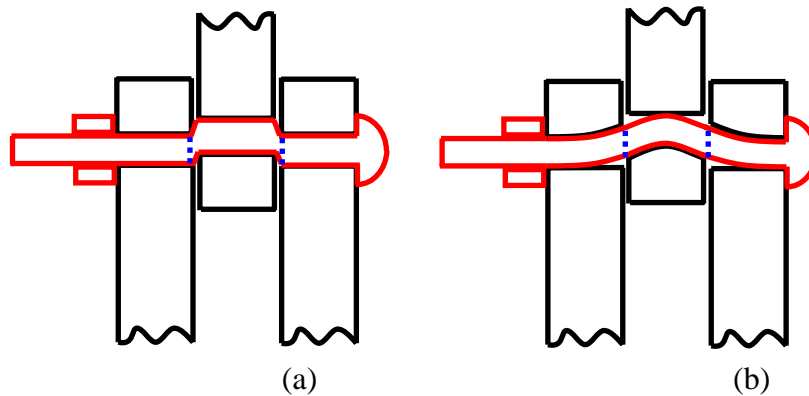
Figure 4-10 (a) Perfect Shear with Undeformed Fixture; (b) Shear and Tension Failure with Deformed Fixture;

**4.4 A490 High Strength Bolts**

As found in double shear tests on A325 bolts, deformation of bushings might affect the shear test results by introducing tension in bolt. New bushings were made with 4340 high strength steel for A490 bolt shear tests. In addition the test sequence was reversed starting with lower temperature tests followed by the higher temperature tests. This reduced the strength loss of bushings due to heat. Therefore A490 bolts were tested in a fixture providing a more distinct shear plane shear than the tests of A325 bolts.

Figure 4-11 shows all the shear failure sections of A490 bolts at different temperature levels. At 25°C, 100°C and 200°C, the failure sections are all shiny and smooth with small ripples. At 300°C, failure surface shows blue color again, which is due to oxidization of steel at this temperature. This indicates steel enters its blue brittleness range. At 400°C, the failure surface begins to be rough and shows light blue color. At 500° and 600°C, the failure surfaces are rough too. At 700°C and 800°C, the failure sections become smooth again with super large shear deformation and scratching lines. That proves the high ductility of steel under these temperature levels.

Figure 4-12 shows the shear capacity of A490 bolt at different temperatures. From 33°C to 300°C, shear capacity of A490 bolt drops by about 5% at 200°C first and then comes back at 300°C again. Beyond 300°C, shear capacity drops almost linearly with temperature. At 400°C, 500°C, 600°C and 700°C, the shear capacity drops by 17%, 40%, 65% and 85% respectively. From 700°C to 800°C, the shear capacity does not change much. Duplicate test results are very consistent at all temperature levels except 100°C. There were four tests performed at 100°C, which gave scattered results, from 50.2 kips to 64.0 kips. This phenomenon does not happen on tests at any other temperature level. Further study is needed to clarify the reason.

Figure 4-13 shows the load displacement curves at different temperatures. The stiffness of A490 bolts only decreases slightly in the temperature range of 33°C to 400°C; while from 400°C to 800°C, the stiffness drops significantly with temperature. From 33°C to 300°C, there is no unloading curve captured, which indicates very abrupt failure with little ductility. At 400°C unloading part occurs for the first time. From 500°C to 800°C, full unloading part is found. A490 bolts have great ductility in this temperature range.



Ripples          Ripples
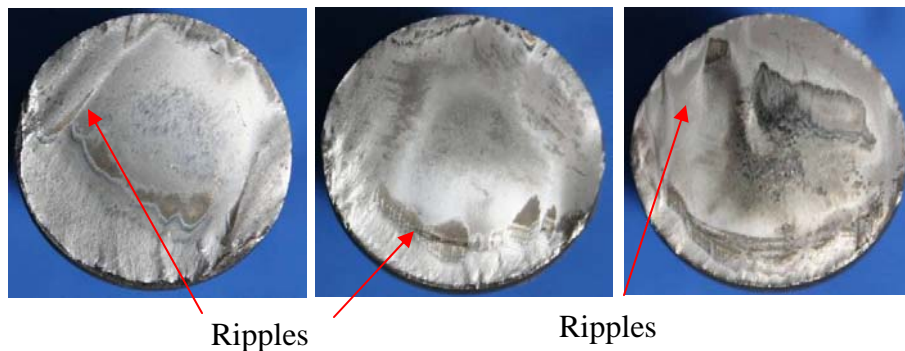
 (a) T=25°C (77°F)          (b) T=100°C (212°F)          (c) T=200°C (392°F)

Figure 4-11 Failure Sections of A490 at Different Temperature Levels (continued)
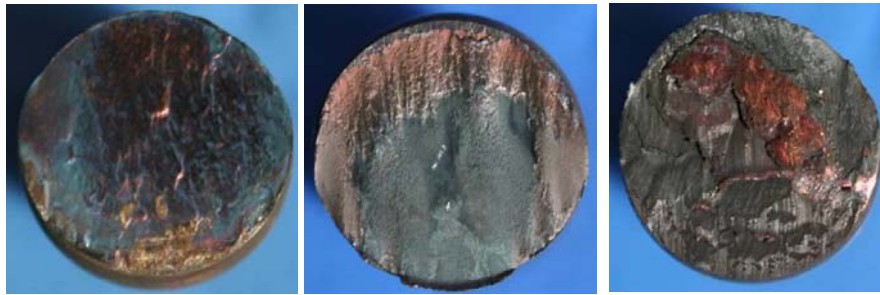
(d) T=300˚C (572˚F)    (e) T=400˚C (752˚F)    (f) T=500˚C (932˚F)



(g) T=600˚C (11    (h) T=700˚C (1292˚F)



(i) T=800˚C (1472˚F)

Figure 4-11 Failure Sections of A490 at Different Temperature Levels
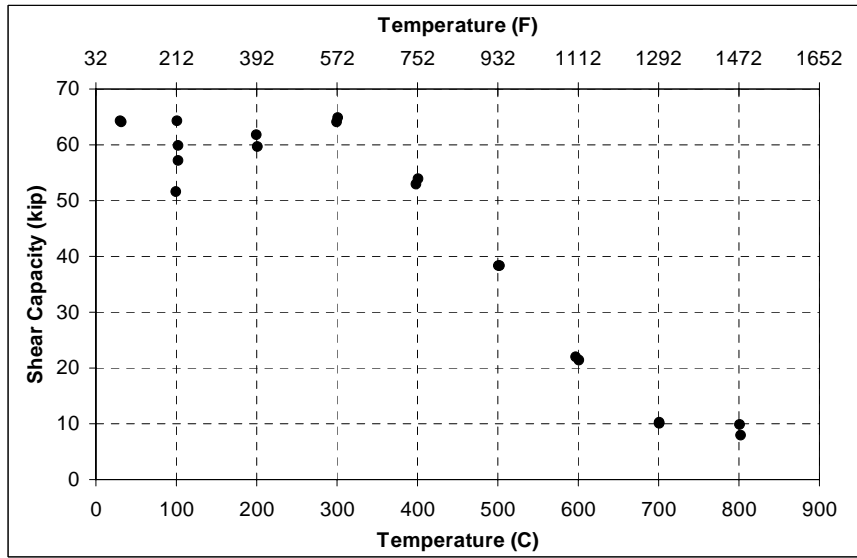
Figure 4-12 Shear Capacity of A490 at Different Temperature Levels
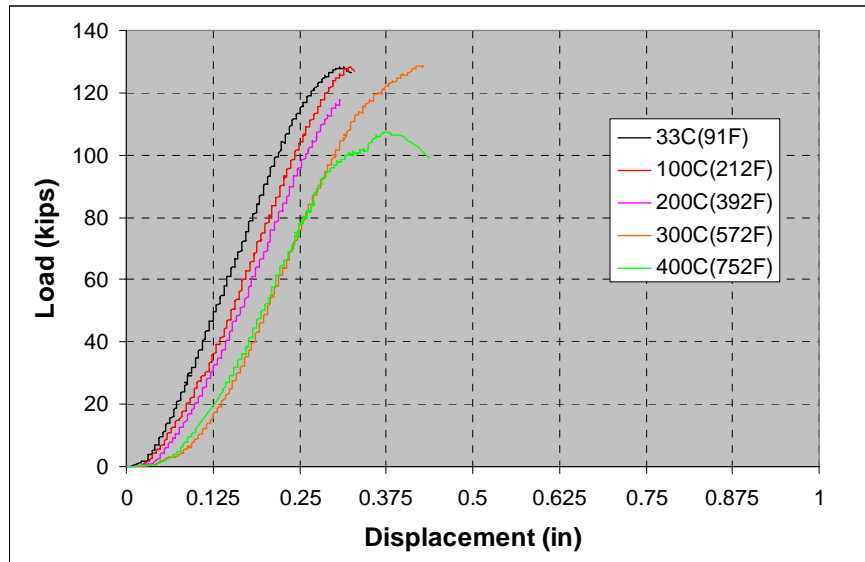


(a) 33˚C to 400˚C
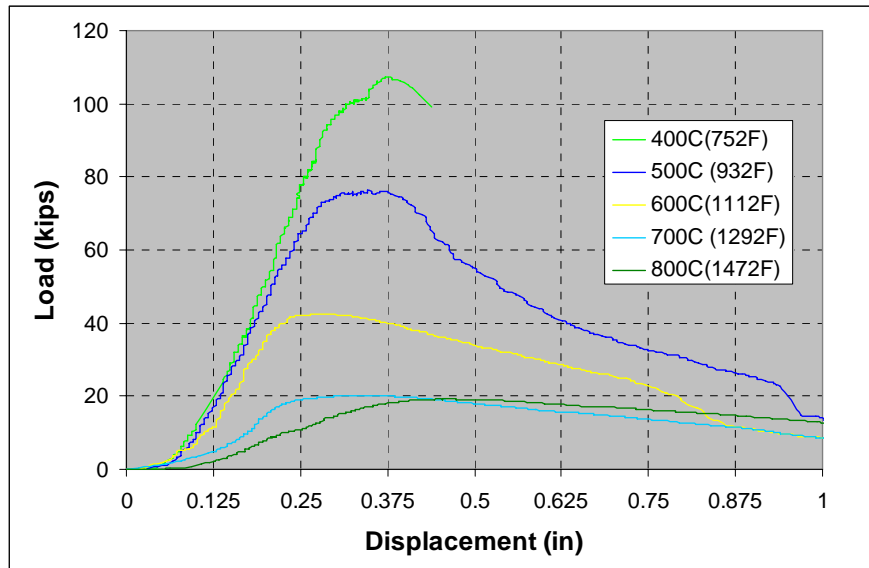
(b) 400˚C to 800˚C

Figure 4-13 Load Displacement Curves of Double Shear Tests on A490 Bolts

## 4.5 Comparison of A325 and A490 High Strength Bolts

Figure 4-14 shows the absolute shear capacity of 7/8 inch diameter A325 and A490 high strength bolts at all temperature levels. The behavior difference of A325 and A490 will be discussed in three ranges, ambient temperature to 300˚C, 300˚C to 700˚C, and 700˚C to 800˚C.

From ambient temperature up to 300˚C, A325 bolt shear capacity drops a little at 100˚C and then rises above its ambient temperature strength at 200˚C. The shear capacity drops back to the ambient temperature value at 300˚C. On the other hand, A490 bolt shear capacity drops slightly from ambient temperature at 200˚C, and then rises back at 300˚C. From 300˚C to 700˚C, the shear capacity of both bolts drops dramatically with an increase in temperature. The shear capacity of A490 bolts drops linearly from 64.0 kips at 300˚C to 10.2 kips at 700˚C, while shear capacity of A325 drops even faster with temperature from 56.0 kips at

300°C to 6.5 kips at 700°C. The difference in the shear capacity between the A325 and A490 bolts is only about 20 kips at ambient temperature, and increases to about 40 kips in the 400°C and 500°C. Between 700°C and 800°C, the shear capacity of the A325 and A490 bolts are almost identical and constant. The strength advantage of the A490 bolt over the A325 bolt gained through quenching and tempering depreciates when temperature is above 700°C.
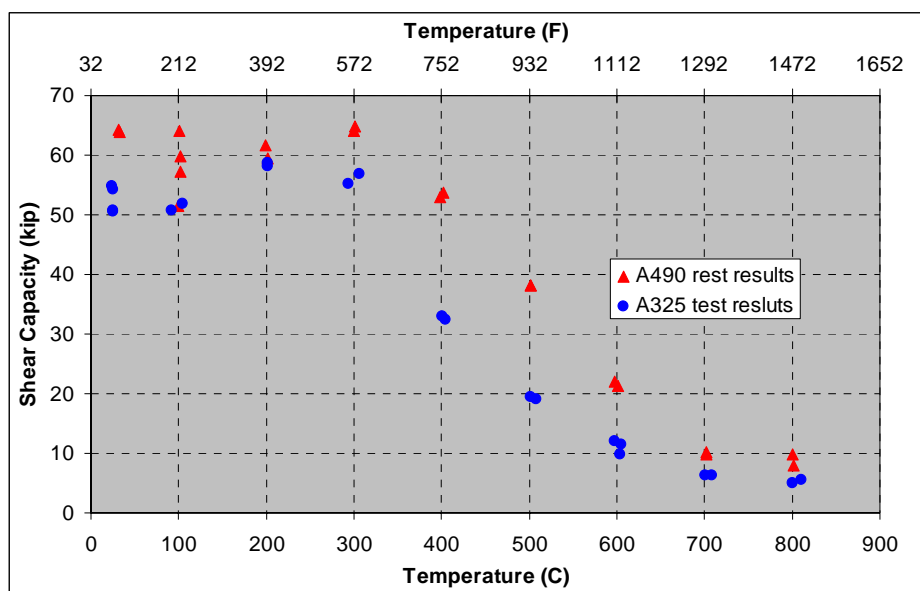


Figure 4-14 Shear Capacity of A325 and A490 Bolts at Different Temperature

Instead of comparing the absolute shear capacity, comparing shear strength relative to the room temperature capacity provides a better measure of a bolts ability to maintain its ambient temperature strength when it is exposed to elevated temperatures. The relative shear capacity, or normalized shear capacity, is defined as the ratio of the shear capacity at elevated temperature to the shear capacity at ambient temperature.
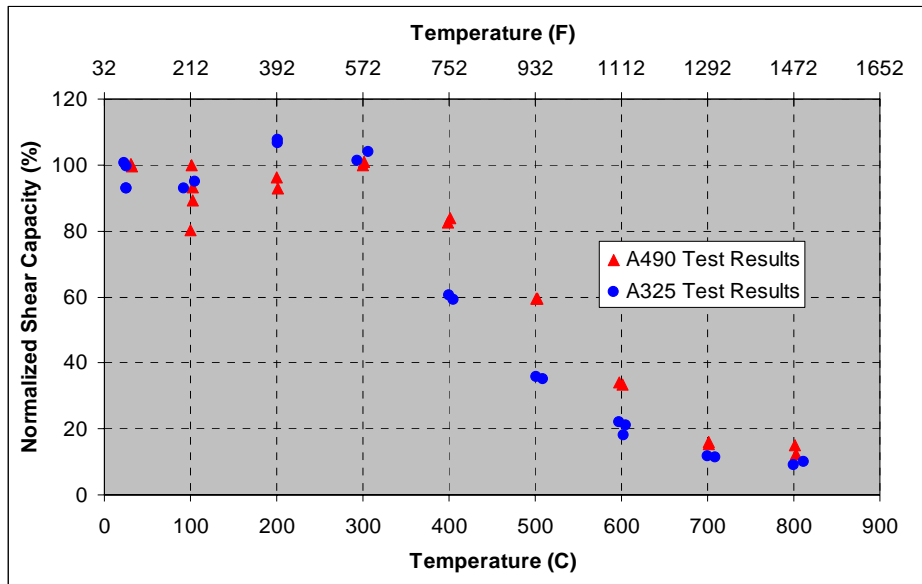
Figure 4-15 Normalized Shear Capacity of A325 and A490 Bolts at Different Temperature

Figure 4-15 shows the relative shear capacity of A325 and A490 bolts changes with temperature. It is found that between 300˚C and 600˚C, A490 bolt, compared with A325 bolt, maintains more of its strength at ambient temperature. The improved high temperature performance of the A490 bolt may be due to its higher molybdenum content of 0.18% versus the A325 bolt 0.01%. Molybdenum is the most important alloy element for steels which work under elevated temperature. It strongly increases the strength and creep resistance of steels in high temperature range because molybdenum introduces carbides. Besides this, molybdenum also increases the hardenability. Generally A325 and A490 bolt steel contains very limited amount of molybdenum, less than 0.2 %. That is one of the reasons why they have dramatic strength loss when they are exposed to temperature above 300˚C. For bolts used in a high temperature environment,

ASTM A193 requires a much larger amount of molybdenum, up to 3.00 %. From the hardness tests on the residual strength of A325 and A490 bolt, it was found that the tempering of A490 was 100°C higher than that of A325. The higher tempering temperature might be another reason for the better performance of the A490 bolt in the temperature range of 300°C to 600°C.

## 4.6 Comparison of A325 and A490 High Strength Bolts with Grade 8.8 M20 High Strength Bolts

B. R. Kirby performed a series double shear tests on M20 Grade 8.8 high strength bolt at elevated temperature levels (B. R. Kirby, 1995). Grade 8.8 high strength bolt is equivalent to A325 bolt. Two different heats of bolts, set A and set C, were tested. The chemical compositions of these two sets of bolts are given in Table 4-1.

Figure 4-16 shows the normalized shear capacity of A325, A490 and Grade 8.8 bolts. The bolt shear strength at elevated temperature is normalized to its shear strength at ambient temperature. It is found that A490 bolt behaves very similarly to Grade 8.8 bolts, while A325 bolt does not. From ambient temperature to 300°C, A490 bolt behaves in the same way as Grade 8.8 bolts, while A325 bolt shows a unique peak at 200°C. From 300°C to 600°C, A490 bolt performs a little bit better than Grade 8.8 bolt in keeping more percentage of its strength at ambient temperature. In the same temperature range, A325 bolt shows significant larger percentage of strength loss compared with other bolts. The difference in molybdenum contents between the bolts maybe the cause of this difference in elevated temperature strength. As discussed in 4.2.6, molybdenum introduced carbide can greatly increase steel strength at medium temperature range. The molybdenum contents of A490, Set C , Set A and A325 bolts are 0.180%, 0.130%, 0.027% and 0.010% separately, which correspond to the sequence of normalized

strength from high to low in the temperature range of 300°C to 800°C. At 700°C and 800°C, the normalized shear capacity of the four groups of bolts converged within 12% to 15%.　When designing bolted connections to work under elevated temperature, a strength reduction factor is used to assess bolt strength at that temperature. Figure 4-16 shows that different reduction factors are needed for the A325 and A490 bolts tested. More test data is needed before general conclusion can be drawn about the shear strength reduction factors of A325 and A490 bolts. Future discussion will be presented in chapter 6.
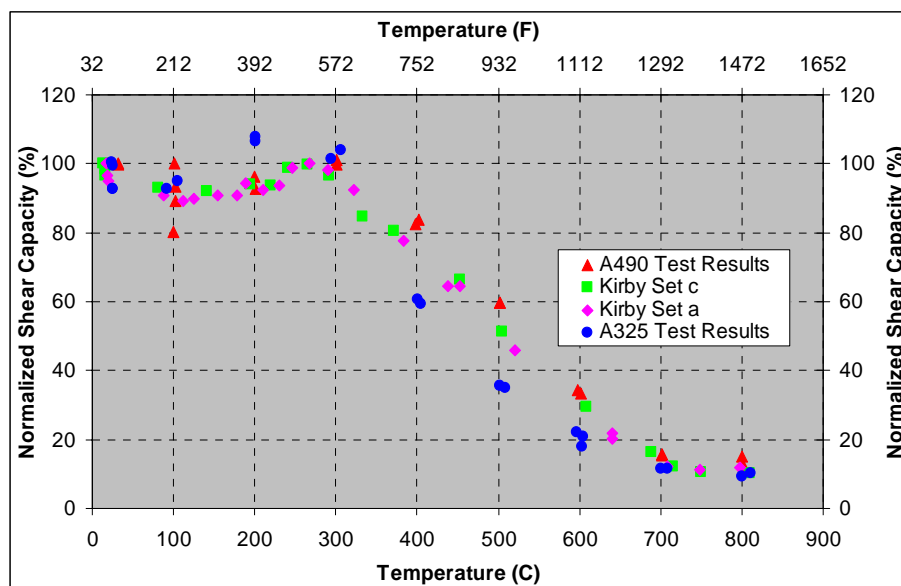


Figure 4-16 Normalized Shear Capacity of Bolts at Different Temperature

# Chapter 5

# Post Fire Residual Shear Strength of Connections

The residual strength of A325 and A490 bolts after exposure to elevated temperatures was studied by direct shear test and estimated from hardness tests. Slip load tests were performed on A490 bolted connections, which had been heated at elevated temperature and cooled to ambient temperature to determine their post fire slip resistance. The test method had been described in chapter 3, 3.3.5.

## 5.1 Single Shear Test Results

After double shear tests at elevated temperature, the bolts were cooled back to ambient temperature. Single shear test on the untested segment of the tested bolts with shear plane away from former shear failure section were performed to determine the post fire strength of the fasteners.

After double shear tests at elevated temperature, the bolts were cooled back to ambient temperature. Exercising a single shear test on the untested segments of previously tested bolts, determined the post fire strength of the fasteners. This shear test was performed with the shear plane apart from the formerly sheared failure section.

These tests were named using the following order:

Bolt type + Double shear test temperature + The sequence number of that test at that temperature + The letter S, which stands for Single shear test.

For example, 325T700-2S was an A325 bolt tested at a temperature of 700°C, the second test in a series of single shear tests. The bolt used in this single shear test had been previously double shear tested at 700°C. Table 5-1 gives the post fire single shear test results of A325 and A490 bolts.

67

Table 5-1 Post Fire Single Shear Test Results of A325 and A490 Bolts

| | A325 Bolts | | | | A490 Bolts | | |
|---|---|---|---|---|---|---|---|
| Test Name | Maximum Exposure Temperature | | Residual Single Shear Capacity | Test Name | Maximum Exposure Temperature | | Residual Single Shear Capacity |
| | ˚F | ˚C | (kips) | | ˚F | ˚C | (kips) |
| 325T25-1S | 77 | 25 | 49.9 | 490T25-1S | 88 | 31 | 62.8 |
| 325T25-2S | 77 | 25 | 50.3 | 490T25-2S | 90 | 32 | 63.7 |
| 325T25-3S | 75 | 24 | 50.5 | 490T100-1S | 212 | 100 | 61.9 |
| 325T100-1S | 197 | 92 | 50.3 | 490T100-2S | 216 | 102 | 61.5 |
| 325T100-2S | 221 | 105 | 50.3 | 490T100-3S | 213 | 101 | 62.8 |
| 325T200-1S | 394 | 201 | 51.6 | 490T100-4S | 216 | 103 | 60.9 |
| 325T200-2S | 395 | 202 | 50.5 | 490T200-1S | 391 | 199 | 61.7 |
| 325T300-1S | 561 | 294 | 51.6 | 490T200-2S | 394 | 201 | 61.3 |
| 325T300-2S | 583 | 306 | 49.4 | 490T300-1S | 574 | 301 | 61.7 |
| 325T400-1S | 753 | 401 | 48 | 490T300-2S | 573 | 300 | 62.4 |
| 325T400-2S | 761 | 405 | 50 | 490T400-1S | 755 | 402 | 61.8 |
| 325T500-1S | 935 | 502 | 44.7 | 490T400-2S | 749 | 398 | 61.2 |
| 325T500-2S | 947 | 509 | 46.4 | 490T500-1S | 935 | 501 | 61.3 |
| 325T600-2S | 1107 | 597 | 42.7 | 490T500-2S | 936 | 502 | 62.2 |
| 325T600-3S | 1118 | 603 | 38.5 | 490T600-1S | 1115 | 601 | 50.7 |
| 325T600-1S | 1121 | 605 | 41 | 490T600-2S | 1108 | 598 | 50.6 |
| 325T700-1S | 1293 | 701 | 33.5 | 490T700-1S | 1295 | 702 | 43.1 |
| 325T700-2S | 1307 | 709 | 34.1 | 490T700-2S | 1295 | 702 | 41.3 |
| 325T800-2S | 1472 | 800 | 29.2 | 490T800-1S | 1476 | 802 | 36.4 |
| 325T800-1S | 1483 | 806 | 29.3 | 490T800-2S | 1473 | 801 | 36.6 |
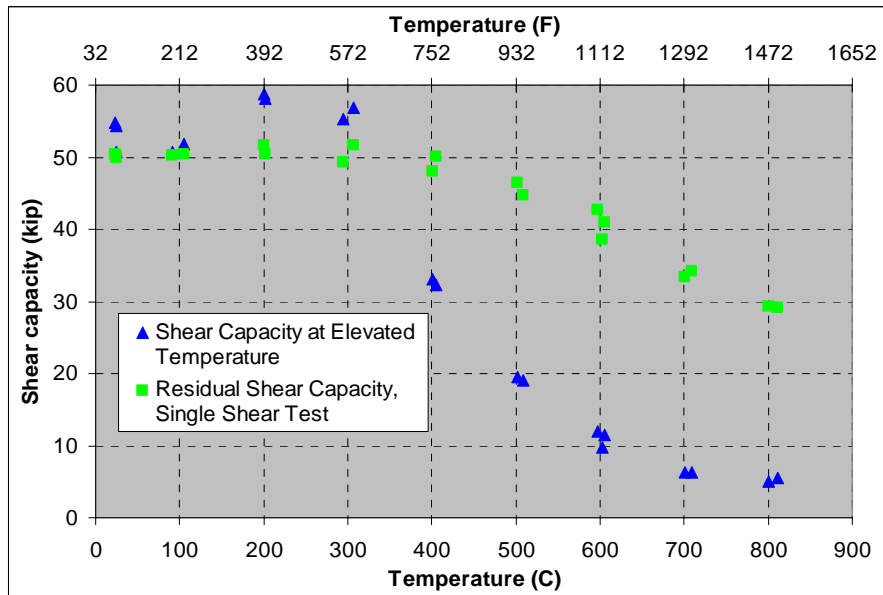
Figure 5-1 Elevated Temperature and Residual Shear Capacity of A325 Bolts
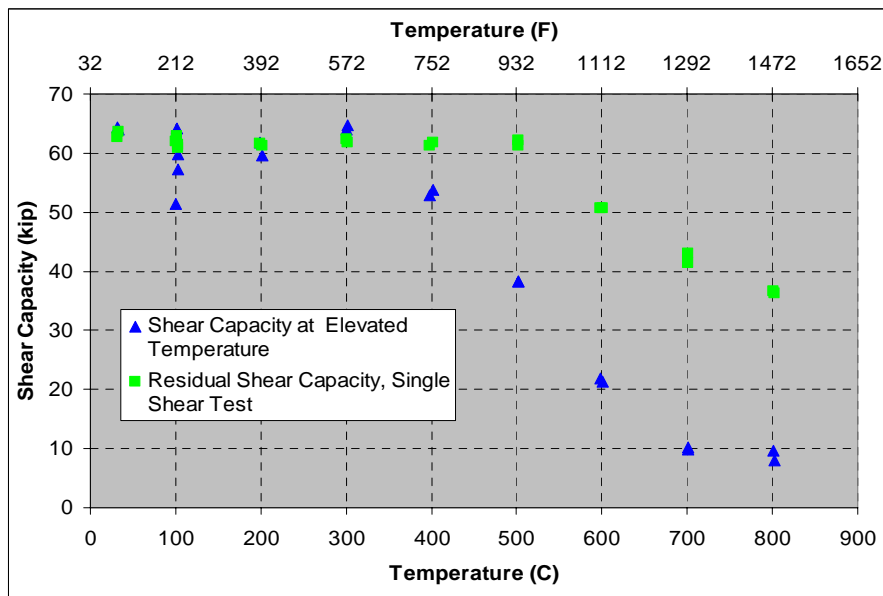


Figure 5-2 Elevated Temperature and Residual Shear Capacity of A490 Bolts

Figure 5-1 compares the residual shear capacity of A325 bolts with their shear capacity at corresponding elevated temperature levels. The test shows that if an A325 bolt is exposed to a temperature lower than 400°C, the bolt strength is fully recovered after cooling back to ambient temperature. If the bolt was exposed to a temperature higher than 400°C, then the bolt loses some of its original strength. The A325 bolt strength loss increased linearly with the maximum temperature between 400°C and 800°C. The loss in strength was up to about 45% after the bolt was exposed to 800°C. It is very interesting that the shear strength at elevated temperatures of 200°C and 300°C are higher than the corresponding residual shear strength. The reason could be the steel microstructure changes in the blue brittle temperature range. This microstructure change may increase steel strength and decrease ductility (R W K Honeycombe, 1981). Chemical composition of steel plays a key role in this phenomenon. Different steels might show different behavior in this temperature range. The A490 bolts tested exhibited a different behavior. The shear capacity from double shear tests at room temperature should be the same as its residual shear capacity from single shear test since the bolt was not exposed to elevated temperature. In Figure 5-1, the residual shear capacities from singles shear test on the three bolts were close to that from double shear tests with un-deformed bushings, specimen 325T25-1. The high shear capacities from double shear tests 325T25-2 and 325T25-3 (Table 4-3) were not supported by their residual shear capacities from 325T25-2S and 325T25-3S. Because the bolt segment in the single shear test had no nut, there was no tension force in the bolt during test. This data support the contention that shear test with deformed bushings gives higher shear strength by causing the bolt to fail in shear and tension.

Figure 5-2 gives the residual shear capacity of A490 bolts along with their shear capacity at corresponding temperature levels. A490 bolts behaved

differently from A325 bolts. From ambient temperature to 300˚C, A490 bolts had similar strength both at elevated temperature and after heating to that temperature and then cooling down to room temperature. Another significant difference between A325 bolt and A490 bolt was the temperature, at which it started to lose strength. The A490 bolt kept its original strength up to temperature of 500˚C. Above 500˚C, A490 bolt lost its strength linearly as the previous exposure temperature increased. It underwent about a reduction of 60% of room temperature strength after exposure to 800˚C.

## 5.2 Hardness Test Results

Hardness test is a very convenient way to estimate the tensile strength of steel. In assessing the strength left in post fire steel structures, this could be an economical method to investigate residual bolt strength after a fire. The process involves using hardness measurements to estimate the tensile strength of the fastener. The tensile strength was estimated using Table 2 and Table 3 in ASTM A370–03a. The shear strength was estimated by multiplying the estimated tensile by 0.6 to approximate the shear strength of the fastener and then multiplying by the gross area of the bolt. The results were compared with single shear test results.

Rockwell hardness tests were performed on a 7/8 inch long bolt segment which was cut from the opposite end of the bolt from where the single shear tests were taken. After machining and grinding the cross section surfaces, hardness tests were performed in accordance with ASTM E18-03.  Both type B and type C hardness scales were used to stay within the established ranges of each scale, 20 and above for the C scale and 100 and below of the B scale. These hardness tests were named as bolt type plus double shear test temperature plus number of test at this temperature plus H, which stands for hardness test. For example, 490T500-

2H is the hardness test on the bolt failure segment from the number 2 A490 bolt tested at 500°C.

In manufacture process, bolts gain their strength through quenching. Because the surface cools faster than the core, tensile strength varies across bolt section. Therefore hardness tests were performed at different locations on the bolt section in order to survey the magnitude of difference. Table 5-2 and Table 5-3 give the hardness test results of the unheated bolts, 325T25-1H and 490T25-1H. "R" in the Tables refers to the radius of the bolt. The readings were taken at 1/4 R increments from the center of the bolt. Four readings were taken equally spaced around the whole circle at each of these radial locations. The A325 bolt had an average HRC 27.9 at core and HRC 30.6 at ¾ R. That is a significant difference. The A490 bolt was hardened more uniformly than A325 bolt, less than one point difference between the center and the ¾ R locations. A weighted hardness value was calculated based on the area of the annulus as shown in the equations below. Figure 5-3 shows the layout of hardness tests locations on the bolt section and a tested section.

Table 5-2 Hardness Test Result of 325T25-1H

| Location | Hardness Value (HRC) | | | | | Weight Coefficient | Weighted Average |
| | Test | | | | Average | | |
| | 1 | 2 | 3 | 4 | | | |
|---|---|---|---|---|---|---|---|
| Center(0) | 27.9 | N/A | N/A | N/A | 27.9 | 1/64 | |
| ¼ R (1) | 29.8 | 29.5 | 28.1 | 29.0 | 29.1 | 8/64 | 30.2 |
| ½ R (2) | 30.0 | 31.4 | 29.0 | 29.6 | 30.0 | 16/64 | |
| ¾ R (3) | 30.5 | 30.8 | 30.7 | 30.4 | 30.6 | 39/64 | |

Table 5-3 Hardness Test Result of 490T25-1H

| Location | Hardness Value (HRC) | | | | | Weight Coefficient | Weighted Average |
|----------|------|------|------|------|---------|--------------------|------------------|
| | Test | | | | Average | | |
| | 1 | 2 | 3 | 4 | | | |
| Center(0) | 35.3 | N/A | N/A | N/A | 35.3 | 1/64 | 36.4 |
| ¼ R (1) | 35.8 | 36.4 | 35.9 | 36.1 | 36.1 | 8/64 | |
| ½ R (2) | 36.9 | 36.5 | 36.9 | 37 | 36.8 | 16/64 | |
| ¾ R (3) | 36.2 | 36.2 | 36.5 | 36.6 | 36.4 | 39/64 | |

Weight Coefficient:

$$\text{Center: } C_0 = \frac{\pi(1/8)^2 R^2}{\pi R^2} = 1/64$$

$$\text{¼ R: } C_1 = \frac{\pi\left[(3/8)^2 - (1/8)^2\right]R^2}{\pi R^2} = 8/64$$

$$\text{½ R: } C_2 = \frac{\pi\left[(5/8)^2 - (3/8)^2\right]R^2}{\pi R^2} = 16/64$$

$$\text{¾ R: } C_3 = \frac{\pi\left[(8/8)^2 - (5/8)^2\right]R^2}{\pi R^2} = 39/64$$

R = the radius of bolt.
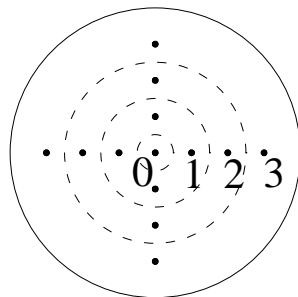


Figure 5-3 Layout of Hardness Test Points on Bolt Section and Tested Bolt Segment

Table 5-4 and Table 5-5 give the hardness test results of A325 and A490. Area weighted hardness values were used to determine estimated tensile strength and calculated shear capacity. The average hardness values at 1/2R location are also shown for comparison. In general the average 1/2R values agree with the hardness calculated using the weighted average.

Figure 5-4 and Figure 5-5 show the estimated residual shear capacity of A325 and A490 bolts based upon area weighted hardness and 1/2R hardness along with the results from single shear tests. For both types of bolts, the estimated shear capacity agrees with direct single shear test results well from ambient temperature to 600˚C. Estimated shear capacity was conservative, compared with shear test results, at 700˚C and 800˚C. The difference between estimated shear capacity from hardness tests and shear test result got larger as the shear strength became lower. That is because when bolt was softened, due to being soaked in temperature higher than its tempering temperature, the shear failure plane was not flat as what we assumed. In Figure 5-6 (a), shear planes of 32525T-2S and 325T400-1S were flat; while in Figure 5-6 (b), double layered shear planes were found on the failure section of 325T700-2S and 325T800-2S. That might generate the error in using hardness test to estimate the shear capacity since the area was taken as a constant in estimating the shear strength. For both types of bolt, the hardness value at 1/2R position provided a good estimation of the area weighted hardness value for the whole section. Therefore it is not necessary to perform all the hardness tests on bolt section to assess the residual strength of bolt post fire.
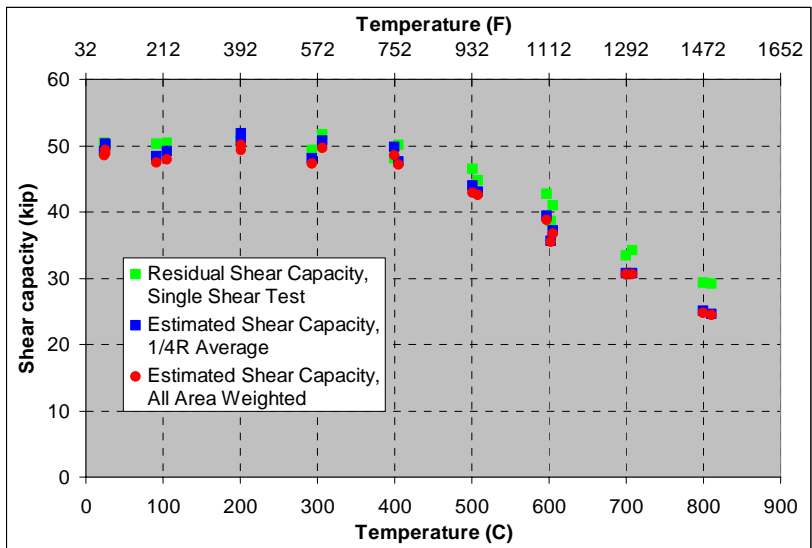
Figure 5-4 Estimated Residual Shear Capacity of A325 Bolt
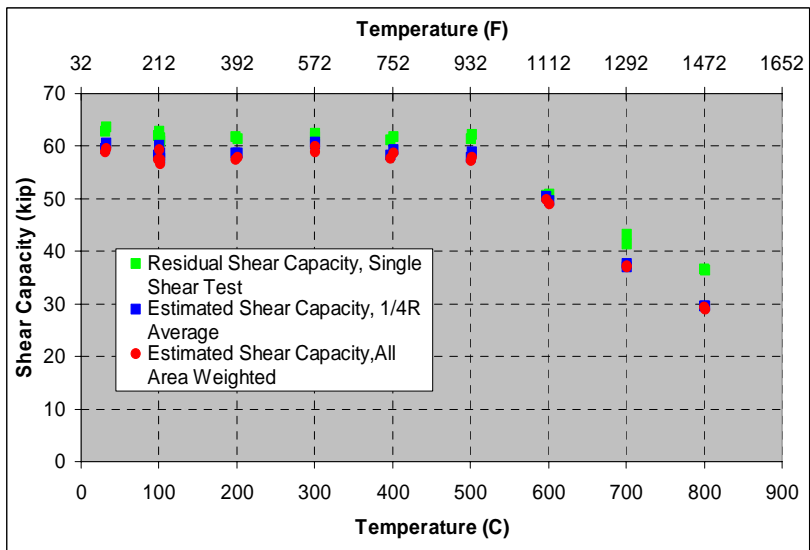


Figure 5-5 Estimated Residual Shear Capacity of A490 Bolt

(a) A325T25-2S (right);
A325T400-1S (left);

Secondary shear plane

(b) A325T700-2S (left);
A325T800-2S (right);

Major shear plane
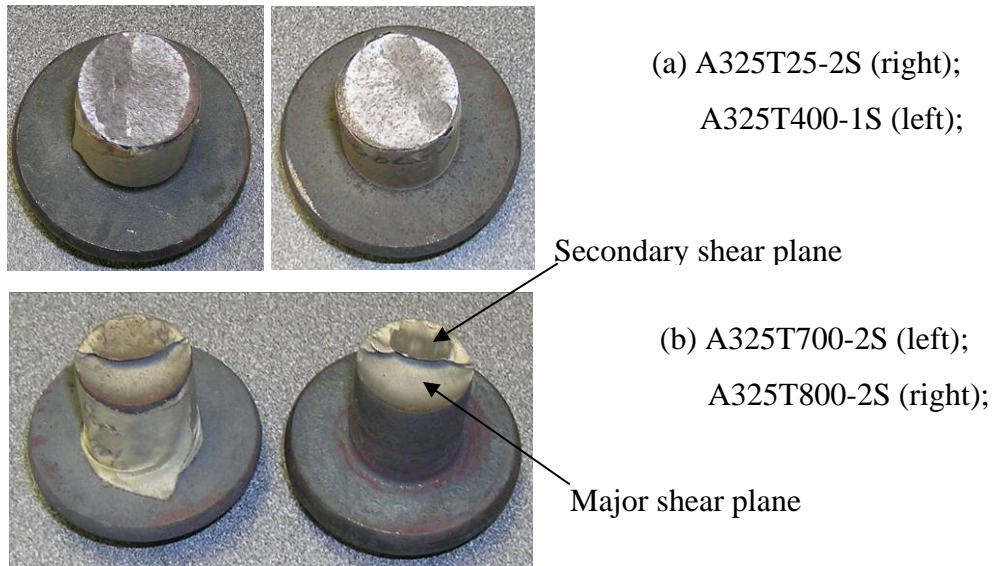
Figure 5-6 Rockwell hardness tests points on each bolt section

## 5.3 Tempering Temperature

Tempering temperature during the manufacturing process is a key variable in determining the residual strength of a bolt after a fire. The bolt lost strength only after it was exposed to a temperature higher than its tempering temperature. Unfortunately the tempering temperature of a high strength bolt is normally not reported in the mill report from the manufacturer. One way to find out the tempering temperature is to cut a bolt into several segments and heat them to different temperatures and measure the hardness of the bolts after heating. A plot of the hardness of each segment against temperature that it experienced provides a means of estimating the tempering temperature. Because reduction in hardness will occur above the tempering temperature, the tempering temperature is where the bolt hardness starts to reduce. All the bolts in each type are from the same heat, which means they were tempered at the same temperature.

Table 5-4 Hardness Test Results of A325 bolts

| Test Name | Maximum Exposure Temperature | | Average Hardness Value at ½ R | Area Weighted Rockwell Hardness Value | Estimated Tensile Strength (ksi) | Estimated Shear Capacity (kips) |
|---|---|---|---|---|---|---|
| | ˚F | ˚C | | | | |
| 325T25-1(S,H) | 77 | 25 | 30.3 (HRC) | 30.1 (HRC) | 136.6 | 49.3 |
| 325T25-2(S,H) | 77 | 25 | 30.4 (HRC) | 30.2 (HRC) | 135.5 | 48.9 |
| 325T25-3(S,H) | 75 | 24 | 29.4 (HRC) | 29.9 (HRC) | 134.4 | 48.5 |
| 325T100-1(S,H) | 197 | 92 | 28.7 (HRC) | 29.3 (HRC) | 131.2 | 47.4 |
| 325T100-2(S,H) | 221 | 105 | 29.4 (HRC) | 29.9 (HRC) | 132.9 | 48 |
| 325T200-1(S,H) | 394 | 201 | 31.5 (HRC) | 30.8 (HRC) | 138.9 | 50.1 |
| 325T200-2(S,H) | 395 | 202 | 30.7 (HRC) | 30.3 (HRC) | 136.8 | 49.4 |
| 325T300-1(S,H) | 561 | 294 | 30.8 (HRC) | 30.5 (HRC) | 137.3 | 49.6 |
| 325T300-2(S,H) | 583 | 306 | 28.6 (HRC) | 29.2 (HRC) | 131.1 | 47.3 |
| 325T400-1(S,H) | 753 | 401 | 30.0 (HRC) | 29.7 (HRC) | 134.3 | 48.5 |
| 325T400-2(S,H) | 761 | 405 | 28.3 (HRC) | 28.8 (HRC) | 130.5 | 47.1 |
| 325T500-1(S,H) | 935 | 502 | 24.0 (HRC) | 24.5 (HRC) | 118.1 | 42.6 |
| 325T500-2(S,H) | 947 | 509 | 24.7 (HRC) | 24.5 (HRC) | 118.9 | 42.9 |
| 325T600-2(S,H) | 1107 | 597 | 98.1 (HRB) | 98.3 (HRB) | 107.5 | 38.8 |
| 325T600-3(S,H) | 1118 | 603 | 94.4 (HRB) | 94.2 (HRB) | 98.3 | 35.5 |
| 325T600-1(S,H) | 1121 | 605 | 96.6 (HRB) | 96.9 (HRB) | 101.9 | 36.8 |
| 325T700-1(S,H) | 1293 | 701 | 87.6 (HRB) | 87.5 (HRB) | 84.5 | 30.5 |
| 325T700-2(S,H) | 1307 | 709 | 87.6 (HRB) | 87.6 (HRB) | 84.5 | 30.5 |
| 325T800-2(S,H) | 1472 | 800 | 77.1 (HRB) | 77.1 (HRB) | 67.6 | 24.4 |
| 325T800-1(S,H) | 1483 | 806 | 78.3 (HRB) | 77.9 (HRB) | 68.5 | 24.7 |

Table 5-5 Hardness Test Results of A490 bolt

| Test Name | Maximum Exposure Temperature | | Average Hardness Value at ½ R | Area Weighted Rockwell Hardness Value | Estimated Tensile Strength (ksi) | Estimated Shear Capacity (kips) |
|---|---|---|---|---|---|---|
| | ˚F | ˚C | | | | |
| 490T25-1(S,H) | 88 | 31 | 36.8 (HRC) | 36.4 (HRC) | 58.9 | 163.3 |
| 490T25-2(S,H) | 90 | 32 | 37.3 (HRC) | 36.8 (HRC) | 59.6 | 165.1 |
| 490T100-1(S,H) | 212 | 100 | 36.1 (HRC) | 35.6 (HRC) | 57.4 | 159.1 |
| 490T100-2(S,H) | 216 | 102 | 36.3 (HRC) | 35.6 (HRC) | 57.4 | 159.0 |
| 490T100-3(S,H) | 213 | 101 | 37.1 (HRC) | 36.6 (HRC) | 59.2 | 164.1 |
| 490T100-4(S,H) | 216 | 103 | 35.7 (HRC) | 35.2 (HRC) | 56.7 | 157.0 |
| 490T200-1(S,H) | 391 | 199 | 35.3 (HRC) | 35.6 (HRC) | 57.4 | 159.0 |
| 490T200-2(S,H) | 394 | 201 | 36.3 (HRC) | 35.9 (HRC) | 57.9 | 160.5 |
| 490T300-1(S,H) | 574 | 301 | 37.3 (HRC) | 36.4 (HRC) | 58.9 | 163.3 |
| 490T300-2(S,H) | 573 | 300 | 37.5 (HRC) | 37.0 (HRC) | 60.0 | 166.2 |
| 490T400-1(S,H) | 755 | 402 | 36.6 (HRC) | 36.3 (HRC) | 58.6 | 162.4 |
| 490T400-2(S,H) | 749 | 398 | 36.1 (HRC) | 35.8 (HRC) | 57.7 | 159.8 |
| 490T500-1(S,H) | 935 | 501 | 35.9 (HRC) | 35.6 (HRC) | 57.3 | 158.8 |
| 490T500-2(S,H) | 936 | 502 | 36.5 (HRC) | 35.9 (HRC) | 57.9 | 160.5 |
| 490T600-1(S,H) | 1115 | 601 | 29.9 (HRC) | 29.2 (HRC) | 48.9 | 135.5 |
| 490T600-2(S,H) | 1108 | 598 | 30.5 (HRC) | 30.0 (HRC) | 49.9 | 138.2 |
| 490T700-1(S,H) | 1295 | 702 | 97.1 (HRB) | 96.6 (HRB) | 37.3 | 103.2 |
| 490T700-2(S,H) | 1295 | 702 | 96.2 (HRB) | 96.1 (HRB) | 36.9 | 102.3 |
| 490T800-1(S,H) | 1476 | 802 | 84.6 (HRB) | 83.3 (HRB) | 28.9 | 80.1 |
| 490T800-2(S,H) | 1473 | 801 | 84.9 (HRB) | 84.1 (HRB) | 29.2 | 80.9 |
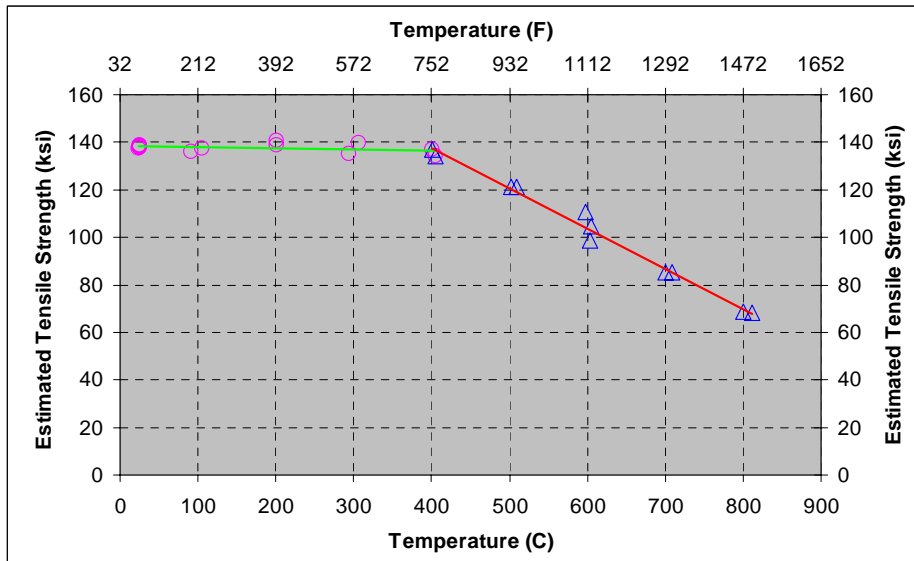
Figure 5-7 Hardness Estimates of the Tempering Temperature of A325 Bolt
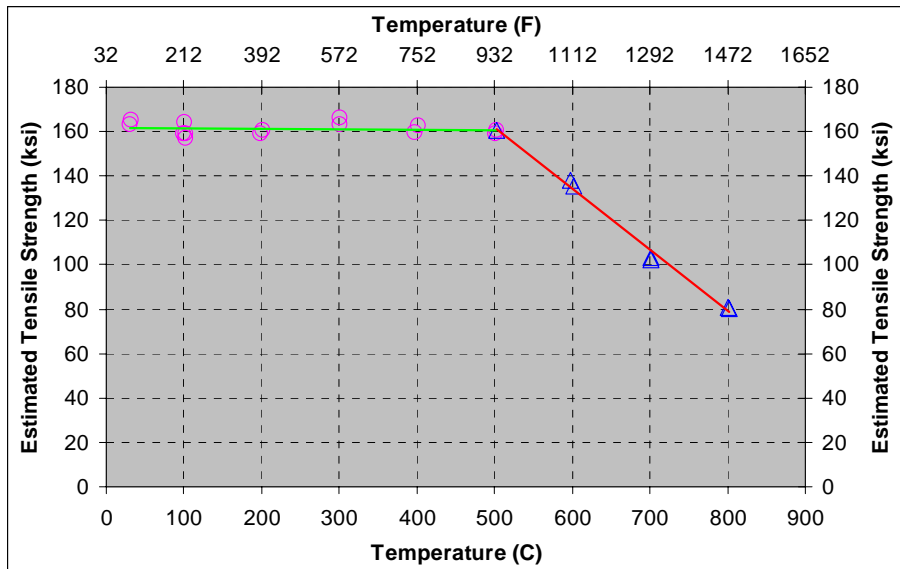


Figure 5-8 Hardness Estimates of the Tempering Temperature of A490 Bolt

Therefore the tempering temperature can be found by plotting the hardness of each bolt after double shear test at elevated temperature. The area weighted average hardness was used here. Because the hardness results involved both HRC and HRB scale, tensile strength was used instead of hardness numbers. The estimated tensile strength of A325 and A490 bolts are shown in Figure 5-7 and Figure 5-8. The data indicates the A325 bolts were tempered at 400°C and the A490 bolts were tempered at 500°C.

**5.4 Effect of Heating Time on Bolt Residual Strength**

In real fire event, the duration of a fire varies depending on fuel load, oxygen supply, and many other factors. Therefore structure members will undergo different time-temperature histories. A series of tests were undertaken to study if the longer time that a bolt was exposed to elevated temperature would result in further strength loss. As discussed above, the bolt has to be exposed to a temperature higher than tempering temperature in order to have a significant loss of strength. The tests were undertaken at a temperature above the estimated tempering temperatures. Two A325 bolt were cut into 5 segments each and exposed to 600°C for different lengths of time. After being cooled back to ambient temperature in room air (about 30°C/85°F), hardness tests were performed. The estimated tensile strength based upon the area weighted hardness versus the length of time that it was kept at 600°C is listed in Table 5-6 and plotted in Figure 5-9.

The results in Table 5-6 and Figure 5-9 show that an additional 330 minutes (5.5 hours) of exposure at 600°C (1112°F) results in about 10% reduction in tensile strength for these A325 bolts. The results also vary from bolt to bolt, even though they are from the same manufacture heat. Bolt #1 shows no strength

loss after 240 minutes, while Bolt #2 shows no change in strength from 120 minutes to 180 minutes but loses another 3% from 240 minutes to 360 minutes.
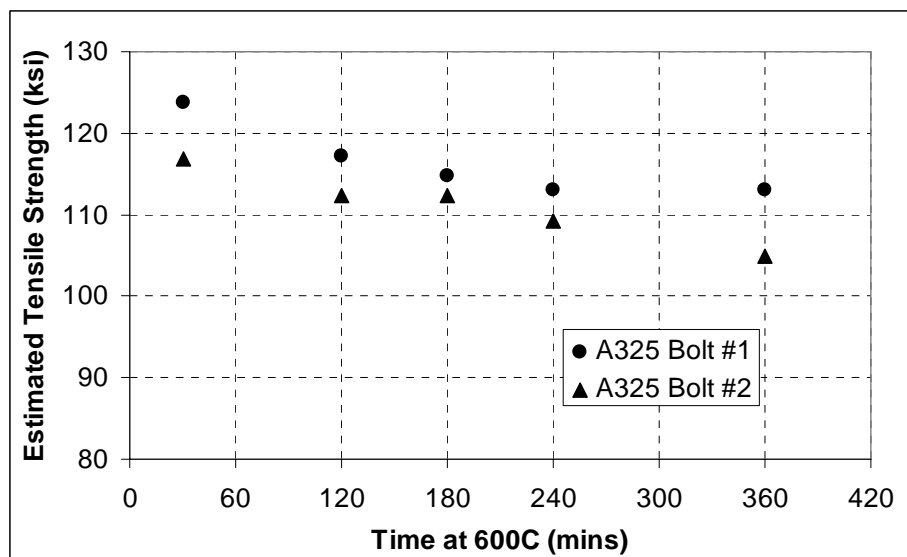


Figure 5-9 Estimated Tensile Strength vs. Heat Time

Table 5-6 Influence of Heating Time on Estimated Residual Tensile Strength of A325 Bolts

| Estimated Residual | Time at 600°C (1112°F) (minutes) | | | | |
|---|---|---|---|---|---|
| Tensile Strength (ksi) | 30 | 120 | 180 | 240 | 360 |
| A325 Bolt #1 | 123.7 | 117.2 | 114.8 | 113.0 | 113.1 |
| A325 Bolt #2 | 116.8 | 112.3 | 112.4 | 109.2 | 105.0 |

**5.5 Effect of Cooling Rate on Bolt Residual Strength**

The same as heating time, the cooling rate of structural members in a real fire event also varies from case to case. For example, if water from fire hose hits the heated structural member, it will be cooled very quickly. Other structural

81

members that have been heated in fire will cool more slowly. A series of tests were performed to study the effect of cooling rate on bolt residual strength. Segments from the same A325 bolts were heated to 600°C for 6 hours and then cooled in room air, in ice water and in furnace separately. The room air temperature was about 30°C and the bolt cooled to this temperature in about 30 minutes. The ice water was approximately 0°C and cooled the bolt segment in about 5 seconds. Even with the power off and its door closed, the furnace cooled down very slowly. Figure 5-10 shows a typical cooling rate of furnace. The results shown in Table 5-7 show that cooling rate has very limited effects on the residual tensile strength of A325 bolt.

Table 5-7 Estimated Residual Tensile Strength with Different Cooling Rate

| Estimated Tensile | Cooling method | | |
|---|---|---|---|
| Strength (ksi) | In Room Air | In Ice Water | In Furnace |
| Bolt #1 | 113 | 112 | 111 |
| Bolt #2 | 105.0 | N/A | 103.7 |
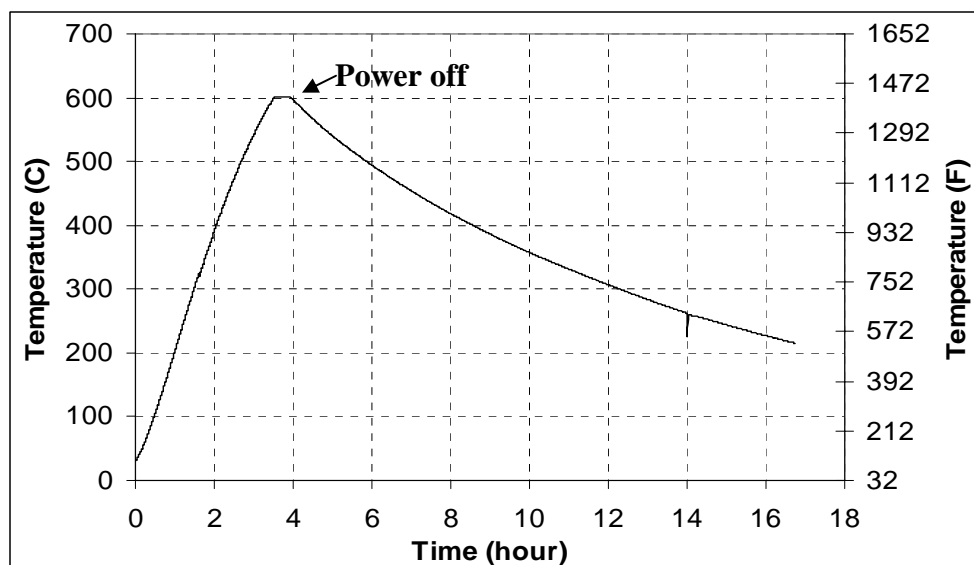


Figure 5-10 Typical Heating and Cooling Rate of Furnace

### 5.6 Slip Load of Fully Tighten A490 Bolt Connection

Slip critical connections are widely used bolted connections. The Research Council on Structural Connection Specification for Structural Joints using ASTM A325 or A490 Bolts provides the standard test method for determining the slip load. The compression test specimen geometry was used to study the residual slip load of slip critical connections after undergoing exposure to elevated temperature.

The slip load is determined by two variables: the tension force in bolt and the slip coefficient of the contact surface of steel plates. The specified tension force in bolt, also known as clamping force in connection, is specified in the AISC Specification and is attained by using one of the approved tightening methods.. The slip coefficient varies with the surface condition of the plates that are connected. Generally, slip tests are performed to determine the mean slip coefficient for designing slip critical connections. .



Figure 5-11 A490 Bolts in Slip Load Tests

Table 5-8 Tension Force in A490 Bolt after Fully Tightened

| Bolt No. | Bolt #1 | Bolt #2 | Bolt #3 | Average |
|---|---|---|---|---|
| Tension Force (kips) | 57.0 | 58.0 | 57.0 | 57.3 |

The first step was to determine the pretension force when the bolt was fully tightened. Three inch long A490 tension control bolts were used in the test

specimens. The bolts are shown in Figure 5-11. The pretension force in A490 bolt when the splined end sheared off at the notched section was measured in a Skidmore load cell. The details of the procedure are given Chapter 3. Table 5-8 gives the tension force in three A490 bolts tested.

Table 5-9 Slip Load Tests Result

| | Exposure Temperature | Ambient Temperature | | | | | |
|---|---|---|---|---|---|---|---|
| Batch #1 | Slip Resistance (kips) | 26.6 | 32.4 | 35.1 | Average Ambient: 31.4 | | |
| | Exposure Temperature | 300˚C | 300˚C | 500˚C | 500˚C | 700˚C | 700˚C |
| | Slip Resistance (kips) | 47.8 | 49.6 | 16.1 | 19.4 | 9.0 | 8.2 |
| Batch #2 | Exposure Temperature | Ambient Temperature | | | | | |
| | Slip Resistance (kips) | 34.0 | 32.7 | 38.7 | Average Ambient: 35.1 | | |
| | Exposure Temperature | 200˚C | 200˚C | 400˚C | 400˚C | 600˚C | 600˚C |
| | Slip Resistance (kips) | 51.4 | 58.8 | 50.1 | 52.7 | 10.0 | 5.0 |
| Batch #3 | Exposure Temperature | Ambient Temperature | | | | | |
| | Slip Resistance (kips) | 54.0 | 30.0 | 36.6 | Average Ambient: 33.3 (54.0 is not included) | | |
| | Exposure Temperature | 100˚C | 100˚C | 800˚C | 800˚C | | |
| | Slip Resistance (kips) | 71.2 | 47.0 | 4.0 | 3.3 | | |

Standard slip test connections were made at room temperature. Then the connections were heated to the desired temperature in furnace. After the connections cooled back to ambient temperature in room air (about 75°F), slip load tests were performed. The loss of slip resistance was determined by comparing the control test results to the remaining batch of connections. Twenty-seven standard slip load test plates were available from previous research studies. Each specimen requires three plates; therefore nine connections could be made with these plates. Three batches of connections were tested by using each plate three times. Before making a connection, all the steel plates were blasted to provide a uniform surface to minimize the variance among connections within a batch. Table 5-9 summarizes the test temperature and the measured slip of all the slip load tests. In each batch, 3 connections were randomly picked as control samples and were tested without being heated. Among the 9 connections, which are tested as control samples, 7 results are between 30 kips and 40 kips. The test results show a good consistency between test batches with two exceptions: a low load of 26.6 kips and a high load of 54.0 kips. The change in the slip coefficient of the plates due to the subsequent heating, testing, and then re-sandblasting, was determined by these control specimens. The average slip load of the control tests neglecting the outlier of the first specimen of batch 3 range was between 31.4 to 33.3 kip corresponding to a slip coefficient of 0.27 to 0.29 using the average bolt tension determine in the Skidmore load cell. The specimens heated and then tested are labeled as T, followed by the temperature they were heated to in degrees Celsius and the replicate number for the batch.

Figure 5-12 gives the absolute slip load of the heated connections. From room temperature to 400°C, the slip load increased from about 35 kips to 50 kips. Therefore slip connections are still safe after being exposed to a temperature lower than 400°C. However, from 400°C to 800°C, the slip capacity dropped

significantly. For comparing slip loads from different batches, slip loads in each batch were normalized to the average slip load (Table 5-9) of that batch. Figure 5-13 shows the normalized slip load against the max temperature that the connection has been heated at. It was found that the normalized slip load in bolted connections increased with a maximum temperature from room temperature to 400˚C, where connection can gain 50% more slip load at most. Beyond 400˚C, slip load starts to drop dramatically with temperature. At 600˚C and 700˚C, there is only about 25% of its original slip load capacity left.
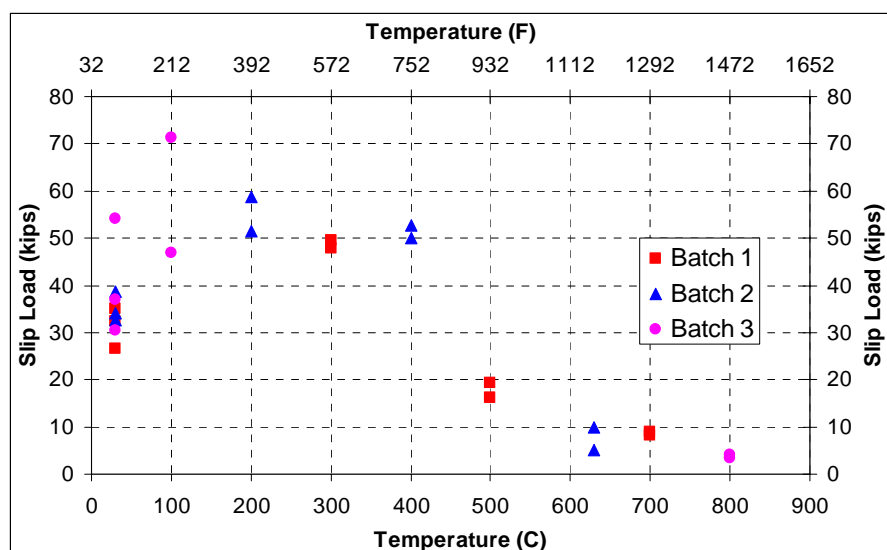


Figure 5-12 Slip Load vs. Temperature

The reason for a slip resistance increase from room temperature to 400˚C might be due to the increase in the surface roughness due to oxidization with the bolt tension evidently remaining constant. During the heating and cooling phases, the connection underwent expansion and shrinkage. That might have resulted in a better contact between the rough surfaces. The rapid drop above 400˚C was probably due to a loss of bolt tension. From Table 4-4, the shear capacity of A490 bolt drops by 40% at 500˚C when compared with its shear capacity at ambient

temperature. It is reasonable to estimate A490 bolt's tensile capacity drops by the same amount also. From the mill report, the tensile strength of this A490 bolt is 75.4kips. At 500˚C, the tensile capacity drops to about 45.2kips. The original pretension force is 57.3kips which is greater than tensile strength of 45.2kips. Therefore A490 bolt stretches plastically. After cooled to ambient temperature, elongated bolt lost most of its pretension force. In turn, connection lost its slip capacity.
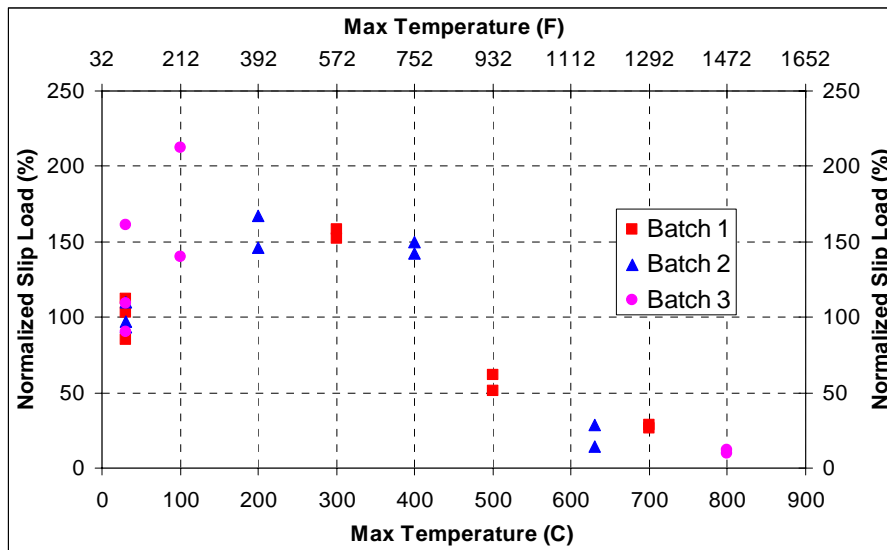


Figure 5-13 Normalized Slip Load vs. Temperature

If we assume that the tension force in the bolt does not change after being heated and cooled, then the residual slip coefficient can be calculated for each temperature level. The result is shown in Figure 5-14.
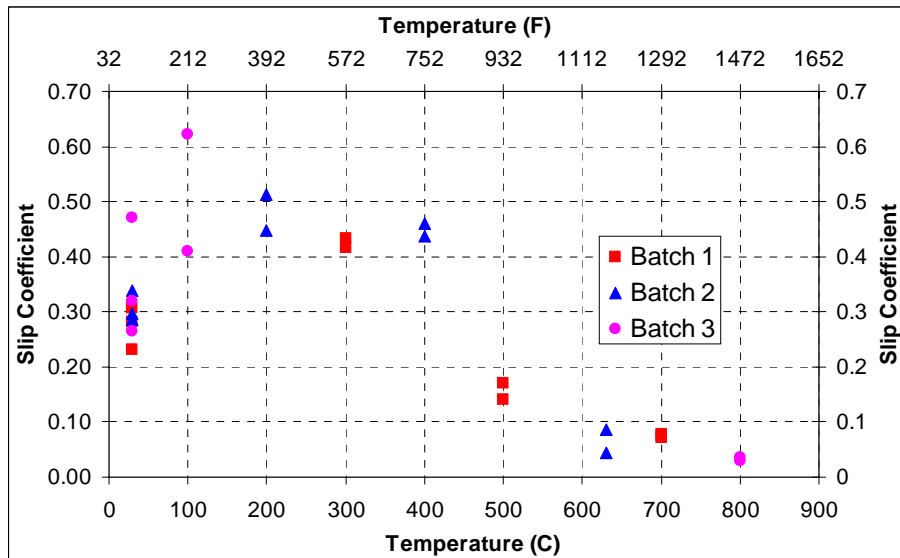
Figure 5-14 "Slip Coefficient" vs. Temperature

Figure 5-15 shows the slip surfaces after slip load tests of connection with different temperature history. On the control connection slip surface, slip marks are small. After the connection was heated to 100°C and 200°C, large slip marks concentrate near the bolt hole, where high clamping force acts on. This indicates better contact of the steel plate surfaces due to expansion and shrinkage in heating and cooling. At 300°C, there is more slip marks occur on the slip surfaces. It corresponds to the high slip load on connections from this temperature. At 400°C, slip marks reduce to as about the same as 100°C connection. From 500°C to 800°C, slip marks almost disappear. This is consistent with the conclusion that A490 bolt loses most of its pretension force after experiencing temperature higher than 500°C. The tempering temperature was estimated to be the same temperature as that of 7 inch long A490 bolt. Bolts heated above this estimated tempering temperature suffered a reduction in tensile strength. The reduced slip load could also be attributed to a loss of bolt pretension due to a loss of bolt strength.
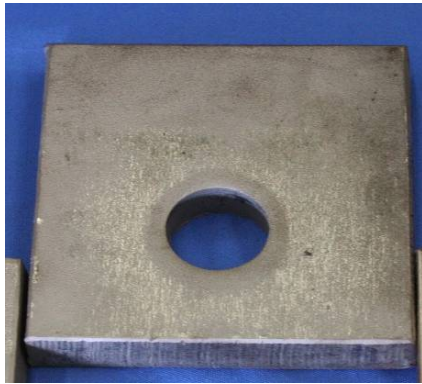
(a) Control Connection (25˚C)   (b) Connection Heated to 100˚C
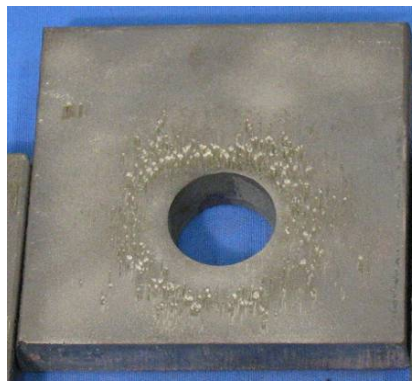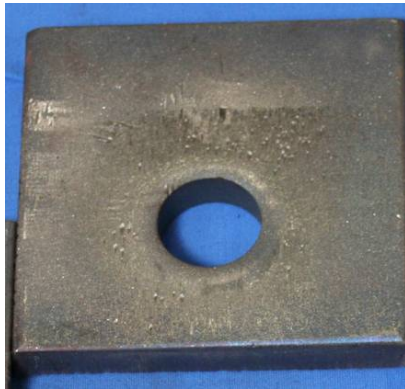
(c) Connection Heated to 200˚C   (d) Connection Heated to 300˚C
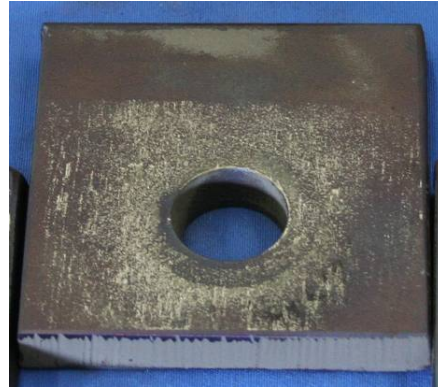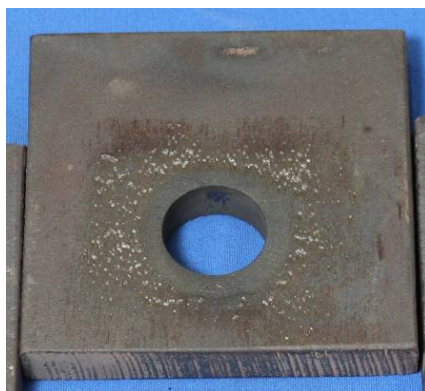
(e) Connection Heated to 400˚C   (f) Connection Heated to 500˚C
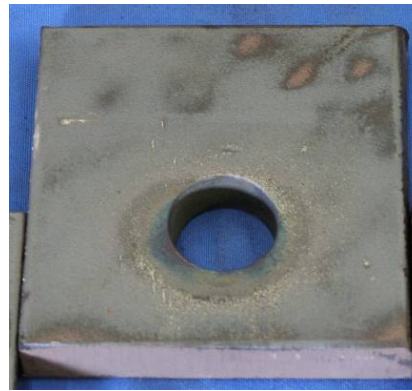
Figure 5-15 Slip Surface of Connections after Heat to Different Temperature Levels and Tested at Room Temperature (continued)
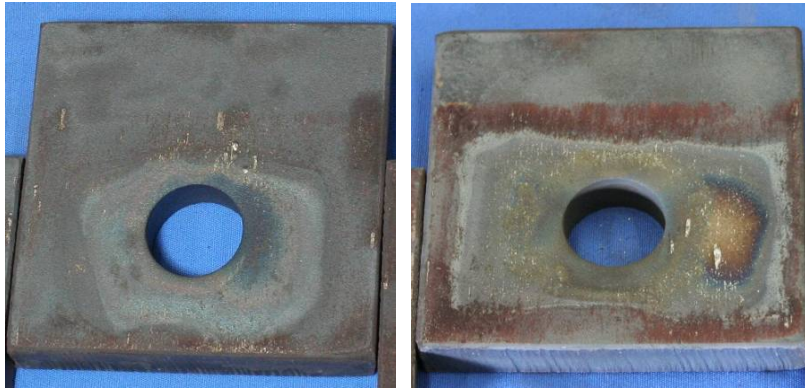
(g) Connection Heated to 600˚C     (h) Connection Heated to 700˚C
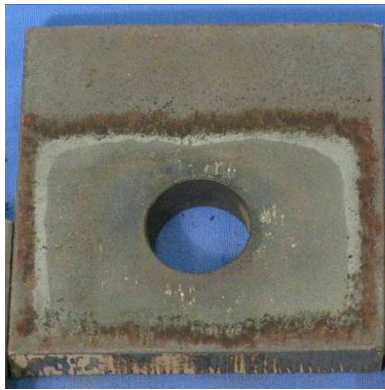


(i) Connection Heated to 800˚C

Figure 5-15 Slip Surface of Connections after Heat to Different Temperature Levels and Tested at Room Temperature

# Chapter 6

# Bolted Connection Behavior at Elevated Temperature

This chapter presents the test results of single bolt connections and two-bolt connections at elevated temperature levels. Single bolt connections were tested in order to study bearing strength and bolt shear strength variation with temperature. Two-bolt connections were designed to investigate the block shear failure capacity at different temperature levels.

## 6.1 Single Bolt Connections

As discussed in Chapter 3, single bolt connection was designed as shown in Figure 3-17. The steel plates were all Grade 50 and 3/8 inches thick. They have measured dynamic yield strength of 57.1 ksi and dynamic ultimate tensile strength of 78.6 ksi at ambient temperature. The shorter plate with the smallest end distance was designed to fail during test, while the longer one served as a loading plate. The bolt used was 7/8 diameter 3 inches long A325 bolt. The bolt was snug tightened only, in order to reduce the friction force between connected plates. Two groups of connections with different bolt hole end distance, 7/8 inch (1.0 D) and 1-5/16 inch (1.5 D), were tested at different temperature levels.

Table 6-1 summarizes all the test results of single bolt connections. Each connection test is named by the description, its temperature, and bolt hole end distance. If there was more than one connection tested under the same temperature, then an ordinal number is added to the end of its name. For example, SC-T25-D10-1 stands for **S**ingle bolt **C**onnection that was tested at a **T**emperature of 25˚C. The bolt hole end distance is $1.0 \times \mathbf{D}$, where D is bolt nominal diameter.

91

Table 6-1 Single Bolt Connection Test Results

| Test Name | Test Temperature | | Measured Clear End Distance (in) | Load Capacity (kips) | Failure Mode |
|---|---|---|---|---|---|
| | (˚F) | (˚C) | | | |
| SC-T25-D10-1 | 72 | 22 | 0.410 | 25.8 | Bearing |
| SC-T25-D10-2 | 75 | 24 | 0.388 | 25.3 | Bearing |
| SC-T100-D10 | 214 | 101 | 0.493 | 27.9 | Bearing |
| SC-T200-D10 | 392 | 200 | 0.472 | 29.3 | Bearing |
| SC-T300-D10 | 574 | 301 | 0.420 | 30.2 | Bearing |
| SC-T400-D10 | 754 | 401 | 0.508 | 29.7 | Bearing |
| SC-T500-D10 | 939 | 504 | 0.476 | 20.2 | Bearing |
| SC-T600-D10 | 1112 | 600 | 0.401 | 10.3 | Bearing |
| SC-T700-D10 | 1305 | 707 | 0.488 | 5.5 | Bolt Shear |
| SC-T800-D10 | 1479 | 804 | 0.474 | 3.8 | Bearing |
| SC-T25-D15-1 | 75 | 24 | 0.843 | 40.8 | Bearing |
| SC-T25-D15-2 | 77 | 25 | 0.894 | 42.8 | Bearing |
| SC-T100-D15 | 216 | 102 | 0.902 | 42.8 | Bearing |
| SC-T200-D15 | 390 | 199 | 0.906 | 43.7 | Bearing |
| SC-T300-D15 | 574 | 301 | 0.850 | 46.4 | Bearing |
| SC-T400-D15 | 752 | 400 | 0.924 | 39.0 | Bolt Shear |
| SC-T500-D15 | 934 | 501 | 0.911 | 23.6 | Bolt Shear |
| SC-T600-D15-1 | 1112 | 600 | 0.848 | 11.9 | Bolt Shear |
| SC-T600-D15-2 | 1116 | 602 | 0.860 | 8.6 | Bolt Shear |
| SC-T700-D15 | 1294 | 701 | 0.905 | 6.0 | Bolt Shear |
| SC-T800-D15 | 1481 | 805 | 0.906 | 4.9 | Bolt Shear |

### 6.1.1  1.0d End Distance
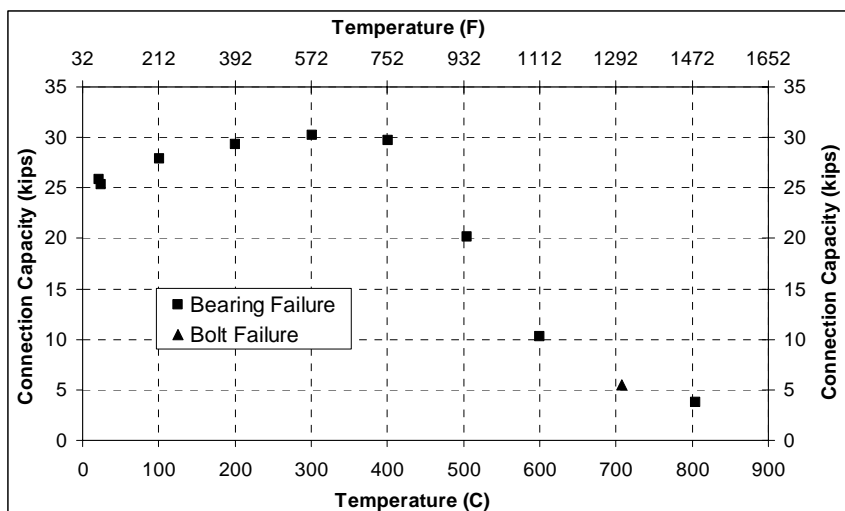


Figure 6-1 Capacity of Connections with 1.0d End Distance at Different Temperature

Figure 6-1 plots the load capacity of single bolt connections with a bolt hole end distance equal to bolt nominal diameter at different temperature levels. From ambient temperature to 300˚C, the connection capacity increased with temperatures from about 26 kips to 31 kips, a 20% increase. From 300˚C to 400˚C, the connection capacity dropped slightly by about 2%. However, from 400˚C to 800˚C, the connection capacity decreased dramatically with temperature. The rate of strength reduction between 400˚C and 600˚C was about 40% of its original capacity at ambient temperature per 100˚C, while the rate decreased to 20% from 600˚C to 700˚C. From 700˚C to 800˚C, the connection capacity only decreases by about 7%.

(a) SC-T25-D10-1          (b) SC-T100-D10          (c) SC-T200-D10

(d) SC-T300-D10          (e) SC-T400-D10          (f) SC-T500-D10

(g) SC-T600-D10          Half Sheared Bolt          (h) SC-T700-D10

Shear Failure Section of Bolt      (i) SC-T800-D10
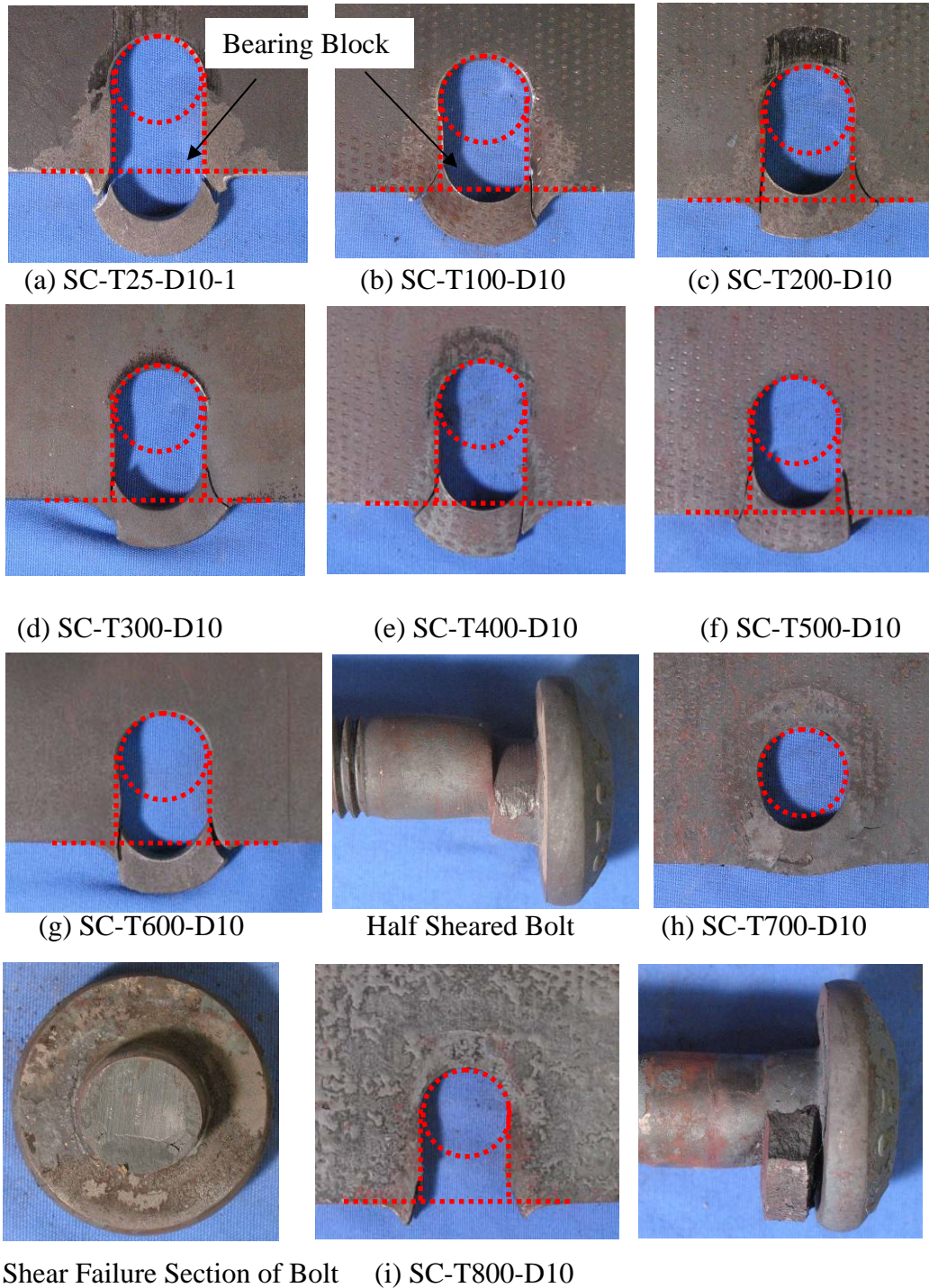
Figure 6-2 Single Bolt Connections (Le = 1.0d) Failures at Different Temperature

Figure 6-2 shows the failure mode and failure paths of single bolted connections with 1.0d end distance. The red dashed lines show the original material boundary before test. The specimens failed in bearing at all the temperatures except 700°C. At ambient temperature, large amounts of shear deformation happened before final failure. The bolt movement created two straight shear paths, which were parallel. Due to the relative small clear end distance, that final ligament of material failed in tension. As temperature went up to 100°C, 200°C and 300°C, connection capacity increased while deformation decreased. The material in the bearing block deformed less. The two shear deformation paths got shorter and flared out instead of being parallel to each other. At 400°C and 500°C, the shear paths showed a greater flare angle and asymmetry. From ambient temperature to 500°C, the shear strength of the A325 bolt was always greater than the bearing capacity of plate. At 600°C, bearing failure still controlled connection capacity. However at this temperature the bolt was halfway sheared which indicated that the capacity of bolt was getting near to that of bearing capacity. The condition of the bolt after the test is shown in the Figure 6-2 (g). At 700°C, bolt shear failure controlled with significant bearing deformation occurred around the bolt hole. At 800°C, a bearing failure occurred with very little bearing deformation evident in the plate. At 800°C the bearing strength again became greater than the bolt shear strength.

Figure 6-3 and Figure 6-4 give the load deformation curves at different temperatures. The deformation of connection was defined as the relative movement of two steel plates $Y_1$-$Y_0$, as shown in Figure 6-5. From ambient temperature to 400°C, connection stiffness did not change much, while significant stiffness loss occurred from 400°C to 800°C.

95
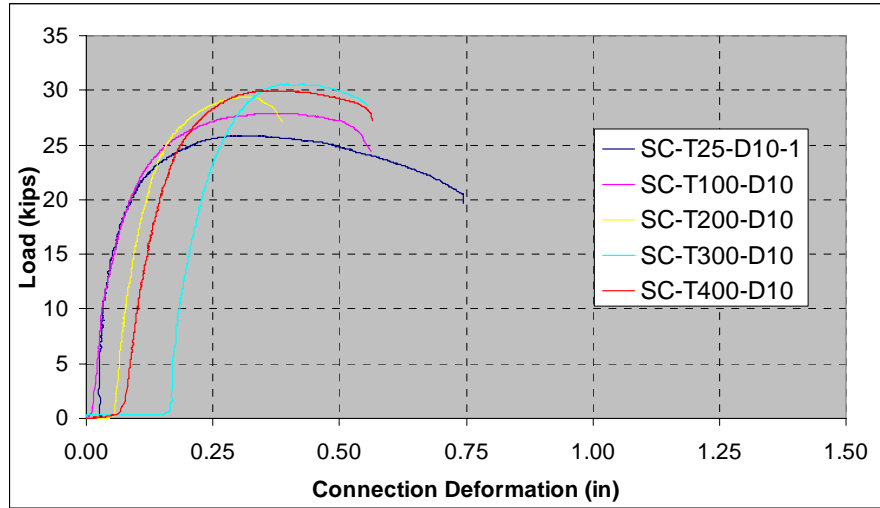
Figure 6-3 Load Deformation Curves of Single Bolt Connection (Le=1.0d)
(Temperature Range: 25°C to 400°C)
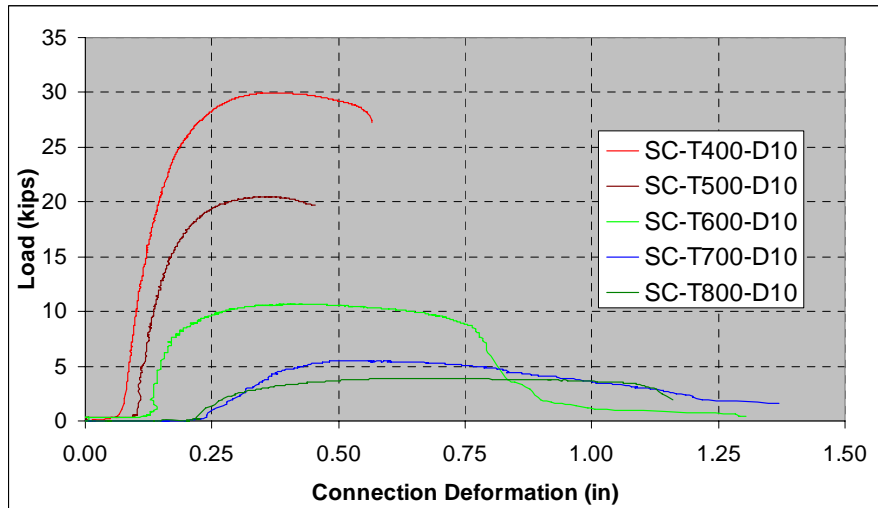


Figure 6-4 Load Deformation Curves of Single Bolt Connection (Le=1.0d)
(Temperature Range: 400°C to 800°C)
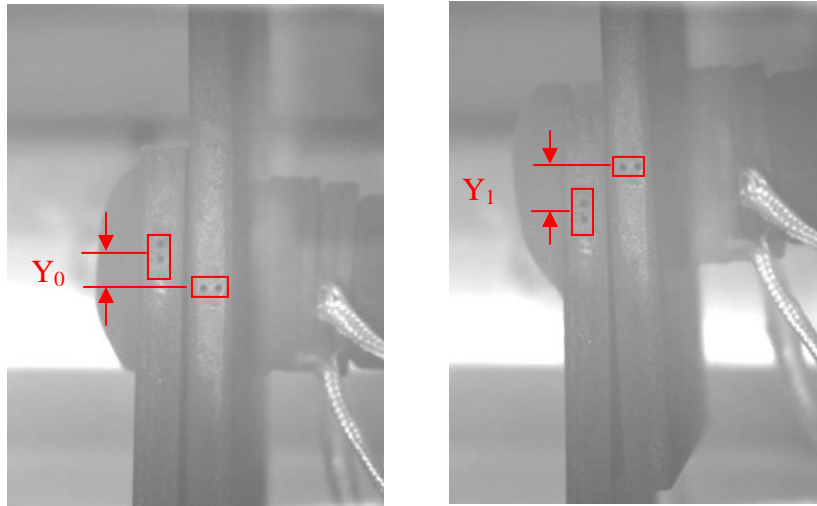
Figure 6-5 Connection Deformation

## 6.1.2   1.5D End Distance

All the conditions were the same as those in 1.0D group except that the end distance was increased to 1.5D. Figure 6-6 shows a plot of the connection capacity at different temperature. A change in the mode of failure from a bearing failure to a bolt shear failure occurred above 300˚C. Comparing the connection failure mode of 1.5D connection with that of 1.0D group, the major difference is the clear failure mode switch between 300˚C and 400˚C from a plate bearing failure to bolt shear failure. Figure 6-7 summarizes the test results from both groups of connection by the mode of failure. Because of the change in the failure mode, the connection capacity started to drop significantly at 400˚C, which was 100˚C earlier than 1.0d connection. The connection with an end distance of 1.5d had about 15 kips more capacity than the 1.0d connection at ambient temperature. At elevated temperatures their capacities became comparable when at 400˚C and beyond.
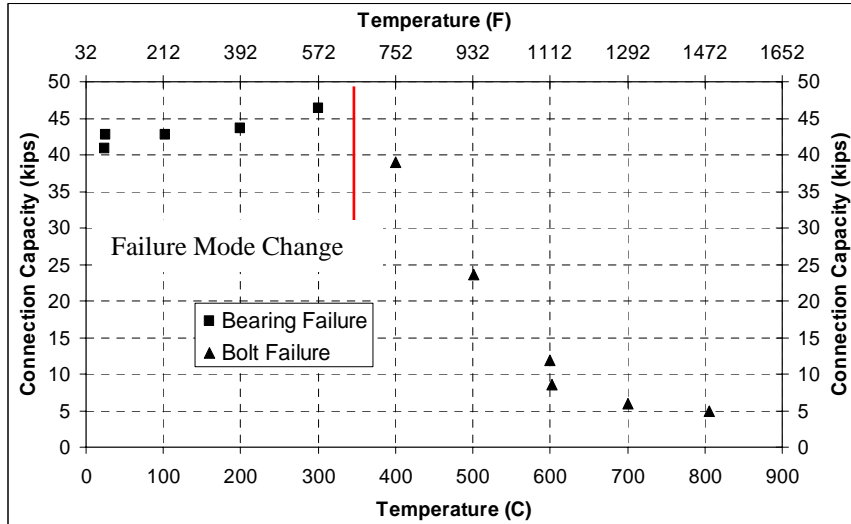
Figure 6-6 Capacity of Connections with 1.5d End Distance at Different
Temperature
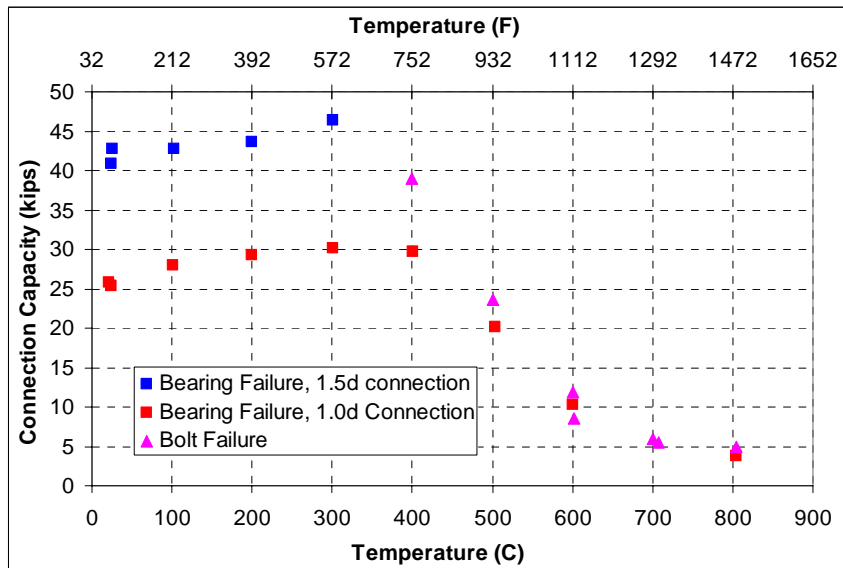


Figure 6-7 Summaries of 1.0d and 1.5d Connections Test Results

(a) SC-T25-D15-1       (b) SC-T100-D15       (c) SC-T200-D15

(d) SC-T300-D15       (e) SC-T400-D15       (f) SC-T500-D15

(g) SC-T600-D15-1       (b) SC-T700-D15       (c) SC-T800-D15
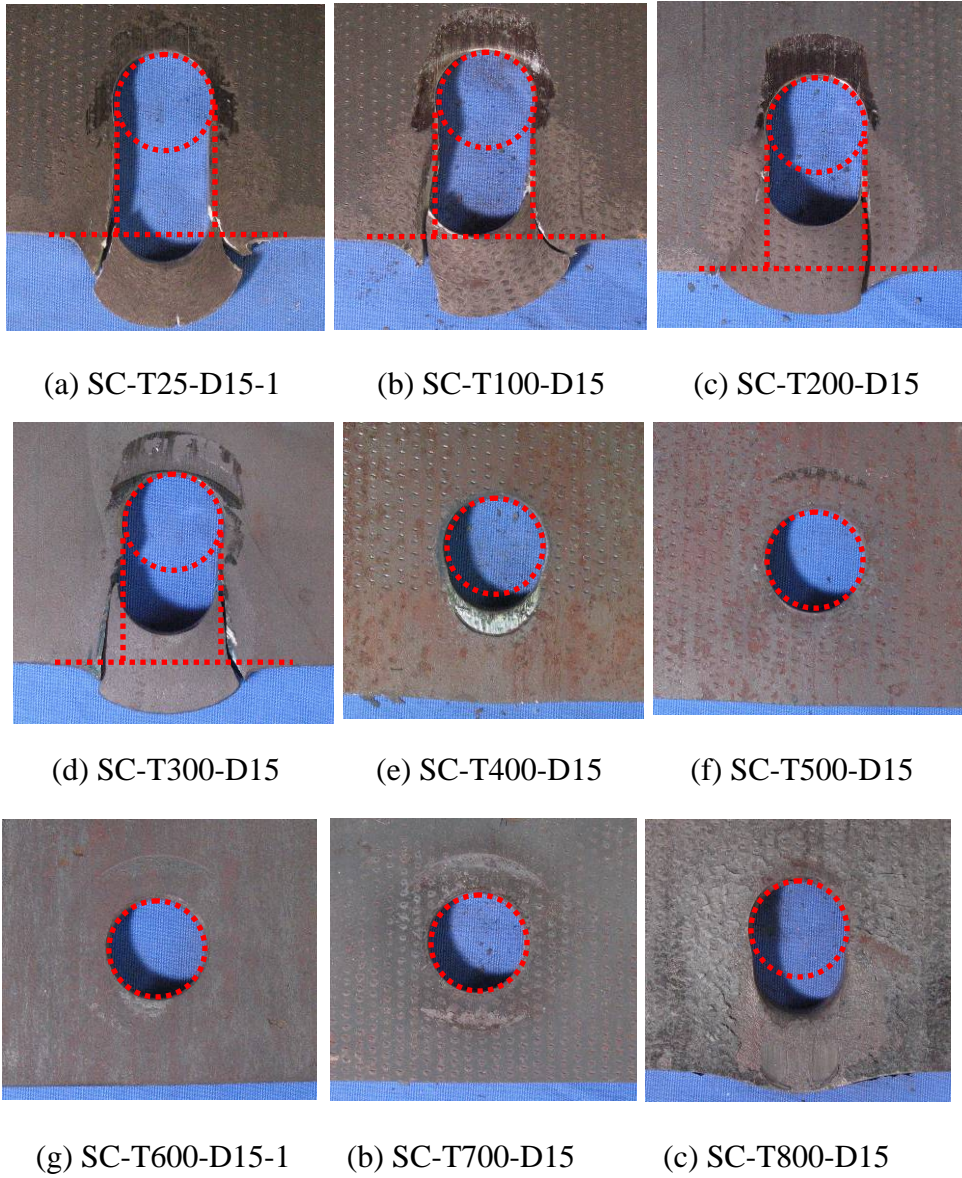
Figure 6-8 Single Bolt Connections (Le = 1.0d) Failures at Different Temperature

Figure 6-8 provides a picture of steel plates after connection failure occurred. From ambient temperature to 200˚C, the deformation capacity of connections decreases with temperature, while simultaneously, the load capacity increased slightly. At 300˚C, both load and deformation capacities increased compared with load capacity at 200˚C. From 400˚C to 800˚C, bolt shear failure controlled. There were significant bearing deformations on steel plates at 400˚C and 800˚C, while bolt holes stayed almost intact at 500˚C, 600˚C and 700˚C. This indicates that the strength reduction rates of A325 bolt is greater than that of Grade 50 steel. A325 bolt started to lose strength at 300˚C, a higher rate than the Grade 50 steel plate; the Grade 50 steel retains its strength up to 400˚C and then began to lose strength at a lower rate than the bolt.
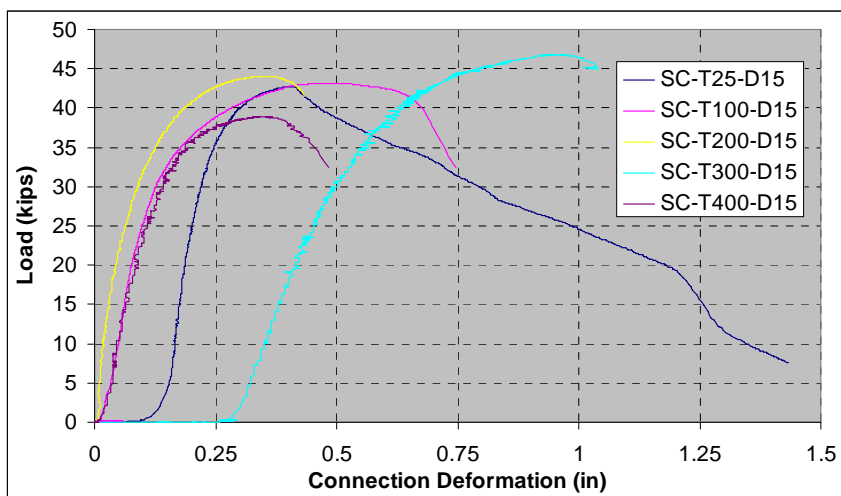


Figure 6-9 Load Deformation Curves of Single Bolt Connection (Le=1.5d) (Temperature Range: ambient temperature to 400˚C)

In Figure 6-9 and Figure 6-10, connection stiffness dropped slightly at 100˚C, compared with ambient temperature. Then connection stiffness increased at 200˚C and went back down at 300˚C. Due to the failure mode change at 400˚C from bearing failure to bolt shear failure, the connection stiffness increased.

Connection stiffness reduced significantly while deformation capacity increased from 500˚C to 800˚C. From 500˚C to 700˚C, connection deformation capacity increased by the increased ductility of bolt. However, the very large deformation capacity at 800˚C was the combination of bolt ductility and bearing deformation on plate.
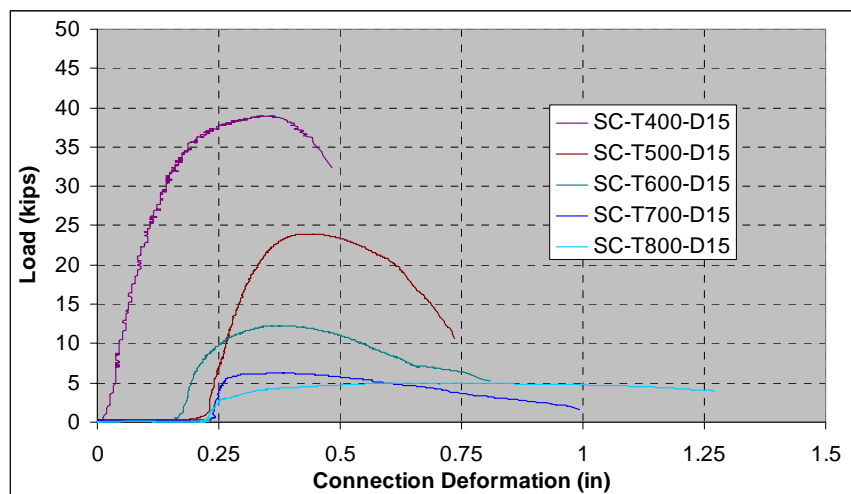


Figure 6-10 Load Deformation Curves of Single Bolt Connection (Le=1.5d) (Temperature Range: 400˚C to 800˚C)

### 6.1.3    Shear Capacity of 3-inch A325 Bolt

Figure 6-11 shows the shear capacity of 3-inch A325 bolts with 7-inch A325 bolt, Kirby's Set A and Set C Grade 8.8 bolts. The chemical composition information is given in Table 6-2. The 7-inch A325, 3-inch A325, Kirby Set A and Kirby Set C contain 0.010, 0.030, 0.027 and 0.130 Molybdenum respectively. Between 300˚C and 600˚C, the bolt shear strength varied in the same sequence. As discussed in chapter 4, Molybdenum is a very powerful alloying element in increasing the strength of steel in the temperature range of 300˚C to 600˚C. However, the advantage from Molybdenum disappeared beyond 600˚C.
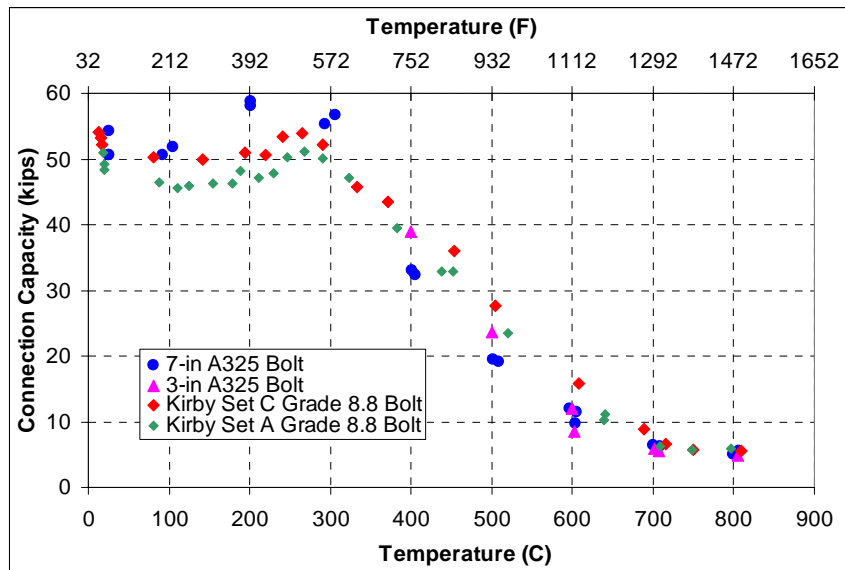
Figure 6-11 Shear Capacity of Different Bolts

## 6.2    Two-Bolt Connections

Two-bolt connections were designed to have block shear failure mode at ambient temperature. Figure 3-19 shows the dimensions of connection plates. The center long plate was designed to fail in block shear, while the two outer short plates served as loading reaction plates only. The steel plate was Grade 50, ½ inch thick, which had a dynamic yielding strength of 56.3 ksi and a dynamic ultimate strength of 73.0 ksi at ambient temperature. Connection deformation was defined as the relative movement between center plate and outer plate, $Y_1$-$Y_0$, as shown in Figure 6-12.

Table 6-2 Chemical Compositions of A325, A490 and Grade 8.8 Bolts

| Bolt | C | Si | Mn | P | S | Cr | Mo | Ni | B | Cu | N |
|---|---|---|---|---|---|---|---|---|---|---|---|
| A325 (L=7in) | 0.29 | 0.27 | 0.76 | 0.006 | 0.010 | 0.05 | 0.010 | 0.06 | 0.0009 | 0.12 | 0.026 |
| A325 (L=3 in) | 0.29 | 0.20 | 0.83 | 0.020 | 0.016 | 0.13 | 0.030 | 0.06 | 0.0018 | 0.18 | 0.028 |
| Kirby Set A (Grade 8.8) | 0.19 | 0.21 | 1.16 | 0.020 | 0.017 | 0.19 | 0.027 | 0.14 | 0.0051 | 0.22 | 0.0080 |
| Kirby Set C (Grade 8.8) | 0.41 | 0.16 | 1.61 | 0.021 | 0.038 | 0.13 | 0.130 | 0.12 | <0.0005 | 0.23 | 0.013 |
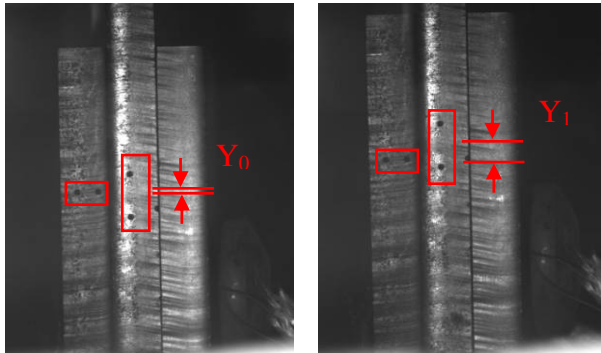
Figure 6-12 Definition of Connection Deformation

There were ten two-bolt connections tested, seven of which were constant temperature tests similar to the tests performed on the single bolt bearing tests and the double shear bolt test. The rest three were constant load tests where the load was held constant while the temperature of the furnace and specimen increased. The constant temperature tests were named as **T**win bolts **C**onnection plus **T**emperature level plus **C**onstant **T**emperature. Table 6-3 summarized constant temperature test results. The constant load tests were named as **T**win bolts **C**onnection plus **L**oad level plus **C**onstant **L**oad. The results were summarized in Table 6-4.

Table 6-3 Two Bolts Connection Test Results (constant temperature tests)

| Test Name | Temperature Level | | Maximum Load (kips) | Connection Deformation at Maximum Load (in) |
|---|---|---|---|---|
| | ˚C | ˚F | | |
| TC-T300-CT | 299.6 | 571.2 | 116.8 | 0.277 |
| TC-T400-CT | 405.4 | 761.7 | 104.7 | 0.280 |
| TC-T500-CT | 502.3 | 936.1 | 73.9 | 0.248 |
| TC-T600-CT-1 | 600.5 | 1112.9 | 44.2 | 0.186 |
| TC-T600-CT-2 | 600.9 | 1113.6 | 43.6 | 0.294 |
| TC-T700-CT | 701.9 | 1295.4 | 21.4 | 0.180 |
| TC-T800-CT | 804.3 | 1479.8 | 13.3 | N/A |

Table 6-4 Two Bolts Connection Test Results (constant load tests)

| Test Name | Temperature at Failure | | Load Level (kips) | Connection Deformation at Failure (in) |
|---|---|---|---|---|
| | ˚C | ˚F | | |
| TC-L75-CL | 419.6 | 916.9 | 75.0 | 0.464 |
| TC-L60-CL | 544.9 | 1012.8 | 60.0 | 0.482 |
| TC-L33-CL | 639.5 | 1183.2 | 33.0 | 0.611 |
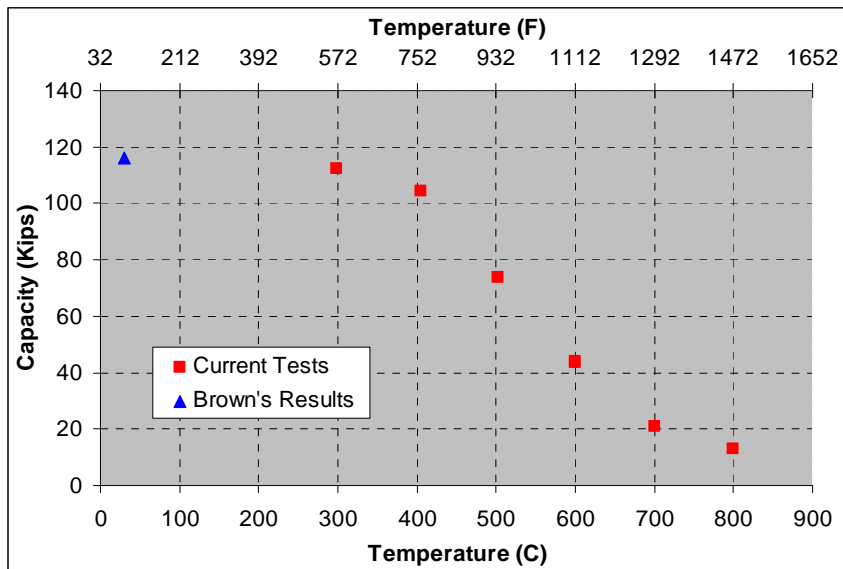


Figure 6-13 Two-Bolt Connection Constant Temperature Test Results

Figure 6-13 shows the two-bolt connection constant temperature test results from 300˚C to 800˚C. At 300˚C, test connection had almost the same capacity as it did at ambient temperature. From 400˚C to 700˚C, the connection capacity dropped linearly with its temperature, from 104 kips to 21 kips. Then the decreasing rate of connection capacity slowed down from 700˚C to 800˚C, in which there was only an 8 kips drop in capacity. It was also noticed that there was a capacity increase at 300˚C and 400˚C similar to the behavior of the single bolt connection. Figure 6-14 shows the load deformation curves for

105

constant temperature tests. As temperature went up, connection stiffness
decreased. Connection ductility increased with temperature, which was shown
by the enlarged unloading parts and large total deformation capacity.
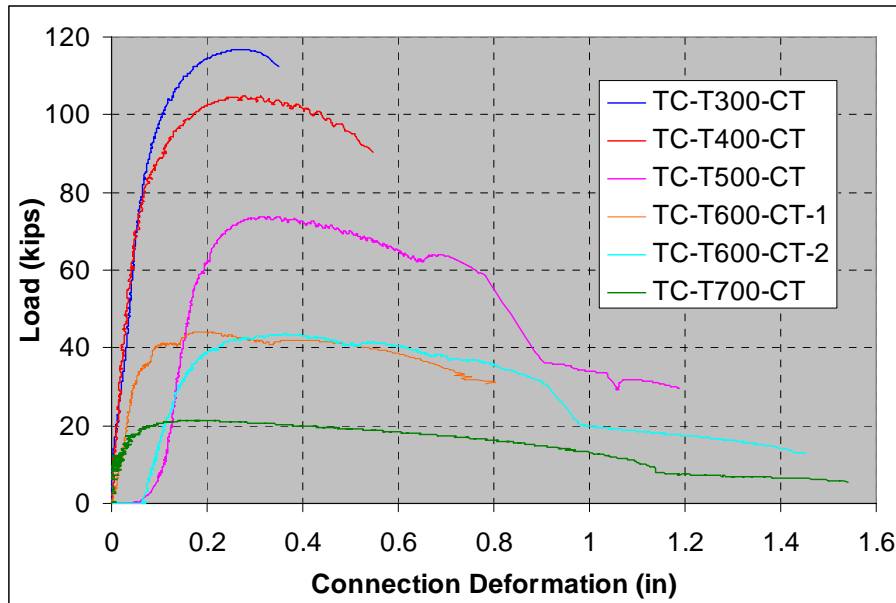


Figure 6-14 Load Deformation Curves of Constant Temperature Tests

Figure 6-15 shows the block shear failures at different temperature
levels. It was found that as temperature went up, the ductility of steel plate
increased significantly. At 300˚C, steel plate was in the blue brittle range and an
unusual failure occurred in the specimen at this temperature as shown in Figure
6-15 (a). A block shear failure only occurred on right hole. The left bolt hole
had a combination of block shear and net section failure. There were brittle
cracks found on the inside surface of bolt hole, as shown in photo in at right
side of fig. 6-17 (a) . At 400˚C, normal block shear failure occurred. Right after
the middle tensile part fractured, shear failure occurred on both shear paths.
From 500˚C to 800˚C, the block failure could be divided into two phases:
tensile failure first and then shear failure. The gap between the failed ends of
tensile part indicated the connection still carried load by shear after the tensile

ligament between the holes fractured. After a large amount of shear deformation, the material included in block shear failed in tension at two tips, as shown in (d). At temperatures lower than 500˚C, A490 bolt had no significant deformation. That showed A490 bolt's shear capacity were much higher than block shear capacity of plate. However from 600˚C to 800˚C, large deformations were found on bolt shank.



Brittle Cracks
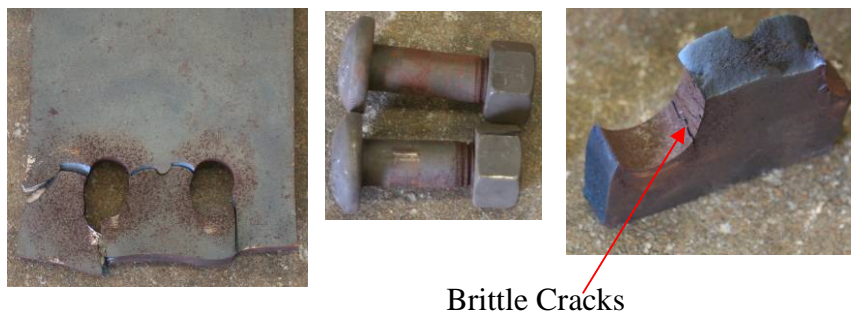
(a) TC-T300-CT



(b) TC-T400-CT



(c) TC-T500-CT

Figure 6-15 Block Shear Failures at Different Temperature Levels (Constant Temperature Tests) (Continued)
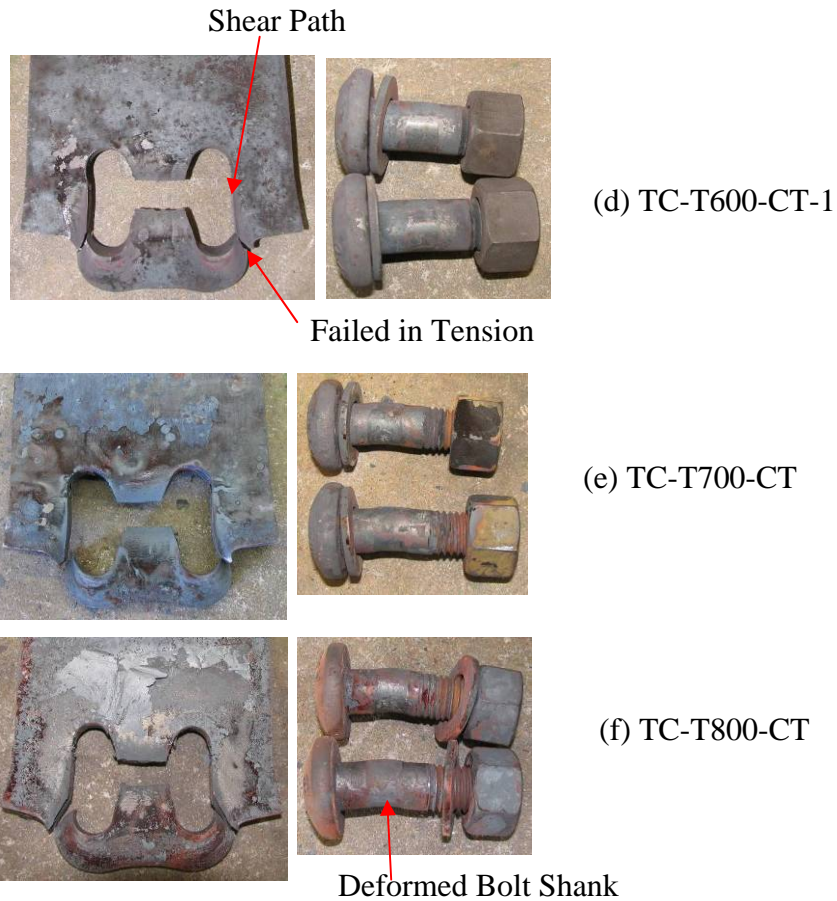
(d) TC-T600-CT-1

(e) TC-T700-CT

(f) TC-T800-CT

Figure 6-15 Block Shear Failures at Different Temperature Levels (Constant Temperature Tests)

Constant load tests were performed to fully simulate the condition of bolted connections in fire event. The connection load was maintained as its temperature was increased gradually. Figure 6-16 shows the constant temperature test results with constant load test results. The two types of tests produced the same strengths. Therefore it appears that test results are not influenced by the heating and loading path taken during the tests. Based upon these results it appears that the constant temperature test results can be used to estimate the behavior of bolted connections regardless of the time temperature that the connection experiences during a fire event. Figure 6-17 shows the

108

failed center plate from constant load tests. TC-T400-CT and TC-L75-CT had similar capacities at similar temperature levels. However, the failure shapes were different, as shown in Figure 6-17 (a). Constant temperature test TC-T500-CT showed a larger shear deformation than transient test TC-L75-CL. Loading rate was the reason for this difference. In constant temperature test, load dropped gradually after peak. This allowed the block of material to deform along shear paths after rapture occurred in tensile section. However, the load was kept constant in transient test. After the tensile part reached its maximum load carrying capacity, the load was transferred to shear section immediately. Under this high loading rate, shear rupture happened before large yielding deformation could occur. Therefore constant load test is a high deformation rate test. On the tensile and shear failure paths, high strain rate deformation occurred. That is why TC-L75-CT showed much less ductility than TC-T500-CT.
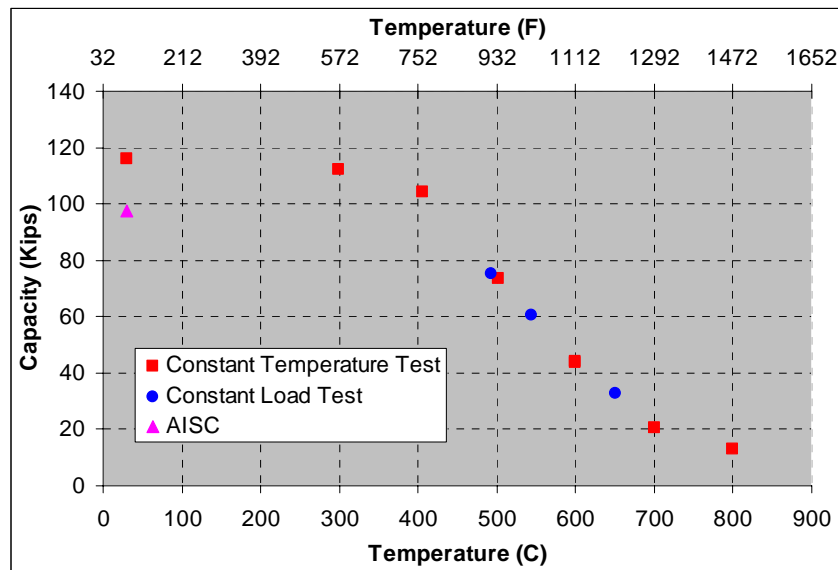


Figure 6-16 Constant Load Test vs. Constant Temperature Test

(a) TC-L75-CL        TC-T500-CT



(b) TC-L60-CL



(c) TC-L33-CL

Figure 6-17 Block Shear Failures at Different Load Levels (Constant Load Tests)

Figure 6-18 shows the time-temperature and time-deformation curves of constant load tests. Three load levels, 33kips, 60kips and 75kips, were tested. All the connections showed very small deformation increase until its temperature reached certain critical level. Then connection deformation started to increase and connection failure occurred a few seconds later. The

temperature at failure point was taken as failure temperature of the connection when it ceased to carry the load. It was also shown that in constant load tests, the connections were exposed to high temperature for longer time than they would experience in the ASTM standard fire test or natural fires. If there were any creep problem, it should show up more obviously in the constant load tests. Because no creep problems were found in the constant load tests, they should not be a concern when dealing with the ASTM standard fire test and natural fires.
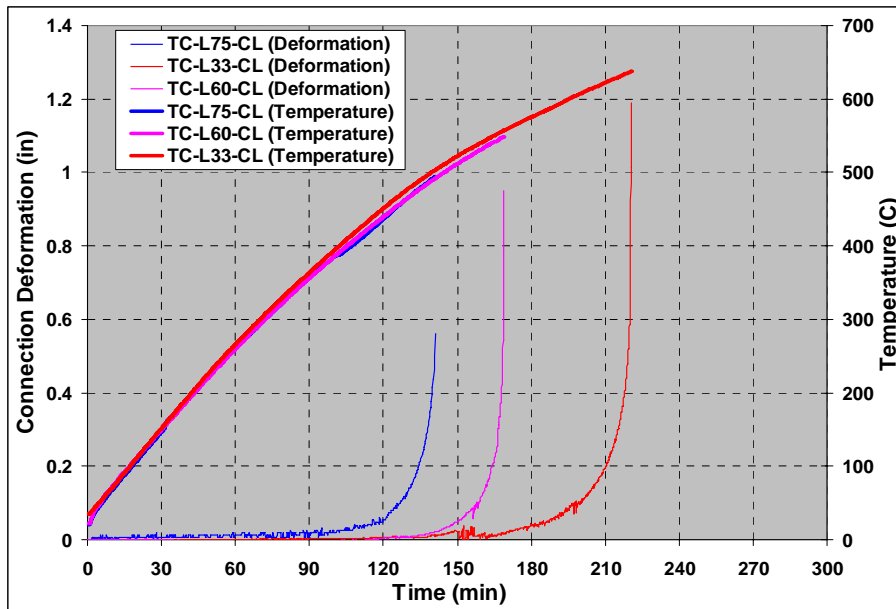


Figure 6-18 Time-Deformation and Time-Temperature Curves of Constant Load Tests

# Chapter 7
# Material Properties of Plate Steels

In connection tests, two heats of A572 Gr. 50 steel were used, which were 3/8 inch and 1/2 inch thick. Coupons were made from the same batch of plates in each heat. Tensile tests were performed at the same temperature levels as connection tests. The results are presented in this chapter.

## 7.1 Terminology

All the coupon tests were performed as constant temperature tests. Coupon was heated to target temperature under zero stress condition. Then with temperature being kept constant, load was applied until fracture occurred. The loading process was under crosshead movement rate control. Two different rates were selected, 0.1 inches per minute and 0.01 inches per minute. During the loading process, 30 second suspensions were carried out several times in order to compare static and dynamic strength.

The stress refers to engineering stress, which is equal to the measured load divided by the measured initial cross section area of coupon's reduced section. The strain is engineering strain, which was measured by extensometer over 1 inch gage length. Punch marks, which were one inch apart, were made along the central axis of coupon to ensure good contact between coupon surface and extensometer ceramic rod tips. The initial error in gage length was about +0.0005 to +0.0007 inch, which resulted in an initial strain reading. After coupon was heated, thermal strain were introduced into gage length also. Therefore strain reading during loading included initial gage length error and thermal strain. When the stress-strain curve was presented, initial error strain and thermal expansion strain were removed from strain readings. Elongation was determined by

measuring the distance between punched marks after fractured coupon had been cooled to ambient temperature again. Area reduction was calculated by (1 – fracture area / initial area).
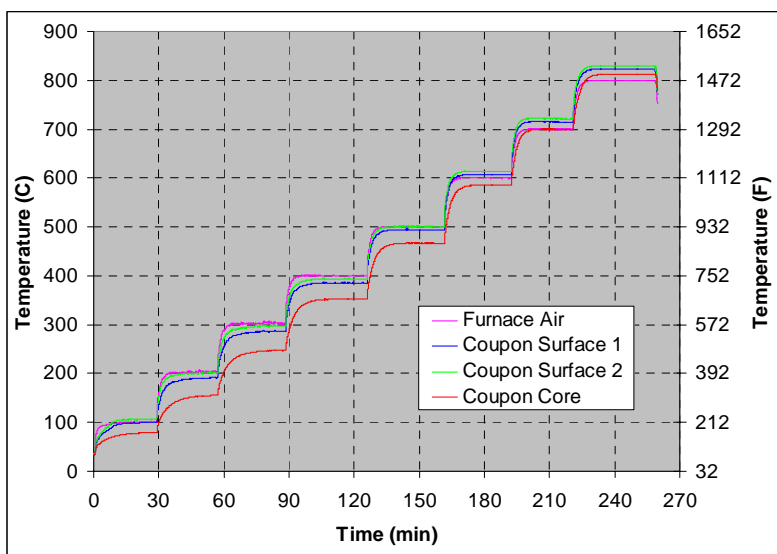


Figure 7-1 Coupon Surface and Core Temperatures

MTS 653 electric furnace was used to maintain coupon temperature during test. It had three heating zones, which had one pair of heating element and one independent, built-in thermal probe. The probes measured air temperature inside furnace. Coupon surface temperatures were measured with three shielded thermal couple probes, which were located along the top, middle and bottom of the reduced section part on coupon. Due to thermal air circulation, cool air enters the furnace from the bottom and hot air escapes from the top. A temperature gradient existed along longitudinal direction of reduced section part of coupon. It was found that the two probes at the top and middle of coupon's reduced section part had similar temperatures readings, while the one at bottom had lower reading. Because most of the fracture section located near middle of coupon reduction section part, the temperature there was taken as coupon surface temperature.

113

The core temperature of a coupon was not monitored because any hole drilled would result in failure there. A dummy coupon with the same geometry as other coupons was used to measure the core temperature and compared with surface temperature. By this method the core temperature could be estimated from its surface temperature. A dead end hole was drilled to mid depth of the reduced section and one thermal probe was inserted into it. The other two thermal probes were put at the same spot, contacting coupon surface. Furnace temperature was set at one hundred degrees Celsius intervals until a stable stage was achieved. Then surface temperature and core temperature were compared. Figure 7-1 shows the time temperature curve and table 7-1 gives the core temperature and surface temperature at stable stage. It was found that maximum temperature difference between core and surface occurred at 200˚C and 300˚C. At all temperature levels, the surface temperatures were higher than core temperature.

Table 7-1 Coupon Surface Temperature and Core Temperature

| Set Temperature (˚C) | Furnace Air Temperature (˚C) | Coupon Surface Temperature (˚C) | | Coupon Core Temperature (˚C) | Surface & Core Difference (˚C) |
|---|---|---|---|---|---|
| | | #1 | #2 | | |
| Ambient | 33.3 | 35.3 | 36.3 | 33.9 | 1.9 |
| 100 | 100.0 | 100.2 | 107.2 | 78.9 | 24.8 |
| 200 | 203.9 | 192.0 | 203.0 | 155.3 | 42.2 |
| 300 | 301.7 | 286.5 | 297.2 | 247.1 | 44.8 |
| 400 | 400.0 | 385.2 | 393.1 | 352.3 | 36.9 |
| 500 | 500.0 | 494.0 | 500.8 | 466.9 | 30.5 |
| 600 | 600.0 | 606.5 | 612.9 | 585.4 | 24.3 |
| 700 | 700.0 | 714.5 | 721.1 | 699.7 | 18.1 |
| 800 | 800.0 | 823.4 | 829.5 | 812.7 | 13.8 |

Table 7-2 Material Properties of 1/2 inch Gr. 50 Steel at Different Temperature

| Temp. (˚C) | Temp. (˚F) | Original Area (in²) | Dynamic F$_y$ (ksi) | Dynamic F$_u$ (ksi) | Fracture Area (in²) | Elongation (%) | Reduction in Area (%) | Stress Drop in 30 seconds Loading Suspension (ksi) | Loading Rate (in/min) |
|---|---|---|---|---|---|---|---|---|---|
| 29.2 | 84.6 | 0.259 | 62.41 | 74.19 | 0.118 | 51.7 | 54.6 | 3.1 | High |
| 102.7 | 216.9 | 0.260 | 56.79 | 70.23 | 0.096 | 54.8 | 63.0 | 2.7 | High |
| 199.9 | 391.8 | 0.264 | 53.07 | 69.83 | 0.130 | 50.8 | 51.0 | 1.9 | High |
| 300.0 | 572.0 | 0.264 | 40.90 | 73.59 | 0.105 | 49.4 | 60.1 | 4.9 | High |
| 399.1 | 750.4 | 0.267 | 33.47 | 60.36 | 0.081 | 41.1 | 69.5 | 5.6 | High |
| 505.4 | 941.7 | 0.266 | 26.34 | 48.32 | 0.060 | 45.0 | 77.3 | 7.5 | High |
| 590.1 | 1094.2 | 0.266 | 16.84 | 28.98 | 0.058 | 54.1 | 78.2 | 8.3 | High |
| 701.6 | 1294.9 | 0.271 | 13.88 | 17.21 | 0.030 | 42.9 | 88.7 | 5.9 | High |
| 803.8 | 1478.8 | 0.264 | N/A | 8.20 | 0.056 | 46.5 | 78.9 | 4.2 | High |
| 807.4 | 1485.3 | 0.264 | 6.23 | 8.41 | 0.104 | 45.9 | 60.5 | N/A | High |
| 27.7 | 81.9 | 0.261 | 57.85 | 72.39 | 0.097 | 60.8 | 62.8 | 1.1 | Low |
| 103.2 | 217.8 | 0.258 | 57.11 | 70.37 | 0.102 | 60.4 | 60.3 | 1.2 | Low |
| 201.1 | 394.0 | 0.265 | 48.69 | 70.99 | 0.114 | 59.7 | 56.8 | 1.5 | Low |
| 300.8 | 573.4 | 0.260 | 40.09 | 76.16 | 0.105 | 60.6 | 59.8 | 2.7 | Low |
| 395.5 | 743.9 | 0.271 | 28.57 | 58.22 | 0.079 | 83.3 | 70.8 | 2.9 | Low |
| 500.5 | 932.9 | 0.262 | 21.98 | 42.26 | 0.067 | 78.3 | 74.3 | 2.7 | Low |
| 596.8 | 1106.2 | 0.261 | 11.47 | 24.32 | 0.064 | 132.6 | 75.3 | N/A | Low |
| 695.0 | 1283.0 | 0.260 | 7.19 | 13.38 | 0.048 | 110.1 | 81.6 | 2.3 | Low |
| 800.5 | 1472.9 | 0.266 | 3.30 | 5.29 | 0.140 | 110.5 | 47.3 | 1.9 | Low |

Loading Rate (crosshead moving rate): High=0.1 in/min; Low=0.01 in/min

From 300˚C to 800˚C, F$_y$ was determined by 0.2% proof method.

## 7.2 1/2 inch Gr. 50 Plate Steel

Table 7-2 gives all test results on 1/2 inch Gr. 50 steel. The temperature was the surface temperature at the middle of reduced section part of coupon. Initial area and fracture area were calculated by measured dimensions. $F_u$ was calculated as maximum load divided by initial area. From ambient temperature to 200°C, $F_y$ was determined directly on stress-strain curves; however from 300°C to 800°C, 0.2% method had to be adopted to determine $F_y$. On stress-strain curve, the part from 0 to ($F_u$/3) was used to determine the slope of 0.2% offset line. Area reduction was calculated by (1- fracture area/ initial area). There were two different loading rates in tests. In high loading rate, test machine crosshead moved at 0.1 in per minute; while in low loading rate, the crosshead moved at 0.01 in per minute.



Figure 7-2 Dynamic Ultimate Strength and Dynamic Yield Strength of 1/2 inch Gr. 50 Steel at Different Temperature Levels

Figure 7-3 Dynamic and Static Ultimate Strength of 1/2 inch Gr. 50 Steel at Different Temperature Levels

Figure 7-2 shows the dynamic yield strength and dynamic ultimate strength of 1/2 inch Gr. 50 steel at different temperatures. Yield strength decreased with temperature almost bi-linearly during the entire temperature range. Loading rate had limited effects on yield strength at most of temperature levels. $F_y$ from high loading rate tests were about 3 ksi to 6 ksi higher than that from low loading rate tests. The ultimate strength did not drop from ambient temperature to 300˚C. Deformation rate had little effects in this temperature range. Beyond 300˚C, ultimate strength decreased linearly with temperature, from 74 ksi at 300˚C to 8 ksi. Loading rate had effects on ultimate strength. $F_u$ from high loading rate test was about 3 ksi to 6 ksi higher than that from low loading rate test. The absolute value of difference did not change much with temperature. This difference was not significant when $F_u$ was still relatively high at 400˚C to 600˚C; while it could not be negligible at 700˚C and 800˚C, where $F_u$ became relatively low. Figure 7-3 shows the static and dynamic ultimate strengths of 1/2 inch Gr. 50

steel. The static ultimate strength equal to the dynamic $F_u$ minus the stress drop in 30 seconds suspensions in Table 7-2. From 400˚C to 800˚C, the static ultimate strength is significantly lower than dynamic ultimate strength.



Figure 7-4 Stress-strain Curves of 1/2 inch Gr. 50 from 29˚C to 400˚C (Deformation rate = 0.1 in/min)
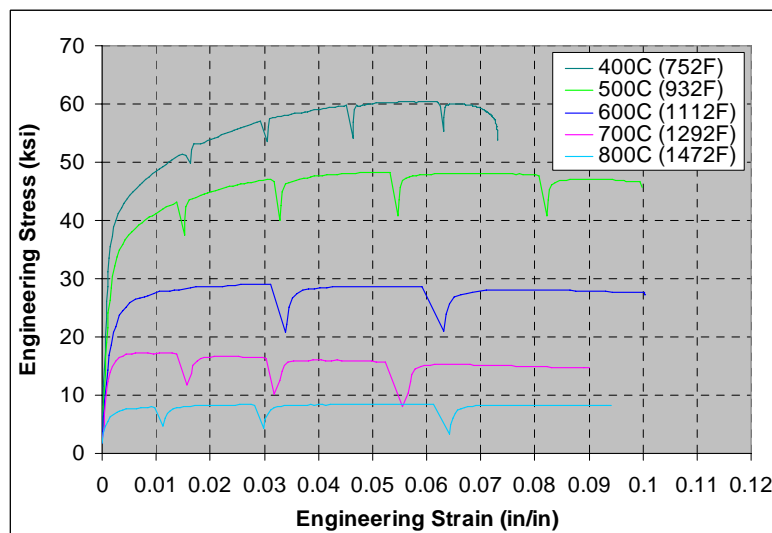


Figure 7-5 Stress-strain Curves of 1/2 inch Gr. 50 from 400˚C to 800˚C (Deformation rate = 0.1 in/min)
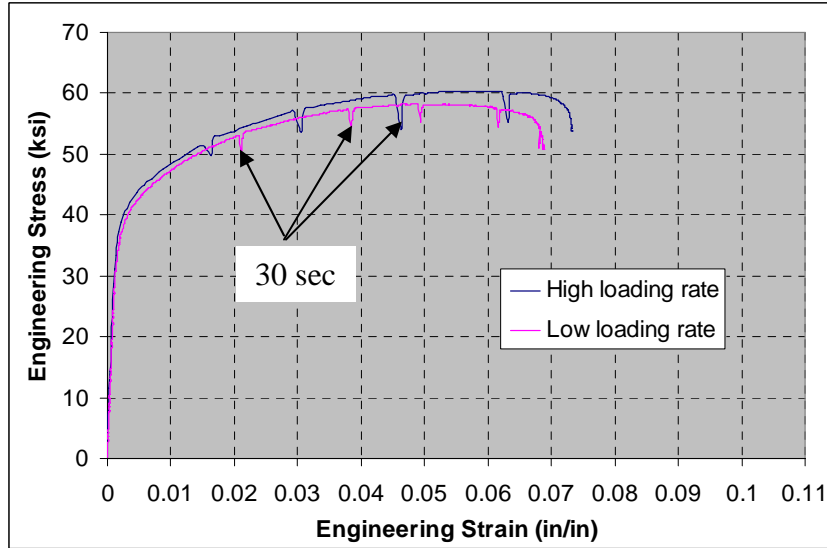
Figure 7-6 Stress-strain Curves of 1/2 inch Gr. 50 Steel at 400°C from High and Low Loading Rate
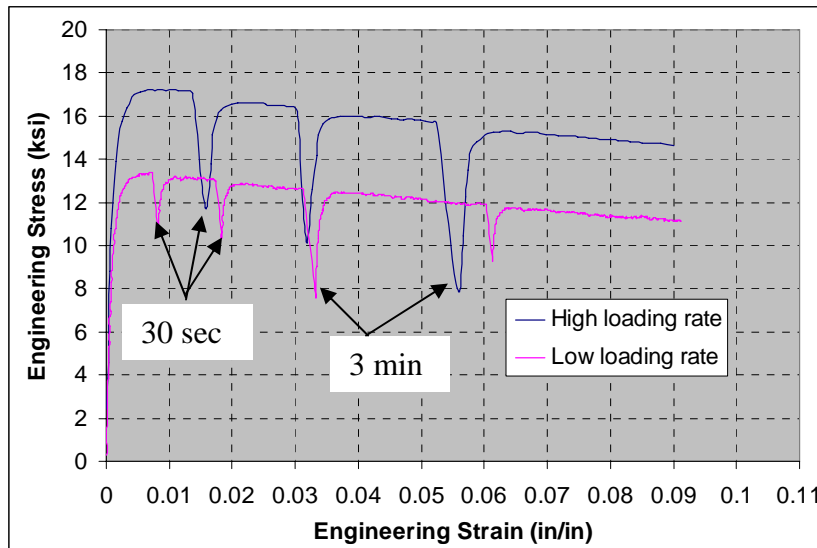


Figure 7-7 Stress-strain Curves of 1/2 inch Gr. 50 Steel at 700°C from High and Low Loading Rate

Figure 7-4 and Figure 7-5 show the stress-strain curves of 1/2 inch Gr. 50 steel at different temperature levels. It was found that from 29˚C to 200˚C, there was clear yield plateau on curve. However beyond 300˚C, no yield plateau existed anymore. At 300˚C, 400˚C, and 500˚C, steel entered hardening status right after elastic part. At 600˚C, 700˚C, and 800˚C, hardening part became shorter, followed by slow unloading.  On each curve, V shapes were created by 30 seconds suspensions in crosshead movement. As temperature went up, the V shapes became larger with wider opening. This indicated more creep and relaxation behavior in steel at higher temperature. From 29˚C to 200˚C, stress went higher than where loading was suspended when loading was resumed. However this phenomenon disappeared from 300˚C to 400˚C. From 500˚C to 800˚C, stress could not reach the level where loading was suspended during resumed loading process. The creep and relaxation behavior of steel from 400˚C to 800˚C indicated that loading rate would have significant effects on yield and ultimate strength in this temperature range. The stress-strain curves shown here were all from high loading rate tests. Stress-strain curves from low loading rate tests showed very similar behavior with lower yield and ultimate strength.

Figure 7-6 and Figure 7-7 show the stress-strain curves from high and low loading rate tests at 400˚C and 700˚C. It was found that at both temperature levels, loading rate did not change the way the steel behaved. Stress-strain curve from a low loading rate test stayed below the curve from high loading rate test. The major difference between curves from two loading rates was the depth of V shapes. On high loading rate curve, V shapes are deeper than that on low loading rate curve. That was because low rate loading allowed more creep and relaxation to occur during loading than high rate loading would allow. Therefore when loading was suspended by freeze crosshead position, less load drop occurred. At 700˚C, three minute suspensions were performed to compare with 30 second

suspension. A further stress drop was found at three minute suspension. Moreover, it was found that after a three minute suspension, the stresses from both high and low loading rates became very close to each other. That indicates that three minutes is enough time to remove the loading rate effects on the1/2 inch Gr. 50 steel at 700°C.
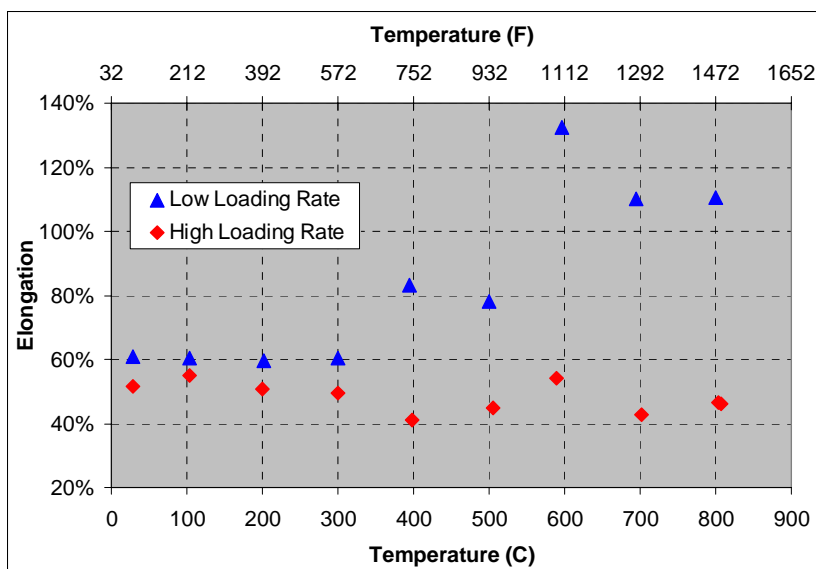


Figure 7-8 Elongation of 1/2 inch Gr. 50 Steel at Different Temperature

Figure 7-8 shows the elongation changes with temperature. It was found that a low loading rate resulted in larger elongation than a high loading rate in the whole temperature range. Elongations from high loading rate tests varied between 40% and 60%, with two low values at 400°C and 700°C. Elongations from low loading rate tests kept at about 60% from 30°C to 300°C. From 400°C to 500°C, elongations increased to about 80%, which was not like those from high loading rate tests. At 600°C, elongation from a low loading rate test increase to its maximum value of 130%, while it dropped to 110% at 700°C and 800°C. Elongations from different loading rate tests varied differently with temperature. One of the reasons is the increased creep and relaxation behavior of steel at

temperature higher than 400˚C. With creep and relaxation, coupons deformed more uniformly and delayed the occurrence of necking. Low loading rate gave more time to allow creep and relaxation happen. Therefore elongation from low loading rate test increased from 400˚C to 800˚C.
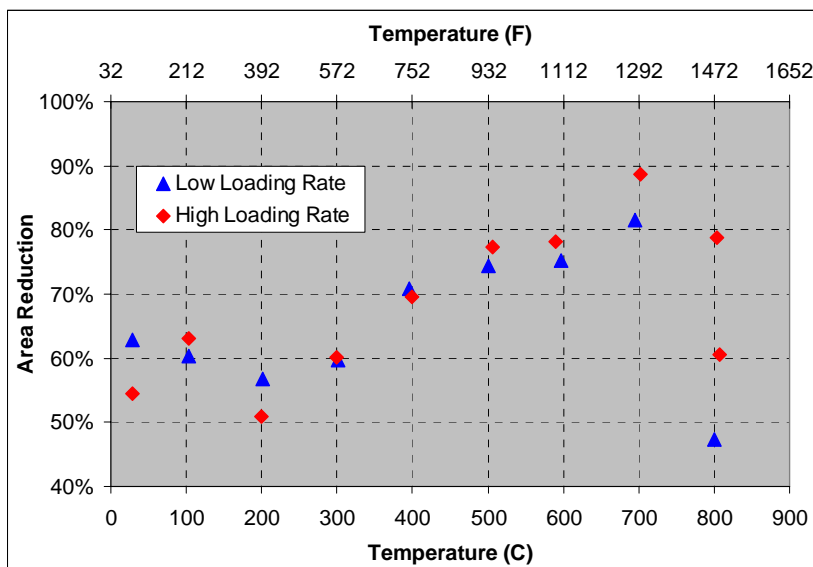


Figure 7-9 Area Reduction of 1/2 inch Gr. 50 Steel at Different Temperature

Figure 7-9 shows an area reduction ratio of 1/2 inch Gr. 50 steel at different temperatures. It was found that area reduction from both high and low loading rate tests followed similar trends in the whole temperature range. From 30˚C to 200˚C, area reduction rate decreased with temperature, while it increased with temperatures from 200˚C to 700˚C. At 800˚C, area reduction dropped again, which was due to the disappearance of necking, as shown in Figure 7-10.

**7.3 3/8 inch Gr. 50 Plate Steel**

Table 7-3 summarizes all test results on coupons of 3/8 inch Gr. 50 plate steel. Because the original plates were not long enough to make coupon, extra steel plate stripes were welded at both ends, as shown in Figure 7-11. Necessary

straighten work was done before test. Tests with high loading rate were performed at all temperature levels, while low loading rate tests were only performed from 500˚C to 800˚C.
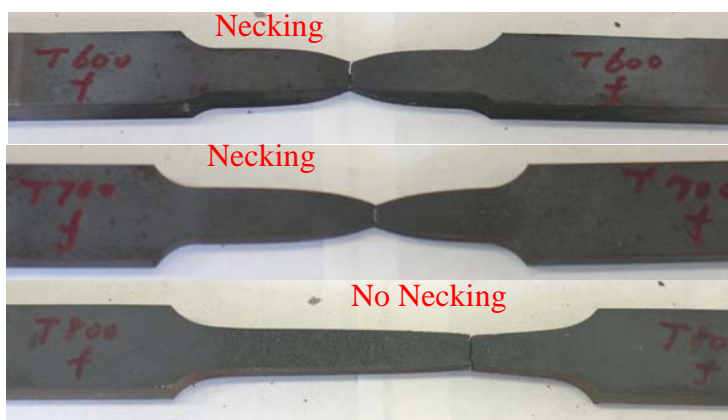


Figure 7-10 Coupons from High Loading Rate Tests at 600˚C, 700˚C and 800˚C



Figure 7-11 Coupon of 3/8 inch Gr. 50 Steel with Welded Extension

Table 7-3 Material Properties of 3/8 inch Gr. 50 Steel at Different Temperature

| Temp. (°C) | Temp. (°F) | Original Area (in²) | $F_y$ (ksi) | $F_u$ (ksi) | Fracture Area (in²) | Elongation (%) | Reduction in Area (%) | Stress Drop in 30 seconds Loading Suspension (ksi) | Loading Rate (in/min) |
|---|---|---|---|---|---|---|---|---|---|
| 29.3 | 84.7 | 0.181 | 57.07 | 78.56 | 0.066 | 45.8% | 63.3% | 2.5 | H |
| 100.2 | 212.4 | 0.182 | N/A | 72.78 | 0.070 | 43.9% | 61.7% | 1.8 | H |
| 199.0 | 390.2 | 0.183 | 50.37 | 74.86 | 0.086 | 37.3% | 53.1% | N/A | H |
| 298.1 | 568.6 | 0.182 | 51.06 | 80.07 | 0.098 | 36.7% | 46.0% | 2.0 | H |
| 400.7 | 753.3 | 0.184 | 38.74 | 74.07 | 0.081 | 36.2% | 55.6% | 4.0 | H |
| 499.7 | 931.5 | 0.182 | 39.23 | 60.80 | 0.112 | 28.3% | 38.3% | 5.8 | H |
| 602.9 | 1117.2 | 0.183 | 27.89 | 35.57 | N/A | N/A | N/A | 5.7 | H |
| 701.2 | 1294.2 | 0.183 | 18.25 | 18.53 | 0.061 | 65.6% | 66.7% | 6.4 | H |
| 702.2 | 1296.0 | 0.179 | 19.76 | 20.00 | 0.053 | 68.7% | 70.5% | N/A | H |
| 801.0 | 1473.8 | 0.180 | 8.02 | 9.36 | 0.096 | 69.5% | 46.7% | 3.8 | H |
| 499.3 | 930.7 | 0.184 | 34.42 | 60.04 | 0.096 | 35.4% | 47.6% | 2.2 | L |
| 602.8 | 1117.0 | 0.182 | 26.04 | 31.47 | 0.109 | 36.4% | 40.0% | 3.0 | L |
| 703.3 | 1297.9 | 0.182 | 14.87 | 15.55 | 0.093 | 48.0% | 48.8% | 2.7 | L |
| 800.1 | 1472.2 | 0.183 | 6.15 | 6.55 | 0.096 | 72.3% | 47.4% | 1.6 | L |

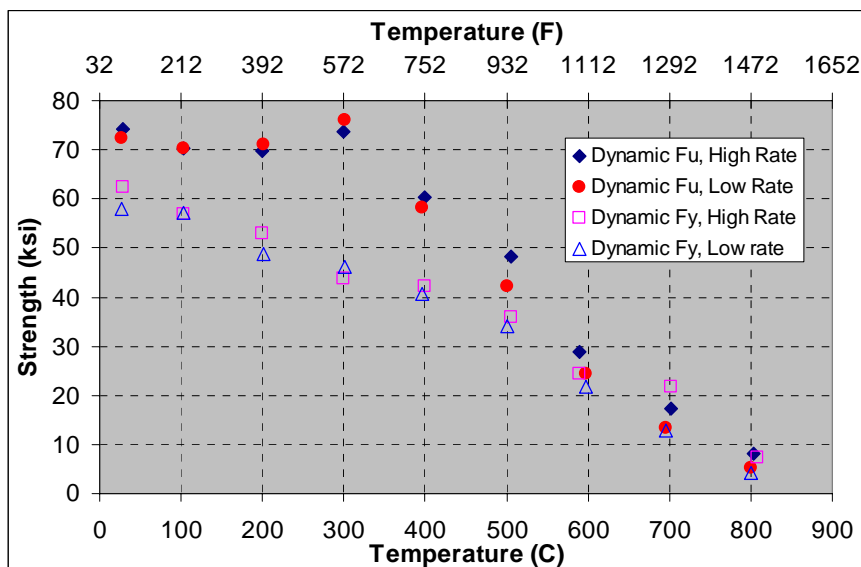Loading Rate (crosshead moving rate): H=0.1 in/min; L=0.01 in/min
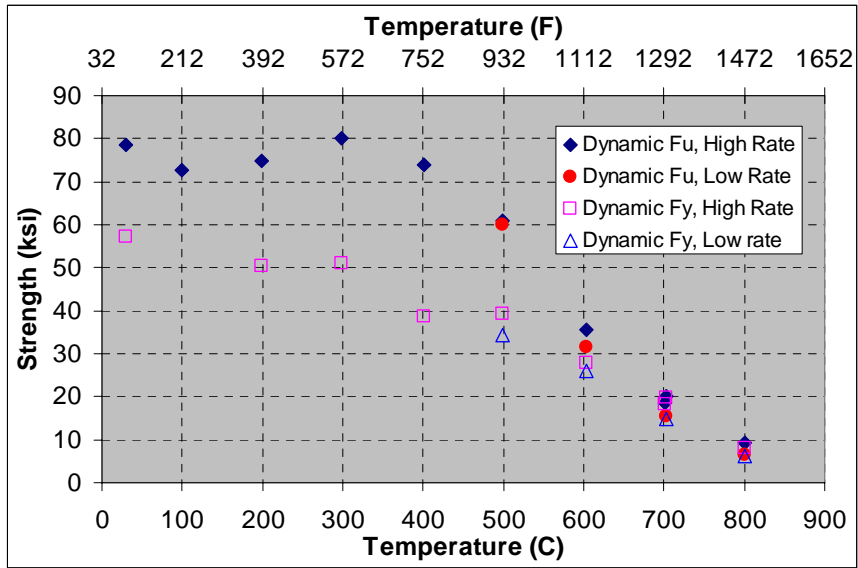
Figure 7-12 Dynamic Yield Strength and Dynamic Ultimate Strength of 3/8 inch Gr. 50 Steel at Different Temperature Levels
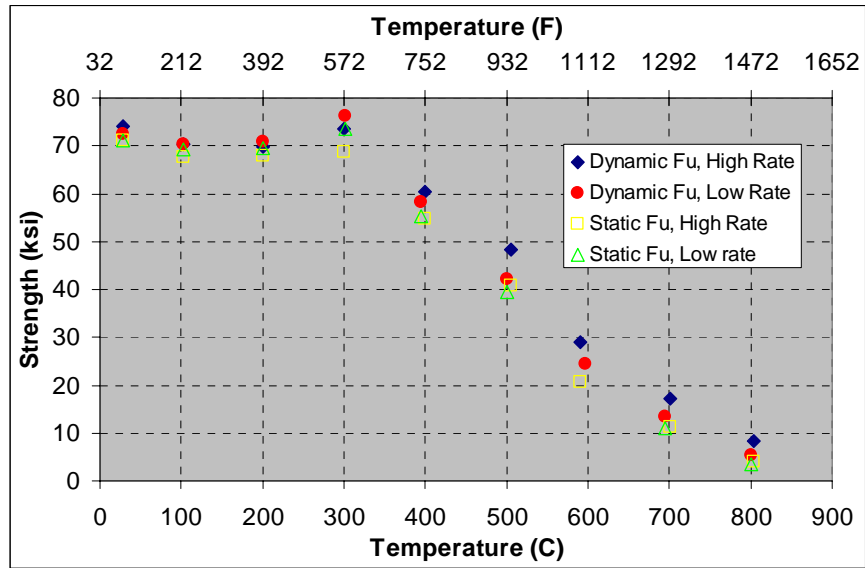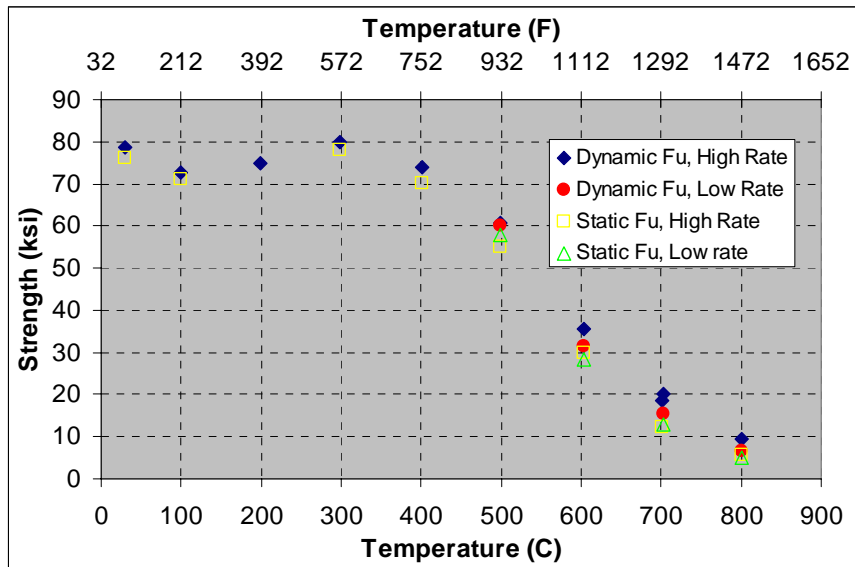


Figure 7-13 Dynamic and Static Ultimate Strength of 3/8 inch Gr. 50 Steel at Different Temperature Levels

Figure 7-12 shows the dynamic yield strength and dynamic ultimate strength of 3/8 inch Gr. 50 steel at different temperatures. Below 400°C, ultimate strength did not change much with temperature. From 400°C to 800°C, ultimate strength decreased linearly with temperature from 74 ksi to 8 ksi. Loading rate effects started at 600°C. There was about three ksi difference between ultimate strengths from high and low loading rate tests from 600°C to 800°C. Yield strength dropped at 100°C first and came back at 200°C and 300°C again. From 400°Cto 500°C, it decreased with temperature. Loading rate had unstable effects on yield strength at different temperatures, which varied from 5 ksi at 500°C and 700°C to about 2 ksi at 600°C and 800°C. Figure 7-13 shows the static and dynamic ultimate strengths of 3/8 inch Gr. 50 steel. The static ultimate strength equal to the dynamic $F_u$ minus stress drop in 30 seconds pauses in Table 7-3. From 500°C to 800°C, the static ultimate strength is significantly lower than dynamic ultimate strength.
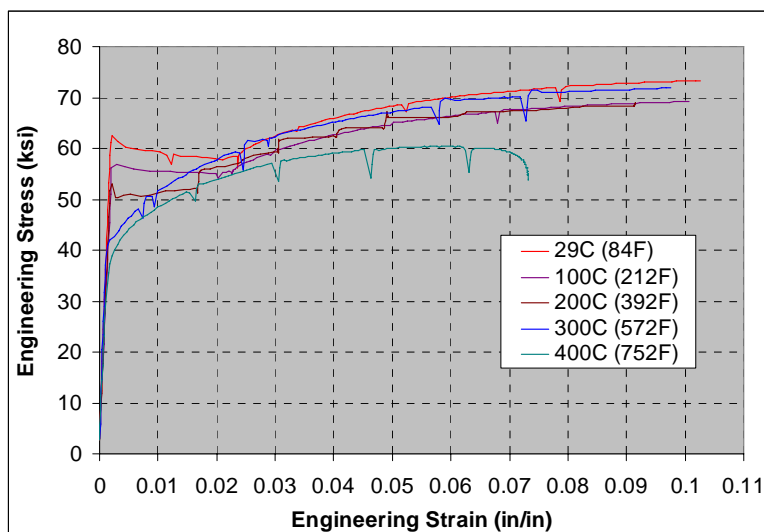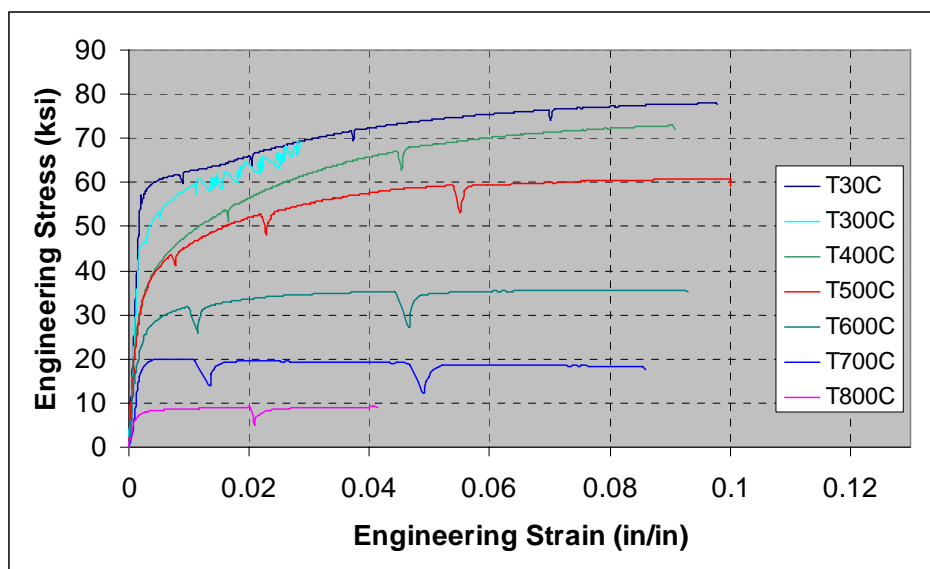


Figure 7-14 Stress-strain Curves of 3/8 inch Gr. 50 Steel at Different Temperatures (Deformation rate = 0.1 in/min)

126

Figure 7-14 shows the stress-strain curves of 3/8 inch Gr. 50. It was a low ductility steel, which had no yield plateau at ambient temperature. As temperature went up to 300°C, the steel entered the hardening phase right after elastic phase. At 400°C, 500°C and 600°C, elastic range got smaller. The difference between yield strength and ultimate strength decreased as well. At 700°C and 800°C, there was no significant hardening at all. During testing, the loading process was suspended several times by freezing the crosshead position for 30 seconds. The V shapes on the stress-strain curve correspond to pauses in loading. At a relatively low temperature range, the V shapes were small. At higher temperature range, the V shapes became larger with a wider opening. That was the result of increased creep and relaxation of steel at high temperature.
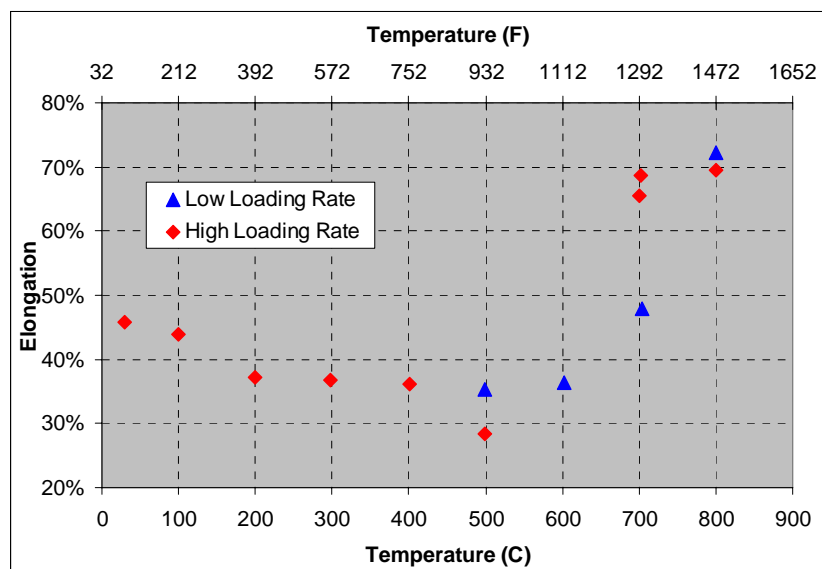


Figure 7-15 Elongation of 3/8 inch Gr. 50 Steel at Different Temperature

Figure 7-15 shows elongation changes over the whole temperature range. Elongations from high and low loading rate tests were presented together. Both groups of data showed the same trends. From 30°C to 500°C, elongation decreased slightly with temperature, which indicated ductility loss in this

127

temperature range. From 500°C to 800°C, elongation increased dramatically with temperature. Figure 7-16 shows area reduction changes with temperature. Area reduction decreased dramatically with temperature from 30°C to 500°C. The high value at 400°C might be an inaccurate data point. From 500°C to 700°C, area reduction increased to its maximum value, which followed by an abrupt drop at 800°C.
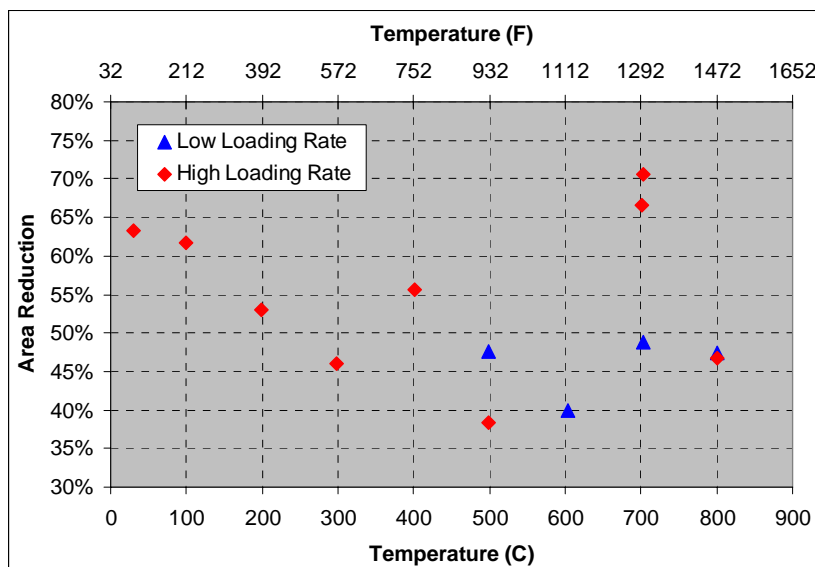


Figure 7-16 Area Reduction of 3/8 inch Gr. 50 Steel at Different Temperature

## 7.4 Comparison of Two Heats of Gr. 50 Steel

Table 7-4 Chemical Composition of Steel

| Heat Description | C (%) | Mn (%) | P (%) | S (%) | Si (%) | Ni (%) | Cr (%) | Mo (%) | Cu (%) |
|---|---|---|---|---|---|---|---|---|---|
| 3/8" Gr. 50 | 0.12 | 0.88 | <0.005 | 0.022 | 0.28 | 0.07 | 0.44 | <0.01 | 0.37 |
| 1/2" Gr. 50 | 0.16 | 0.81 | 0.018 | 0.021 | 0.15 | 0.04 | 0.02 | <0.01 | 0.02 |

Table 7-4 shows the chemical composition of both heats of steel. They have similar content of most elements, except Chromium and Copper. The 3/8 inch Gr. 50 steel had much more Chromium and Copper than 1/2 inch Gr. 50 steel does. Copper does not affect steel strength much at elevated temperatures, while Chromium does. Chromium is the major alloy element of stainless steels for elevated temperature service. (Harold E. McGannon, 1970)
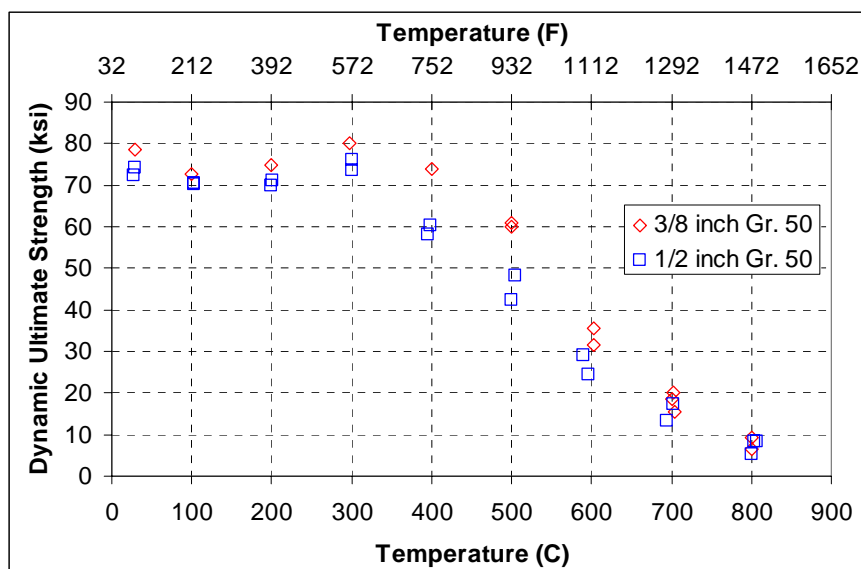


Figure 7-17 Comparison of Dynamic Ultimate Strength of 3/8" and 1/2" Steel

Figure 7-17 shows the dynamic ultimate strength of both heats of steel at elevated temperatures. It was found that both steel behaved similarly. Below 300°C, no significant ultimate strength loss occurred. From 300°C to 800°C, both steels lost their ultimate strength dramatically with temperature. From 400°C to 600°C, 3/8 inch Gr. 50 steel had higher strength than 1/2 inch Gr. 50. Figure 7-18 presents the dynamic yield strength of both steel at elevated temperatures. Yield strength varied in similar way over whole temperature range. It dropped significantly with temperature. The decreasing rate against temperature could be divided into two ranges. From 30°C to 500°C, yield strength dropped at about

four ksi for each 100°C; while from 500°C to 800°C, the decreasing rate increased to about nine ksi each 100°C.
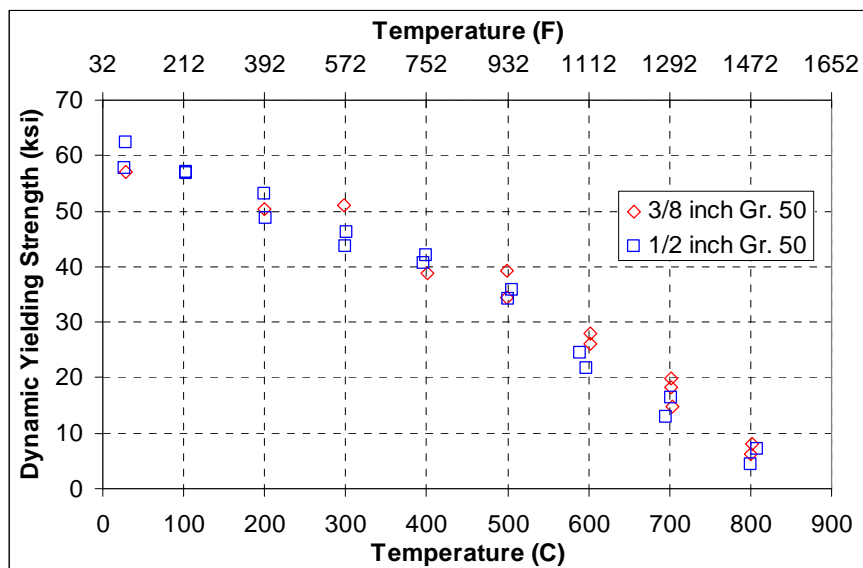


Figure 7-18 Comparison of Dynamic Yield Strength of 3/8" and 1/2" Steel
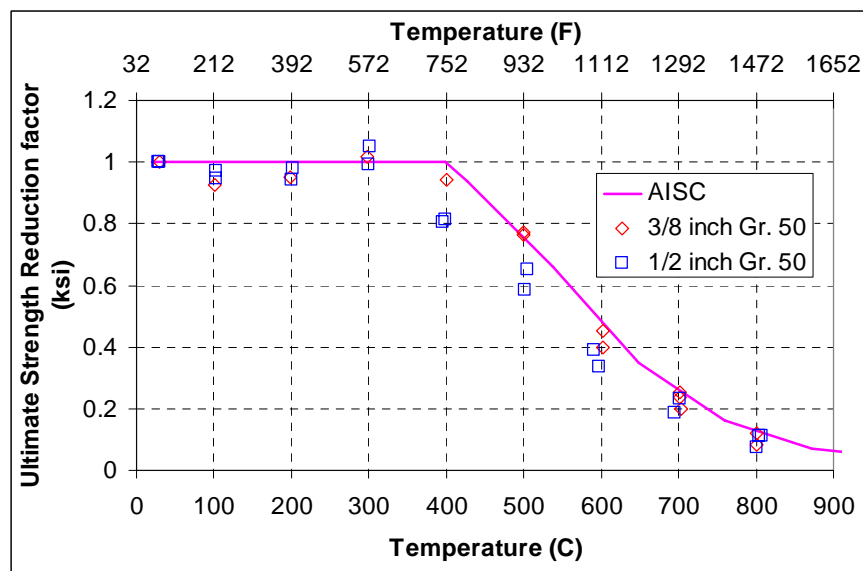


Figure 7-19 Comparison of Dynamic Ultimate Strength Reduction Factor of 3/8 inch and 1/2 inch Steels with AISC Values
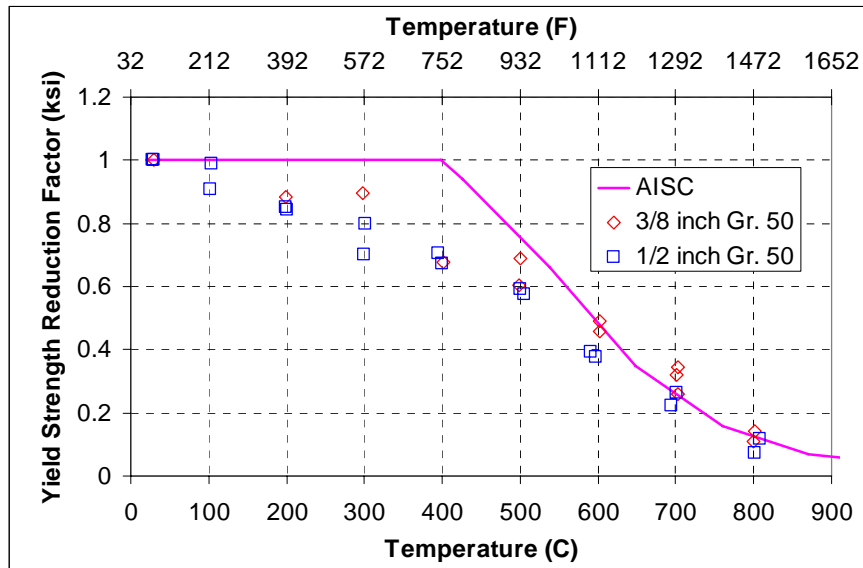
Figure 7-20 Comparison of Dynamic Yield Strength Reduction Factor of 3/8 inch and 1/2 inch Steels with AISC Values

Figure 7-19 compares the dynamic ultimate strength reduction factor of 3/8 inch and 1/2 inch steels at elevated temperature with AISC values. It is shown that AISC is not conservative, especially between 400°C and 600°C. Figure 7-20 compares the dynamic yield strength reduction factors of both steels at elevated temperature with AISC values. AISC over estimates yield strength significantly between 200°C and 600°C.

# Chapter 8

# Behavior of Steel Beams and Composite Beams in Fire

# Finite Element Analysis

Because the mechanical properties of steel and concrete change with temperature, steel beams and composite beams behave quite differently at elevated temperatures compared with their behavior at ambient temperature. The forces in connections change from their original values at ambient temperature. The connection has to be designed to carry different loads at different temperatures. Experimental studies provide a means to determine the capacity of bolted connections at elevated temperature. The forces in connection will be discussed in this chapter. Due to the relatively low strength and Young's modulus of both steel and concrete at elevated temperature, large deformation occurs on beams. Nonlinear Finite Element Analysis is required to assess connection force as temperature changes.

In this chapter, a typical floor beam from a high rise hotel building design was taken as an example (provided by Walter P. Moore). The beam was analyzed as either non-composite or composite beam with both design gravity loads and temperature loads. Beam behavior and connection forces variation with temperature will be compared and discussed. ABAQUS 6.5-1 was used to perform all the Finite Element Analysis.

The purpose of performing Finite Element Analysis on beams is to understand the changes of their behaviors as temperature rises, and provide an estimation of loads on their bolted connections during a fire. Since the details of internal forces distribution in W-shape beams and in concrete slab are not of interest, highly simplified Finite Element models were adopted to minimize calculation time. W-shape steel beams were modeled with beam elements and

132

concrete slabs were modeled with shell elements. Connector elements were used to model shear studs. There are some imperfections associated with these highly simplified models.

1. The local buckling of the lower flange and web of W-shape beams can not be considered;
2. The stiffness and deformation of bolted connections are not revealed;
3. The cracking of concrete slab is not simulated well;
4. The interaction between shear studs and concrete slab is not modeled well; stress concentration occurs at where connector elements joint shell elements;

Despite of these imperfections, the simplified models can still provide reasonably accurate results of forces on bolted connections in fires. Because the purpose of this research is to study beams behavior change after their temperature is raised, no heat conduction analysis was performed. Temperature is applied as load in analysis.

The mesh density was determined by checking the convergence of results. For example, the mesh density of steel beam model was increased by a factor of 2 each time. The mid-span deflection from each mesh was compared. The minimum mesh density, which could provide reasonable close deflection results as finer mesh does, was adopted. For steel beam model, 36 elements were used along the whole span. For composite beam, W-shape beam was meshed into 42 elements and concrete slab was meshed into 62 by 14 elements. The calculation time was less than 20 minutes on a PC with Pentium 3.0GHz processor and 3.5GB RAM.

There are future improvement can be done. Full scale tests of composite and non-composite beams will provide good benchmarks for the validation of Finite Element models. Non-continuous boundary conditions at the edges of concrete slab need be considered because of its popularity. If calculation time and cost are

not considerations, modeling W-shape with shell elements and concrete slab with solid element can serve as a better simulation and overcome the imperfections mentioned above.

Secondary Floor Beam                                        Main Girders



Figure 8-1 Floor Plan
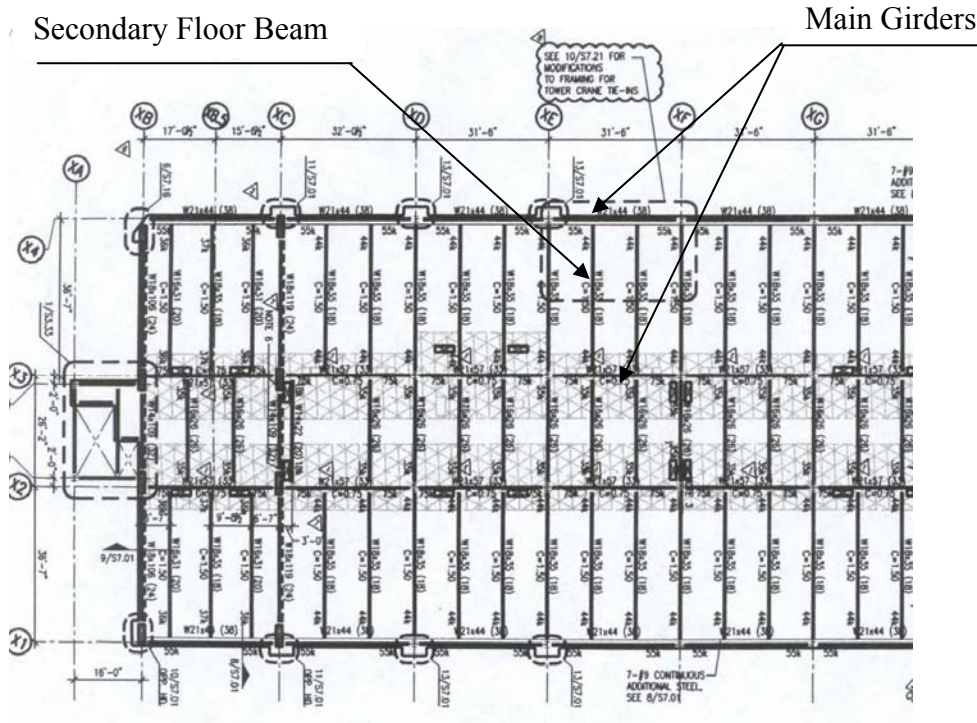


Secondary Beam
W18×35
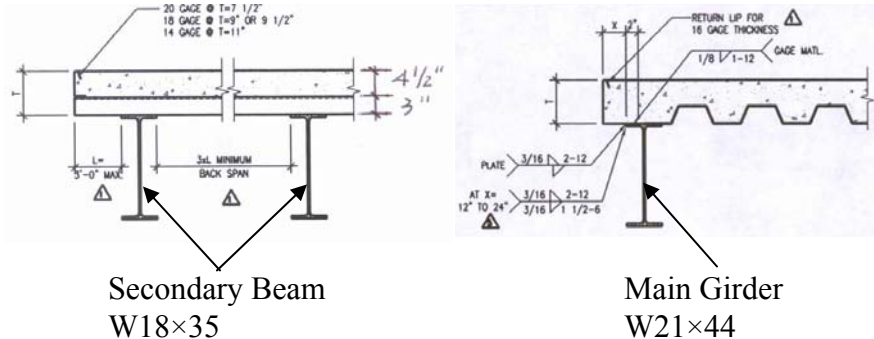
Main Girder
W21×44

Figure 8-2 Details of Composite Floor

## 8.1 Floor Beam Design

As shown in Figure 8-1, the secondary floor beam was selected. It spans 36'-7" between exterior and interior main girders. The steel section is a W18×35 and simply supported at both ends. Figure 8-2 shows the details of the composite floor cross section. Height of the corrugated metal deck is 3 inch and thickness of the concrete slab is 4-1/2 inch. Welded shear studs were not shown here. SFRM (Spray Fire Resistance Material) is specified as fire protection in design.

## 8.2 Material Properties

### 8.2.1 Steel

ASTM 992 or ASTM 572 Grade 50 steel was specified in the original design. Their material properties at elevated temperatures were assumed to be the same as those of the 1/2 inch Grade 50 steel used in block shear tests in this research program. The material properties were obtained from coupon tests at different temperature, which had been presented in Chapter 7. Table 8-1 summaries the material model of steel used in Finite Element Analysis. The engineering stress and strain from coupon test were converted into true stress and true strain. Assuming that both elastic and plastic deformations are incompressible, then

$$\varepsilon_{true} = \ln\left(1 + \varepsilon_{eng}\right) \qquad\qquad (8\text{-}1)$$

$$\sigma_{true} = \sigma_{eng}\left(1 + \varepsilon_{eng}\right) \qquad\qquad (8\text{-}2)$$

$\varepsilon_{eng}$ = Engineering strain;

$\varepsilon_{true}$ = True strain;

$\sigma_{eng}$ = Engineering stress;

$\sigma_{true}$ = True stress;

135

In ABAQUS, an elastic and multi-linear plastic material model was selected for steel, see in Figure 8-3. The Young's modulus at elevated temperature was obtained from the recommended values in AISC Steel Construction Manual (13th Edition). The Poisson's ratio is assumed to be 0.28 in the whole temperature range. Thermal expansion coefficient of steel varies from $1.186 \times 10^{-5}$ /°C at 30°C to $1.596 \times 10^{-5}$ /°C at 800°C (ASCE Manual and Reports, No. 78). AISC Manual takes the average $1.4 \times 10^{-5}$ /°C as thermal expansion coefficient of steel at temperature higher than 65°C. For the calculation here, the AISC value was selected.
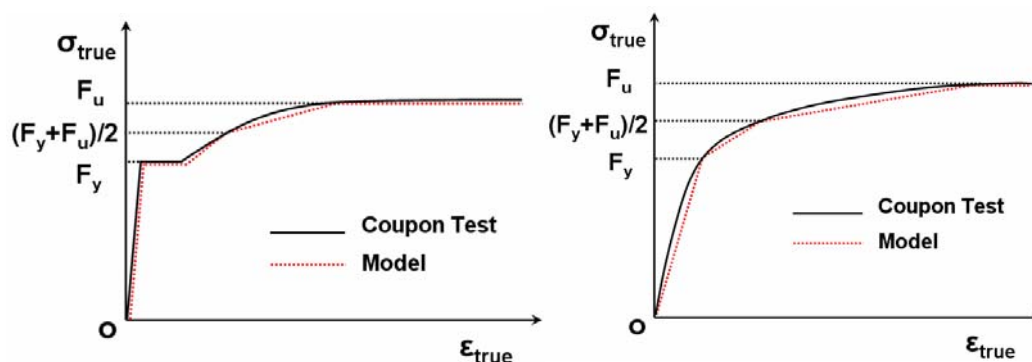


Figure 8-3 Material Models of Structural Steel at Ambient Temperature (left) and Elevated Temperature (right)

### 8.2.2 Concrete

In the original design, the slab concrete was specified to have $f_c' = 3.5ksi$ at ambient temperature. It was assumed that the concrete "yielding strength" is 3.5 ksi and the "ultimate strength" is 5.0 ksi. The recommended properties of concrete at elevated temperature from the AISC Steel Construction Manual (13th Edition) were adopted. Table 8-2 gives the variables for the concrete model at elevated temperature. It is assumed that Poisson's ratio and thermal

expansion coefficient are constant over all temperature ranges, which are 0.15 and $1.8 \times 10^{-5} / °C$ respectively.

Table 8-1 Properties of Steel at Elevated Temperature

| Temperature (°C) | True Fy (ksi) | True Strain at Fy (%) | True Fu (ksi) | True Strain at Fu (%) | Young's Modulus (ksi) |
|---|---|---|---|---|---|
| 29.2 | 62.54 | 0.207 | 85.32 | 13.976 | 29000 |
| 102.7 | 56.96 | 0.295 | 80.76 | 13.976 | 26500 |
| 199.9 | 53.18 | 0.211 | 80.31 | 13.976 | 24700 |
| 300.0 | 43.87 | 0.326 | 84.63 | 13.976 | 20300 |
| 399.1 | 42.30 | 0.453 | 63.97 | 5.796 | 19600 |
| 505.4 | 35.99 | 0.373 | 50.89 | 5.175 | 16300 |
| 590.1 | 24.57 | 0.380 | 29.85 | 2.964 | 11000 |
| 701.6 | 16.45 | 0.321 | 17.36 | 0.847 | 7600 |
| 807.4 | 7.24 | 0.322 | 8.85 | 5.141 | 3600 |

Table 8-2 Properties of Concrete at Elevated Temperature

| Temperature (°C) | Yielding Stress (ksi) | Ultimate Stress (ksi) | Plastic Strain at Ultimate Stress (%) | Young's Modulus (ksi) |
|---|---|---|---|---|
| 20 | 3.500 | 5.000 | 0.1035 | 3412 |
| 93 | 3.325 | 4.750 | 0.1903 | 3173 |
| 204 | 3.150 | 4.500 | 0.2842 | 2559 |
| 288 | 3.010 | 4.300 | 0.3734 | 2081 |
| 316 | 2.905 | 4.150 | 0.4066 | 1945 |
| 427 | 2.485 | 3.550 | 0.5262 | 1297 |
| 538 | 1.890 | 2.700 | 0.6643 | 682 |
| 649 | 1.330 | 1.900 | 0.7147 | 314 |
| 760 | 0.735 | 1.050 | 1.0084 | 249 |
| 871 | 0.350 | 0.500 | 1.2236 | 188 |

**8.2.3 Shear Connectors**

A 3/4 inch diameter by six inch long headed shear stud was chosen to connect the concrete slab with top flange of W shape beam in the original design.

The shear stud strength is determined using the strength equations in the $13^{th}$ Edition of the AISC specifications:

$$Q_n = 0.5 A_{sc} \sqrt{f_c' E_c} \leq R_g R_p A_{sc} F_u \qquad (8\text{-}3)$$

Where $Q_n$ = shear stud strength;

$A_{sc}$ = cross section area of stud;

$E_c$ = Young's modulus of concrete;

$f_c'$ = compressive strength of concrete;

$w$ = concrete density in pound per cubic foot;

$F_u$ = tensile strength of stud;

$R_g$, $R_p$ are reduction factors;

For shear stud orientation and welding method in original design,

$R_g = 0.85$, $R_p = 0.60$

The density of slab concrete is,

$w = 150 lb / ft^3$

$E_c = w^{1.5} \sqrt{f_c'} = 150^{1.5} \times \sqrt{3.5} = 3437 ksi$

Shear stud strength,

$F_u = 60 ksi$

$A_{sc} = \pi \times \left(\dfrac{3}{4}\right)^2 / 4 = 0.442 in^2$

$Q_n = 0.5 A_{sc} \sqrt{f_c' E_c} = 0.5 \times 0.442 \times \sqrt{3.5 \times 3437} = 24.2 kips$

$Q_n < R_g R_p A_{sc} F_u = 0.6 \times 0.85 \times 60 \times 0.442 = 13.5 kips$

$Q_n \leq 0.6 F_u A_{sc} = 0.6 \times 60 \times 0.442 = 15.9 kips$

The room temperature shear stud strength is calculated as 13.5kips.
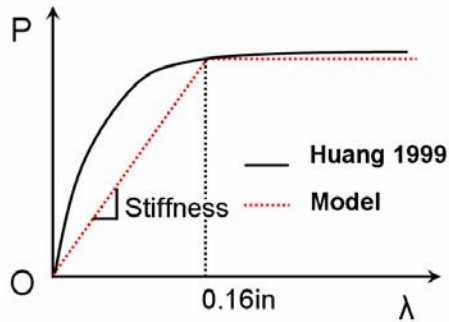
Figure 8-4 Model of Shear Stud Behavior

Since both concrete and steel lose their stiffness and strength as temperature rises, stiffness and strength of shear stud decrease also. Huang (Huang, Burgess, Plank, 1999) gave an empirical formula for the load-slip relationship of shear stud at elevated temperatures, based on the Kruppa and Zhao's (Kruppa and Zhao, 1995) experimental results.

$$P / P_u = A(1.0 - e^{-B\lambda})$$  \hfill (8-4)

Where $P_u = F_u \left( \dfrac{\pi d^2}{4} \right)$ and $\lambda$ is stud deformation.

Table 8-3 Shear Stud Strength and Stiffness at Elevated Temperature

| Temperature (°C) | A | B | Shear Force P (kips) at 0.1575 inch Deformation | Stiffness (P/0.1575) (kip/in) |
|---|---|---|---|---|
| <100 | 1.0000 | 1.2789 | 13.42 | 100.4 |
| 200 | 1.0000 | 1.0297 | 13.42 | 100.4 |
| 300 | 0.9063 | 1.0095 | 13.28 | 99.4 |
| 400 | 0.8567 | 0.9781 | 12.02 | 90.0 |
| 500 | 0.5909 | 0.9163 | 11.33 | 84.8 |
| 600 | 0.3911 | 0.7985 | 7.77 | 58.2 |
| 700 | 0.1964 | 0.9251 | 5.06 | 37.9 |
| 800 | 0.1472 | 0.8967 | 2.59 | 19.4 |

Based on Eq. (8-4), the shear stud strength and stiffness were taken as values in Table 8-3. It is assumed that the stud will not break if subjected to loads and temperature. The temperature of the shear stud is assumed to be the same as the concrete slab. Figure 8-4 shows the bi-linear model of stud behavior in composite beam analysis.

## 8.3 Analysis of Steel Beam

The steel beam was modeled with beam elements in ABAQUS. The beam was simply supported at both ends. Elastic axial constraint was simulated by adding an elastic spring connector, KA, at the roller end. Rotational restraint was simulated with rotational springs, KR, at both ends as shown in Figure 8-5. The analysis was performed in two steps. In the first step, the beam was loaded with evenly distributed gravity loads under ambient temperature. Beam temperature was raised from 30°C (86°F) to 800°C (1472°F) in the second load step with gravity load being kept constant, which simulated the condition in fire event.

The load ratio on beam is defined as the ratio of maximum moment on beam to beam's plastic moment capacity at ambient temperature. $W18 \times 35$ has $M_p$ equals to 346 kip-ft without considering factor $\Phi_b$. In calculating $M_p$, actual yielding strength from material test, $62.4ksi$, was used instead of the nominal yielding strength $50.0ksi$. Figure 8-3 shows the calculation model of $W18 \times 35$ steel beam, in which KA is axial restraint stiffness and KR is rotational restraint stiffness.
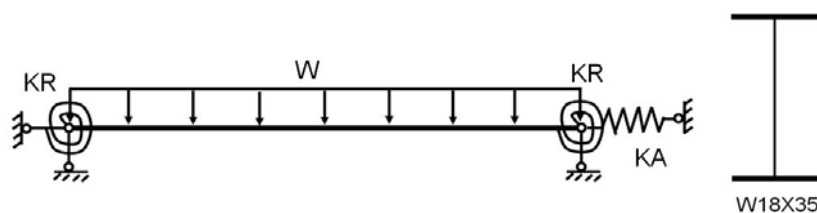


Figure 8-5 Model of Steel Beam

### 8.3.1 Load Ratio

Three load ratios were studied, which were 0.374, 0.624 and 0.874. The load ratio is defined as the ratio of maximum moment in beam to the plastic moment capacity of beam section. The plastic moment capacity of $W18 \times 35$ at ambient temperature:

$$M_p = Z_x F_y = 66.5 \times 50 = 277 kip - ft$$

Load ratio (example of 0.62 kip/ft):

$$LR = \frac{M_{max}}{M_p} = \frac{(1/8)wl^2}{M_p} = \frac{(1/8) \times 0.62 \times (439/12)^2}{277} = 0.374$$

$LR$ = load ratio; $l$ = beam span; $w$ = uniform load on beam;
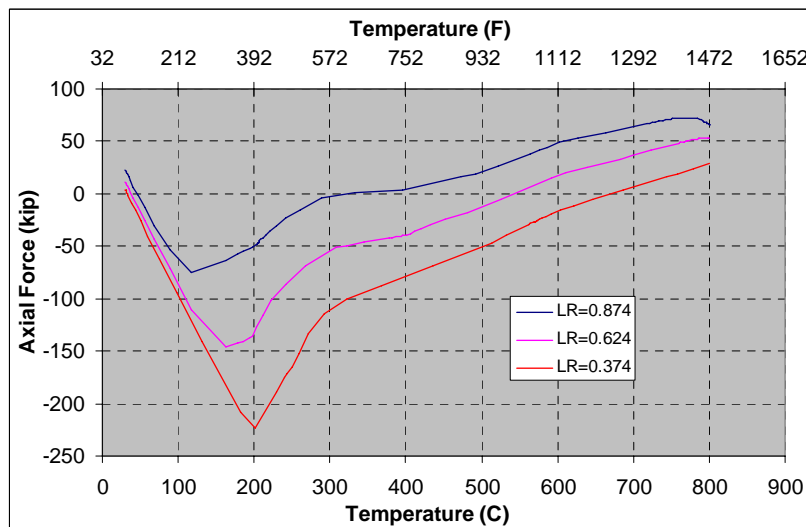


Figure 8-6 Axial Force Changes with Temperature, Different Load Ratios

In steel frame buildings with concrete deck (assume non-composite), the dead load from concrete deck is almost equal or even greater than live load on steel beam. Therefore it is assumed that dead load is 1.2 times of live load,

$$D = 1.2L$$

Based on AISC specification on load combinations, the design loads are:

Normal condition: $1.2D + 1.6L$

Fire: 1.2D+0.5L

Therefore the load ratio is:

$$\frac{q_{normal}}{q_{fire}} = \frac{1.2D + 1.6L}{1.2D + 0.5L} = \frac{1.2(1.2L) + 1.6L}{1.2(1.2L) + 0.5L} = 1.567$$

Table 8-4 Summary of Loads on Non-composite Beam

| Load Ratio to Beam Capacity | Applied Load (kip/ft) | Maximum Moment (kip-ft) | End Shear (kip) | Ratio to Design Load in Fire |
|---|---|---|---|---|
| 0.374 | 0.62 | 103.6 | 11.3 | 0.374×1.567=0.586 |
| 0.624 | 1.03 | 172.8 | 18.8 | 0.624×1.567=0.978 |
| 0.874 | 1.45 | 242.1 | 26.5 | 0.874×1.567=1.370 |
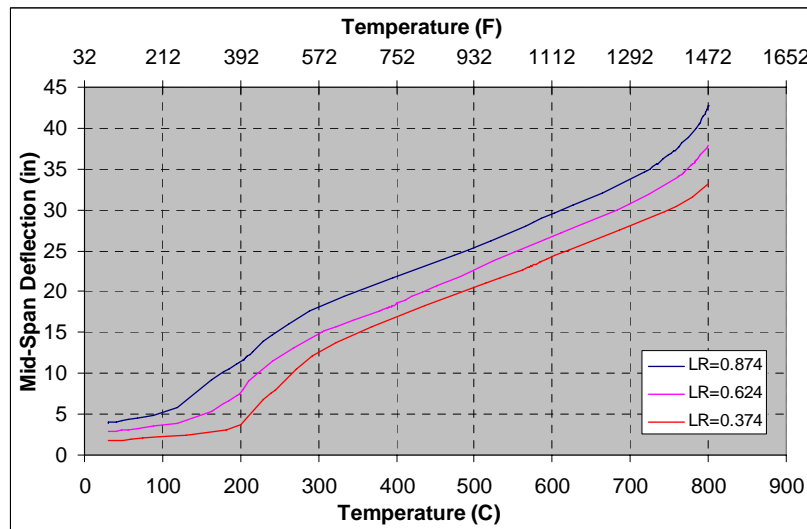


Figure 8-7 Mid-Span Displacement Changes with Temperature

Beams were set to have zero rotational restraint, no temperature gradient through the depth of the section and 400 kip/in axial restraint. Figure 8-6 shows the axial force changes in beam with temperature, in which positive axial force

means tension and negative axial force means compression. From ambient temperature to 200˚C, smaller flexural deflection of the beam with lower load ratio allowed higher compressive force to occur due to thermal expansion. Beams with a higher load ratio had tensile force at lower temperatures than beam with lower load ratio. In Figure 8-6, tensile force occurred in beam with LR=0.7 at about 350˚C; while beam with LR=0.3 did not have axial tensile force until 700˚C. The large tension in the higher load ratios is the result of catenary behavior in the beam at high temperature. Figure 8-7 shows the middle span deflection with temperature. The maximum deflection of LR=0.5 is about 1/12 span. Load ratio affected beam deflection at temperature below 300˚C only. From ambient temperature to 300˚C, the largest increase in rate of deflection was recorded on the beam with the smaller load ratio.

The magnitude of vertical shear force for each load ratio was 26.5kips, 18.8kips and 11.3kips (see Table 8-4), which stayed constant over the whole temperature range. The maximum axial tensile forces that occurred in each load case were 72.1kips, 53.0kips and 28.5kips. For the geometry, loads and boundary conditions of this $W18 \times 35$ beam, the catenary tensile forces were 2.7, 2.8 and 2.5 times of the vertical shear forces for the three load ratios at maximum temperature.

### 8.3.2 Axial Restraint Stiffness

Four axial restraints with different stiffness were studied: 100, 400, 600 and 2000 kips per inch. It was assumed that the beams had zero rotational restraint, zero temperature gradient, and load ratio at 0.624. Figure 8-8 shows the axial force changes in beam with temperature. It was found that the axial restraint could significantly increase axial compressive force in beam below 300˚C. However after axial compressive force surpassed the maximum value and began

143

to decrease, the effects of axial restraint disappeared. The four curves in Figure 8-8 merged together. Figure 8-9 shows the middle span deflection changes with temperature. Beam with stiffer axial restraint has higher axial compression force as the beginning of temperature increase. This force creates extra moment (PΔ effect) at middle span and in larger deflection.
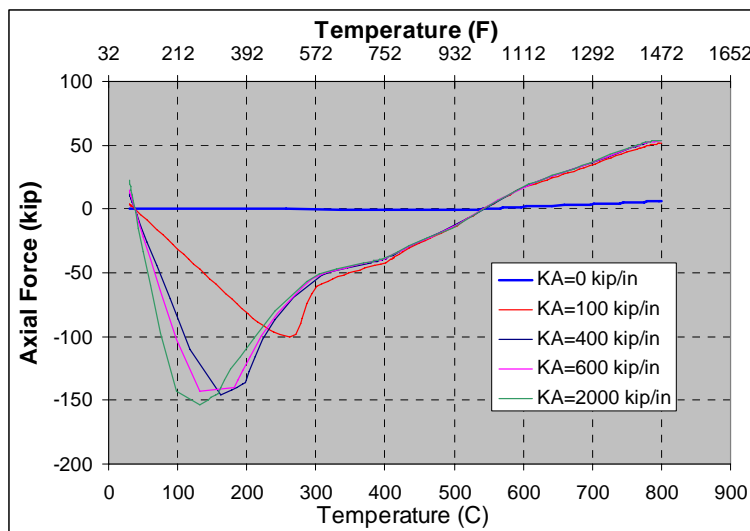


Figure 8-8 Axial Force Changes with Temperature, Different Axial Constraint Stiffness

Figure 8-9 also shows the importance of catenary effect in beam behavior at elevated temperature. When axial restraint stiffness is zero, there is no catenary effect in beam. Beam deflection at mid-span increases dramatically after temperature reaches the temperature, where reduced plastic moment capacity of the beam is equal to the moment at mid span. A plastic hinge is formed and deflection theoretically goes to infinite. On the contrary, beams with axial restraint can have catenary effect, which prevents beam deflection from "run away" above the critical temperature.
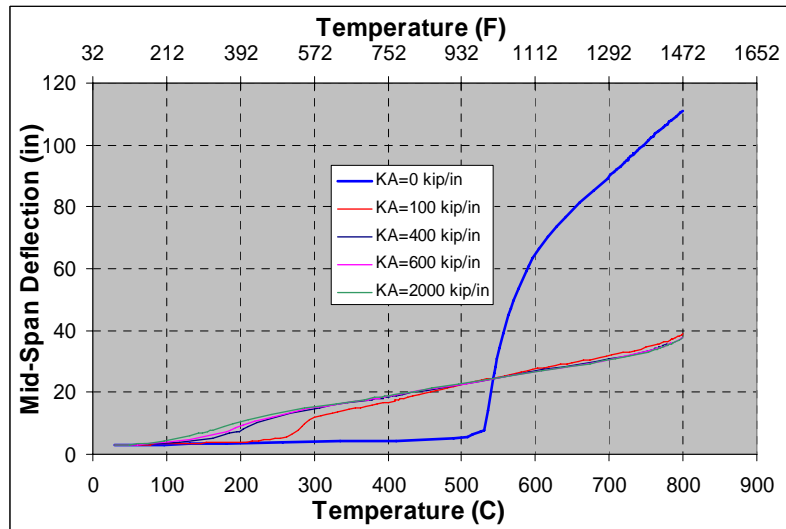
Figure 8-9 Mid-Span Deflection Changes with Temperature, Different Axial Constraint Stiffness

### 8.3.3 Rotational Restraint Stiffness
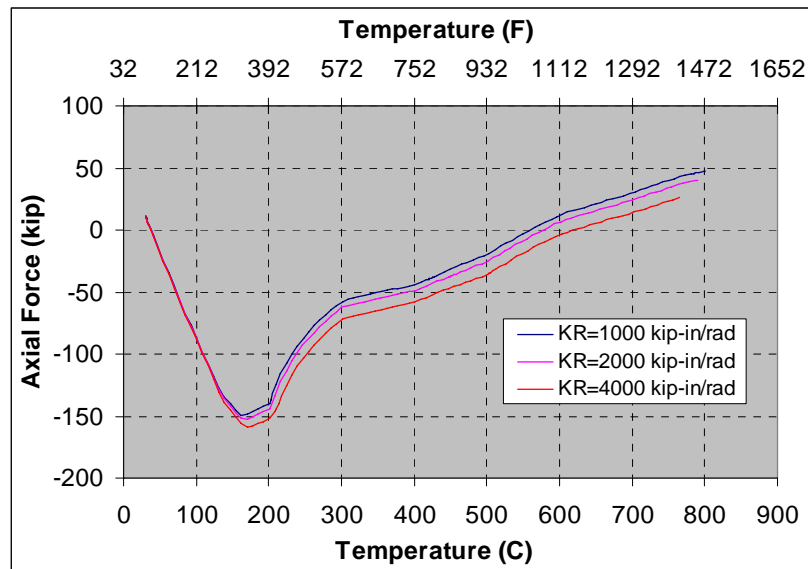


Figure 8-10 Axial Force Changes with Temperature, Different Rotational Restraint Stiffness

Even though the beam connection was designed to be simple connection, it has a certain amount of rotational restraint stiffness. The magnitude varies with connection geometry, manufacture tolerance, and other various uncertain factors. Beams with different rotational restraint stiffness were analyzed and compared here. All the beams were assumed to have zero temperature gradient over depth of the cross section, load ratio of 0.624, and axial restraint of 400 kip/in.

Figure 8-10 shows the axial force change with temperature. Higher rotational restraint stiffness resulted in a smaller increase in compressive force at lower temperatures and decreased in tensile force at higher temperatures.
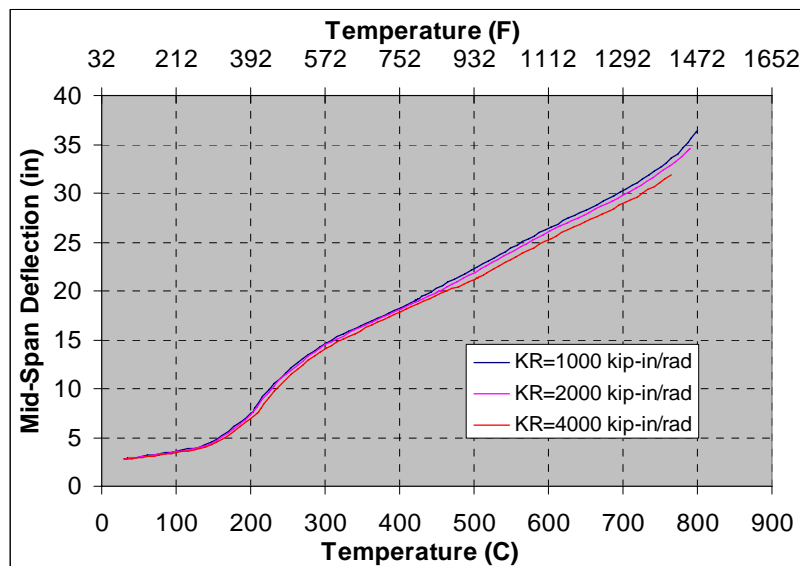


Figure 8-11 Mid-Span Displacement Changes with Temperature, Different Rotational Restraint Stiffness

Figure 8-11 shows the middle span deflection changes with temperature. Stiffer rotational restraints reduce the middle span deflection slightly. Figure 8-12 shows the end moment changes with temperature. Beams with stiffer rotational restraint at their ends have higher end moment.
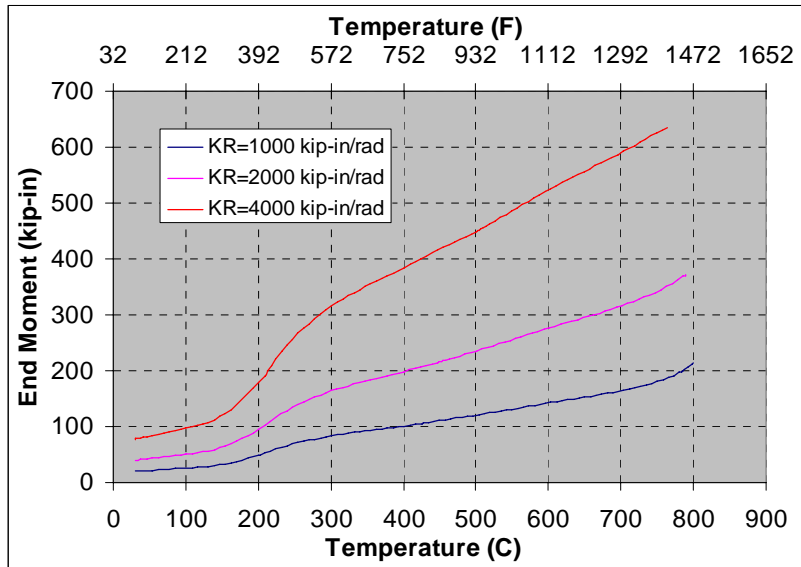
Figure 8-12 End Moment Changes with Temperature, Different Rotational
Restraint Stiffness
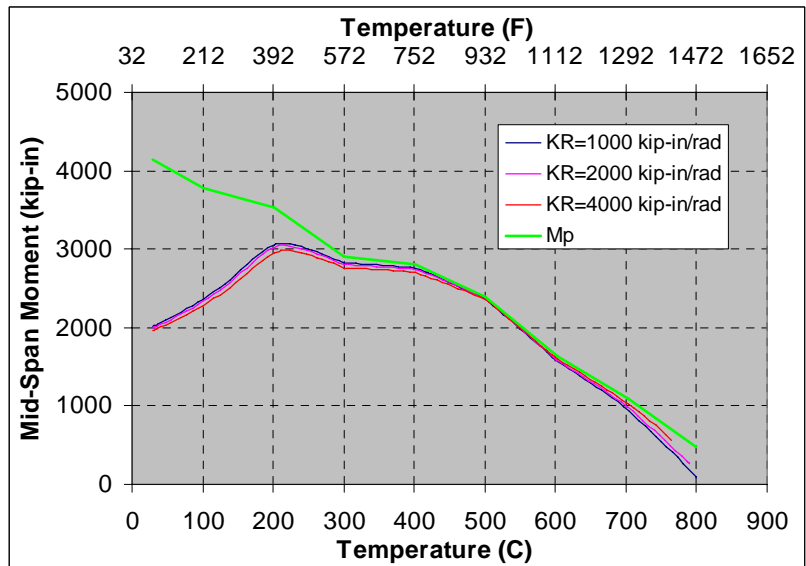


Figure 8-13 Mid-Span Moment Changes with Temperature, Different Rotational
Restraint Stiffness

Figure 8-13 shows the mid-span moment changes with temperature. It is found that rotational restraint stiffness does not affect moment at mid-span much. The reason is that moment in beam at mid-span is affected by not only end moment but also catenary force. Figure 8-14 shows the equilibrium of beam. The relationship between end moment, mid-span moment, catenary force and deflection is $M_m + M_e + T_c\Delta = \frac{1}{8}WL^2$. Higher rotational restraint at beam ends generates higher end moment; however that reduces catenary force and mid-span deflection at the same time. For this example, the magnitude of end moment increase is about the same as decrease in $T_c\Delta$. Therefore mid-span moment in beam does not change much with as rotational restraint stiffness increases.
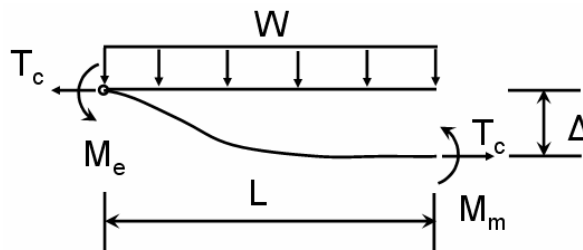


Figure 8-14 Equilibrium Diagrams of Beam

Figure 8-13 shows the plastic moment capacity of the beam at different temperatures also. It is found that a "plastic hinge" is formed at mid-span at 500˚C.

### 8.3.4 Temperature Gradient along the Height of Beam Section

Due to the heat sink effect of concrete deck, a temperature gradient may exist through the depth of the beam cross section, as shown in Figure 8-15. The temperature gradient is defined as $(T_1-T_0)/h$, where h is the section height. Combined with the rotational restraint on beam connections, this temperature gradient generated negative end moment and thermal deflection at middle span.

Beams were assumed to have load ratio of 0.624, axial restraint of 800 kips/in and rotational restraint of 1000 kip-in/radius.
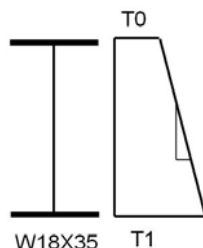


Figure 8-15 Temperature Distribution on Beam Section
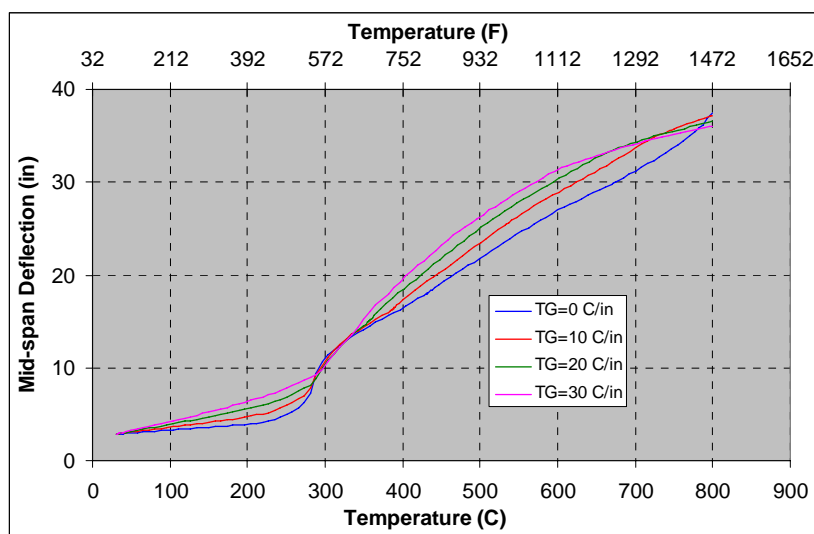


Figure 8-16 Mid-span Deflection changes with Temperature, Different Temperature Gradient

Figure 8-14 shows the middle span deflection of beams with different temperature gradients.  Beams with higher temperature gradient had larger deflection during the entire temperature range except between about 275˚C and 350˚C where mid-span deflection of beams with different temperature gradients merged together. This range corresponds with when the beam axial compressive force passed peak and started to drop, as seen in Figure 8-15. From ambient

149

temperature to about 250°C, higher temperature gradient reduces the thermal expansion of the beam which produces a lower axial compressive force. From 300°C to 400°C, the lower the temperature gradient the faster compressive force dropped. From 400°C to 800°C, higher temperature gradient introduced higher axial tensile force. The axial tensile force converged at about 800°C.
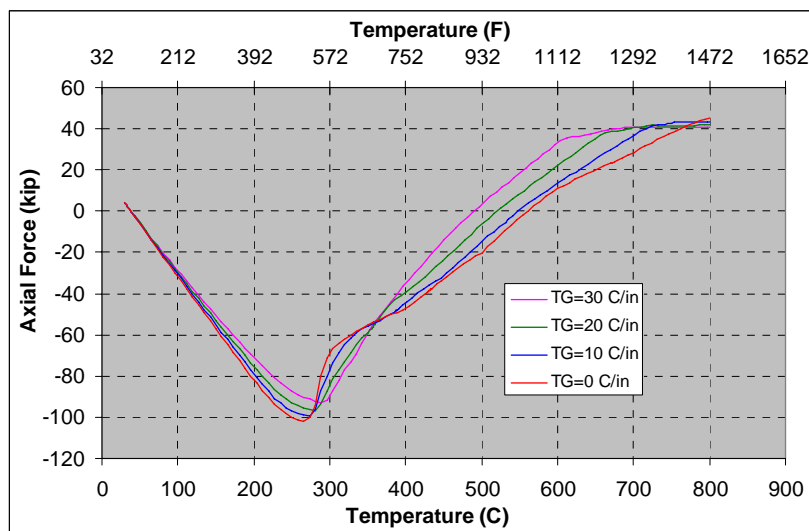


Figure 8-17 Axial Force Changes with Temperature, Different Temperature Gradient

## 8.4 Analysis of Composite Beam
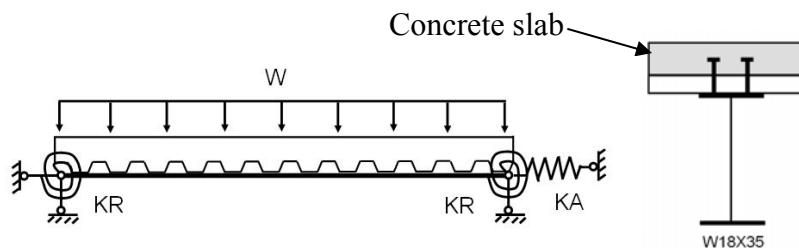


Figure 8-18 Model of Composite Beam and Cross Section

Figure 8-18 shows the composite beam model and cross section. In ABAQUS, beam element was used to model steel beam and shell element was chose to model concrete slab. Shear studs were modeled with connector element. All the boundary restraints were applied on steel beam.

Since concrete slab has a large heat capacity, its temperature is not as high as steel beam in most fire events. It is assumed that the steel beam temperature rises four times faster than temperature of concrete deck. In other word, the concrete slab temperature is 1/4 the temperature of lower flange of steel beam. The temperature of the steel beam was uniform in the initial studies.

### 8.4.1 Load Ratio

The load ratio is defined as the ratio of maximum moment in beam to plastic moment capacity of composite section.

Effective width of concrete deck is the smaller of 1/4 span and beam spacing: $b_e = 109.75in$

Determine plastic neutral axis position:

$0.85 f_c' A_{con} = 0.85 \times 3.5 \times 109.75 \times 4.5 = 1469 kips$

$A_s F_y = 10.3 \times 50 = 515 kips < 1469 kips$

Neutral axis locates in concrete deck.

Depth of concrete in compression at limit state:

$$a = \frac{A_s F_y}{0.85 f_c' b_e} = \frac{515}{0.85 \times 3.5 \times 109.75} = 1.58in$$

Plastic moment capacity of composite section is:

$$M_p = A_s F_y (d/2 + h_{deck} + t_s - a/2)$$

Here the metal deck height is:

$$h_{deck} = 3in$$

151

Concrete deck thickness is:

$t_s = 4.5in$,

$M_p = 515 \times (17.7/2 + 3 + 4.5 - 1.58/2) = 8013.4kip - in = 667.8kip - ft$

Load ratio (example of 1.462 kip/ft):

$$LR = \frac{M_{max}}{M_p} = \frac{(1/8)wl^2}{M_p} = \frac{(1/8) \times 1.462 \times (439/12)^2}{667.8} = 0.366$$

$LR$ = load ratio; $l$ = beam span; $w$ = uniform load on beam;

In steel frame buildings with composite floors, the dead load of concrete deck is almost equal to or even greater than live load. Therefore, it is assumed that dead load is 1.2 times of live load.

$D = 1.2L$

Under normal condition, design load on beam is: $1.2D + 1.6L$

In fire, reduced load combination is used: 1.2D+0.5L

Therefore the load ratio is:

$$\frac{q_{normal}}{q_{fire}} = \frac{1.2D + 1.6L}{1.2D + 0.5L} = \frac{1.2(1.2L) + 1.6L}{1.2(1.2L) + 0.5L} = 1.567$$

Table 8-5 Summary of Loads on Composite Beam

| Load Ratio to Beam Capacity | Applied Load (kip/ft) | Maximum Moment (kip-ft) | End Shear (kip) | Ratio to Design Load in Fire |
|---|---|---|---|---|
| 0.366 | 1.462 | 244.6 | 26.7 | 0.366×1.567=0.574 |
| 0.488 | 1.949 | 326.1 | 35.7 | 0.488×1.567=0.765 |
| 0.610 | 2.436 | 407.5 | 44.6 | 0.610×1.567=0.956 |

Figure 8-19 shows the axial force changes in composite beam with steel section temperature, in which positive axial force means tension and negative axial force means compression. All these composite beams had axial restraint of 800 kip/in, zero rotational restraint and zero temperature gradient over steel beam section. It was found that load ratio did not affect the axial force in composite

beam significantly. No tension forces were developed in the beams. Figure 8-20 shows the middle span deflection of steel beam and composite beam at different temperatures. Compared with steel beam, composite beam had smaller deflection due to the moment of inertia of the composite section.
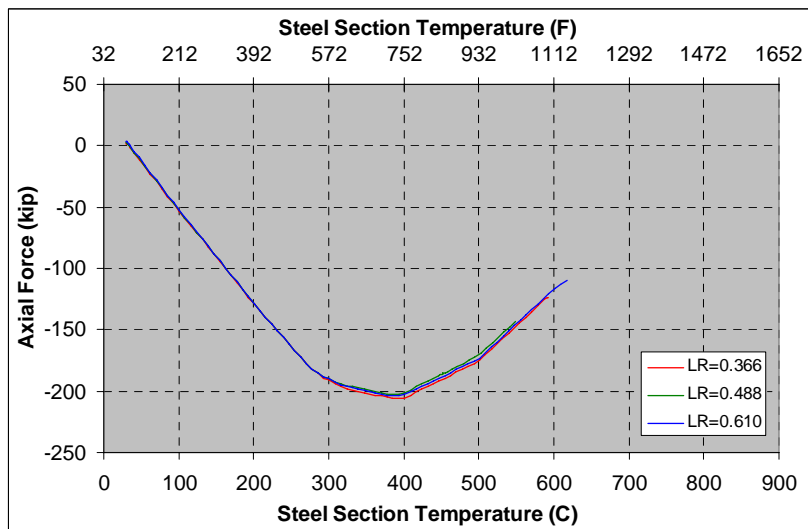


Figure 8-19 Axial Forces Changes with Steel Section Temperature, Different Loading Ratio
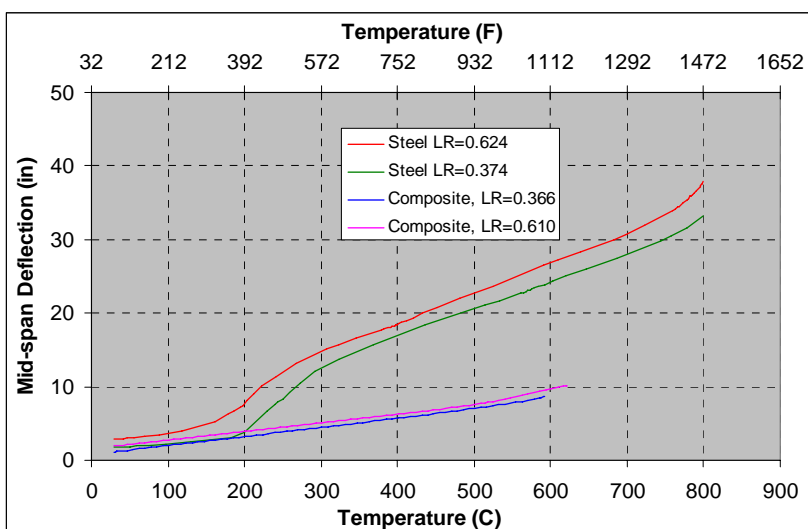


Figure 8-20 Mid-Span Deflection with Temperature of Steel and Composite Beam

### 8.4.2 Axial Restraint Stiffness

Axial restraints with different stiffness were applied to roller end of composite beams. Figure 8-19 shows the axial force changes with temperature in composite beams with different axial restraints. All these composite beams had loading ratio of 0.610, zero rotational restraint, and zero temperature gradient over the steel beam section. The axial restraint stiffness had a significant effect upon the magnitude of axial compression force in the composite beams. Thermal expansion, combined with higher axial restraint stiffness, resulted in higher compressive force in beam. However after the compression started to decrease as a result of beam deformation, axial restraint stiffness showed no effects when the compression force started to decrease as the tensile forces in composite beam started to develop.
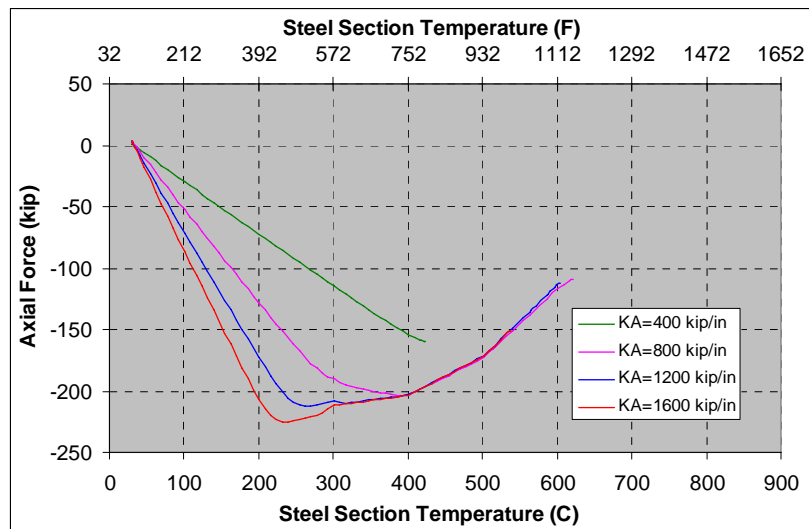


Figure 8-21 Axial Force Changes with Temperature, Different Axial Restraint Stiffness

### 8.4.3 Rotational Restraint Stiffness

Rotational restraints with different stiffness were added to both ends of composite beam model. All these composite beams had loading ratio of 0.610, axial restraint of 800 kip/in, and zero temperature gradient over steel section. Figure 8-20 shows the axial force changes with temperature. It was found that rotational restraint had no effects on compression force when it was increasing. After axial compressive force started to decrease, higher rotational restraint stiffness delayed its rate of decrease. However this effect was quite limited.
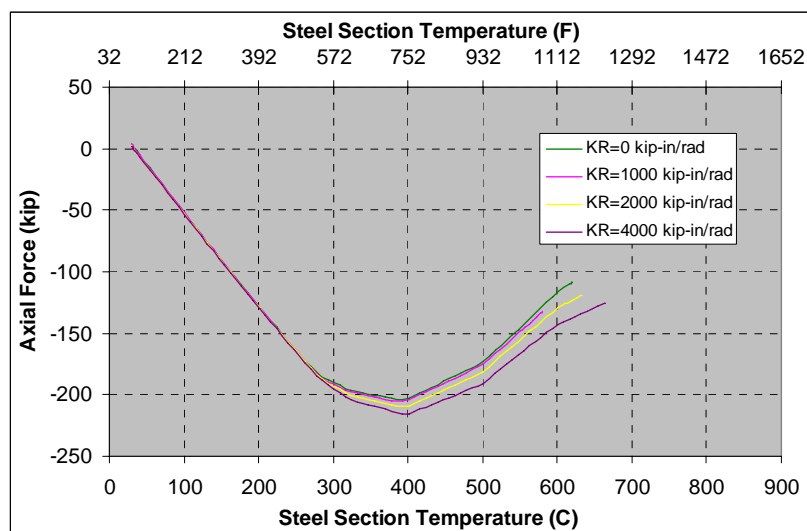


Figure 8-22 Axial Force Changes with Temperature, Different Rotational Restraint Stiffness

### 8.4.4 Temperature Gradient along the Height of Beam Section

Different temperature gradients along the height of the steel beam section were applied to composite beam model, while the concrete slab temperature was still assumed to be uniform through its depth and equal to 1/4 the temperature of lower flange of steel beam. The temperature gradient is shown in Figure 8-21. All

the composite beams had a load ratio of 0.610, axial restraint of 800 kip/in, and zero rotational restraint. Figure 8-22 shows the axial force changes with temperature in composite beams with different temperature gradient in steel section. The higher the temperature gradient, the earlier the axial compression force reached its maximum and began to drop.
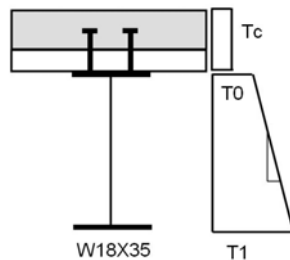


Figure 8-23 Temperature Distribution on Composite Beam Section
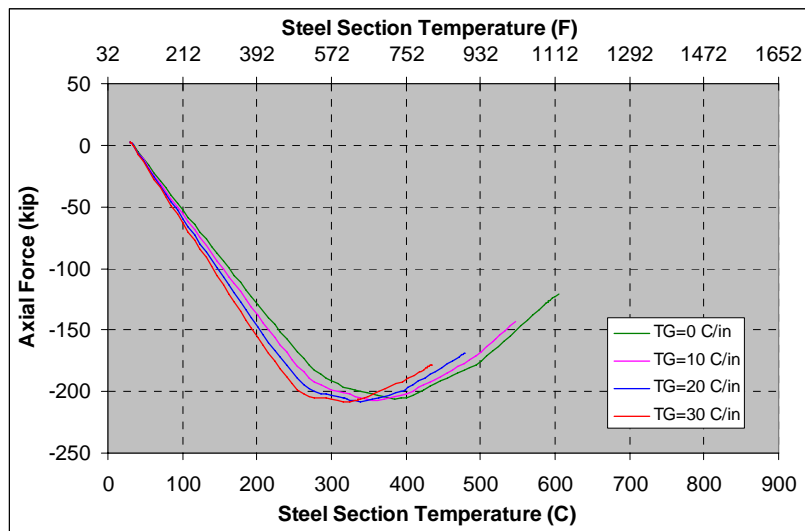


Figure 8-24 Axial Force Changes with Temperature, Different Temperature Gradient through Steel Section

156

## 8.5 Summary

Under gravity loads and temperature loads, steel beam can have deflection as large as 1/12 of beam span. Catenary effect plays an important role in beam behavior. Axial tensile force, as high as 2.5 to 3 times the maximum vertical shear force, may occur in beam. However axial tensile force was not found in composite beam.

Among boundary restraints and temperature gradient, only axial restraint had significant effects on axial compressive force in beam at the beginning of temperature increasing. The rest had limited effect on beam behavior.

From Finite Element Analysis, the beam end forces were obtained in both vertical and horizontal direction. If the beam is assumed to be simply supported, then beam end rotates freely. Figure 8-23 (left) shows the relationship of support reaction forces $R_v$, $R_h$ and beam tension $T$ and shear $V$. However simple connection has significant moment capacity. In fire, this rotation constraint induces local buckling near connection in the lower flange, as shown in Figure 8-23 (right). Therefore vertical reaction force is taken as vertical shear force and horizontal reaction force as tension force on the connection.
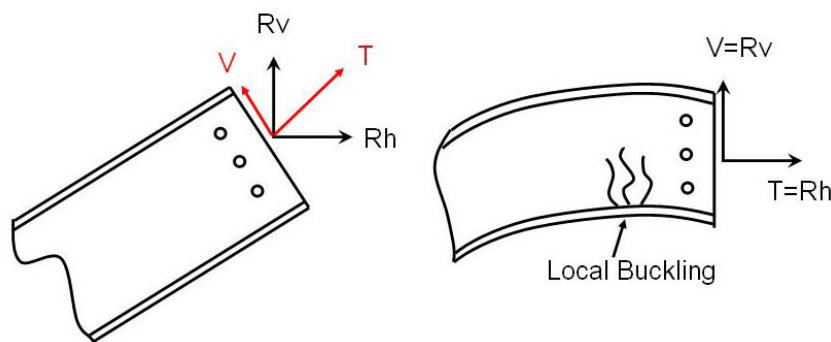


Figure 8-25 Beam End Rotation and Connection Forces

# Chapter 9

## Bolt Connection Design at Elevated Temperature

This chapter summarizes the strength reduction factor for A325, A490 bolt and Grade 50 steel at elevated temperature. Methods for determining bearing capacity, block shear capacity, and bolt shear capacity are put forward and compared with connection test results. The connection on the typical floor beam design example used in Chapter 8 was checked at elevated temperature for safety.

### 9.1 Strength Reduction Factors of Bolt at Elevated Temperature

As discussed in Chapter 4, shear strength of A325 and A490 bolts varied with temperature. Strength reduction factors are defined as dividing the shear capacity of bolt at each elevated temperature level with its shear capacity at ambient temperature. Table 9-1 shows the shear strength reduction factors for A325 and A490 bolts at each tested temperature level. The averaged shear capacity at ambient temperature was taken as the control value $V_c$. The actual temperatures and shear capacities of tests at each temperature level were averaged to stand for shear capacity $V_t$ at that averaged temperature $T_a$. Then the shear strength reduction factor at temperature $T_a$ is calculated as $V_t/V_c$. If $V_t/V_c$ is greater than 1.0, then it is assumed to be 1.0. Linear interpolation method will be used in determining the reduction factor at a temperature between adjacent test temperatures.

As discussed in Chapter 2, the bolt strength is estimated very conservatively in current AISC Manual. For example, ASTM A325 specifies A325 bolt have 120ksi minimum tensile strength when bolt diameter is 1.0 inch or less. In AISC, the nominal shear strength of A325 and A490 bolt is taken as

0.62F$_u$, where F$_u$ is the minimum tensile strength. Strength reduction factor 0.8 is introduced for considering non-evenly load distribution among bolts in long connections. For shear, $\Phi_v$ equals to 0.75. Therefore the design bolt strength is only 0.8×0.75=0.6 of its minimum strength manufactured. Compare the bolt strength reduction factor at elevated temperatures, A325 and A490 bolt will be safe up to 400˚C and 500˚C even if their capacities were fully used in design.

Table 9-1 Shear Strength Reduction Factor of Bolts

| A325 | | | A490 | | |
|---|---|---|---|---|---|
| Temperature($T_a$) | | Reduction | Temperature($T_a$) | | Reduction |
| ˚C | ˚F | Factor | ˚C | ˚F | Factor |
| 25 | 77 | 1.00 | 32 | 89 | 1.00 |
| 99 | 209 | 0.96 | 101 | 214 | 0.91 |
| 202 | 396 | 1.00 | 200 | 393 | 0.95 |
| 300 | 572 | 1.00 | 301 | 573 | 1.00 |
| 403 | 757 | 0.61 | 400 | 752 | 0.83 |
| 506 | 943 | 0.36 | 502 | 935 | 0.60 |
| 600 | 1112 | 0.21 | 600 | 1111 | 0.34 |
| 705 | 1301 | 0.12 | 702 | 1295 | 0.16 |
| 803 | 1477 | 0.10 | 801 | 1475 | 0.14 |

**9.2 Strength Reduction Factors of Bolt Post Exposure to Elevated Temperature**

After exposure to temperatures higher than tempering temperature during the manufacture process, bolts suffered strength loss after being cooled to ambient temperature. Single shear test results have been presented in Chapter 5. The average shear capacity of the bolts, which had been exposed to ambient temperature only, was taken as control value $V_{rc}$. From single shear test, the residual shear capacities of the bolts that had been exposed to each elevated temperature level were averaged as the residual shear capacity of bolt $V_{rt}$. The

159

maximum temperature that the bolt had been exposed to was averaged as $T_{a,\max}$.
Then post exposure to temperature $T_{a,\max}$ is calculated as $V_{rt}/V_{rc}$. Shear strength
reduction factor is taken as 1.0 if $V_{rt}/V_{rc}$ is greater than one. Table 9-2 gives the
reduction factor of residual shear capacity of both bolts.

Table 9-2 Residual Shear Strength Reduction Factor

| A325 | | | A490 | | |
|---|---|---|---|---|---|
| Maximum Exposure | | Reduction Factor | Maximum Exposure | | Reduction Factor |
| °C | °F | | °C | °F | |
| 25 | 77 | 1.00 | 32 | 89 | 1.00 |
| 99 | 209 | 1.00 | 101 | 214 | 0.98 |
| 202 | 396 | 1.00 | 200 | 393 | 0.97 |
| 300 | 572 | 1.00 | 301 | 573 | 0.98 |
| 403 | 757 | 0.98 | 400 | 752 | 0.97 |
| 506 | 943 | 0.91 | 502 | 935 | 0.98 |
| 600 | 1112 | 0.81 | 600 | 1111 | 0.80 |
| 705 | 1301 | 0.67 | 702 | 1295 | 0.67 |
| 803 | 1477 | 0.58 | 801 | 1475 | 0.58 |

**9.3 Slip Capacity Reduction Factors of A490 Bolt Connection Post Exposure
to Elevated Temperature**

Chapter 5 presented the residual slip resistance capacity of fully tightened
A490 bolt connections after exposure to elevated temperatures. The slip resistance
reduction factor is defined as the ratio between residual slip resistance post
exposure to elevated temperature and the original slip resistance. The average slip
resistance of control specimen connections was taken as the original slip
resistance. Table 9-3 gives the slip resistance reduction factors of A490 bolt
connection post exposure at different elevated temperature levels. Even the
factors are named as slip resistance reduction factors; they are greater than 1.0 at
temperature from 100˚C to 400˚C.

Table 9-3 Slip resistance Reduction Factor

| Maximum Exposure Temperature | | Slip Resistance Reduction Factor |
|---|---|---|
| (˚C) | (˚F) | |
| 33 | 91 | 1.00 |
| 100 | 212 | 1.40 |
| 200 | 392 | 1.57 |
| 300 | 572 | 1.55 |
| 400 | 752 | 1.46 |
| 500 | 932 | 0.57 |
| 630 | 1166 | 0.21 |
| 700 | 1292 | 0.28 |
| 800 | 1472 | 0.11 |

**9.4 Properties of Grade 50 Steel at Elevated Temperature**

**9.4.1 1/2 inch Grade 50 Steel**

As presented in Chapter 7, the material properties of 1/2 inch Grade 50 steel were determined from coupon test at elevated temperature with high and low rates loading. Load rate affected dynamic yield strength and dynamic ultimate strength, which was found to be relatively more significant at temperature above 500˚C. Therefore the results from both loading rate tests were used here to represent material properties of the 1/2 inch Grade 50 Steel. Table 9-4 gives the ratio of dynamic yield strength and dynamic ultimate strength at each temperature level to its ambient temperature values. The ratio is named as reduction factor for design purpose. The data in clear background cells were from high loading rate tests and those in shaded cells were from low loading rate tests. The reduction factors for each loading rate were base on the room temperature values under the same loading rate.

Table 9-4 Material Properties of 1/2 inch Grade 50 Steel at Elevated Temperature

| Temperature ˚C (˚F) | Yield Strength, $F_y$ (ksi) | Ultimate Strength, $F_u$ (ksi) | Reduction Factor of $F_y$ | Reduction Factor of $F_u$ |
|---|---|---|---|---|
| 29.2 (84.6) | 62.41 | 74.19 | 1.00 | 1.00 |
| 102.7 (216.9) | 56.79 | 70.23 | 0.95 | 0.91 |
| 199.9 (391.8) | 53.07 | 69.83 | 0.94 | 0.85 |
| 300.0 (572.0) | 40.90 | 73.59 | 0.99 | 0.70 |
| 399.1 (750.4) | 33.47 | 60.36 | 0.81 | 0.67 |
| 505.4 (941.7) | 26.34 | 48.32 | 0.65 | 0.57 |
| 590.1 (1094.2) | 16.84 | 28.98 | 0.39 | 0.39 |
| 701.6 (1294.9) | 13.88 | 17.21 | 0.23 | 0.26 |
| 807.4 (1485.3) | 6.23 | 8.41 | 0.11 | 0.12 |
| 27.7 (81.9) | 57.85 | 72.39 | 1.00 | 1.00 |
| 103.2 (217.8) | 57.11 | 70.37 | 0.99 | 0.97 |
| 201.1 (394.0) | 48.69 | 70.99 | 0.84 | 0.98 |
| 300.8 (573.4) | 40.09 | 76.16 | 0.80 | 1.05 |
| 395.5 (743.9) | 28.57 | 58.22 | 0.70 | 0.80 |
| 500.5 (932.9) | 21.98 | 42.26 | 0.59 | 0.58 |
| 596.8 (1106.2) | 11.47 | 24.32 | 0.38 | 0.34 |
| 695.0 (1283.0) | 7.19 | 13.38 | 0.22 | 0.18 |
| 800.5 (1472.9) | 3.30 | 5.29 | 0.07 | 0.07 |

**9.4.2 3/8 inch Grade 50 Steel**

Table 9-5 gives the reduction factors of dynamic yield strength and dynamic ultimate strength of 3/8 inch Grade 50 steel at each elevated temperature level. The methodology of test and calculation of reduction factors are the same as those for 1/2 inch Grade 50 steel except that only high loading rate results were present here.

Table 9-5 Material Properties of 3/8 inch Grade 50 Steel at Elevated Temperature

| Temperature ˚C (˚F) | Yield Strength, $F_y$ (ksi) | Ultimate Strength, $F_u$ (ksi) | Reduction Factor of $F_y$ | Reduction Factor of $F_u$ |
|---|---|---|---|---|
| 29.3 (84.7) | 57.07 | 78.56 | 1.00 | 1.00 |
| 100.2 (212.4) | N/A | 72.78 | N/A | 0.93 |
| 199.0 (390.2) | 50.37 | 74.86 | 0.88 | 0.95 |
| 298.1 (568.6) | 51.06 | 80.07 | 0.89 | 1.02 |
| 400.7 (753.3) | 38.74 | 74.07 | 0.68 | 0.94 |
| 499.7 (931.5) | 39.23 | 60.80 | 0.69 | 0.77 |
| 602.9 (1117.2) | 27.89 | 35.57 | 0.49 | 0.45 |
| 701.2 (1294.2) | 18.25 | 18.53 | 0.32 | 0.24 |
| 702.2 (1296.0) | 19.76 | 20.00 | 0.35 | 0.25 |
| 801.0 (1473.8) | 8.02 | 9.36 | 0.14 | 0.12 |

## 9.5 Design of Bolted Connections at Elevated Temperature

## 9.5.1 Bearing Failure

In the AISC Steel Construction Manual (13th Edition), the bearing strength of standard size bolt hole is specified as:

$$R_n = 1.2L_c tF_u \leq 2.4dtF_u \tag{9-1}$$

$d$ = nominal bolt diameter, inch.

$F_u$ = specified minimum tensile strength of the connected material, ksi.

$L_c$ = clear distance, in the direction of the force, between the edge of the hole and the edge of the adjacent hole or edge of the material, inch.

$t$ = thickness of connected material, inch.

Eq. (9-1) is valid when deformation at the bolt hole at service load is a design consideration. If it is not a design consideration, Eq. (9-2) can be used.

$$R_n = 1.5L_c tF_u \leq 3.0dtF_u \tag{9-2}$$

The above design equations are specified for use at ambient temperature only. They were developed based on experimental data. A theoretical model was developed to deal with the end tear-out failure mode, see Figure 9-1.



Theoretical Failure Block
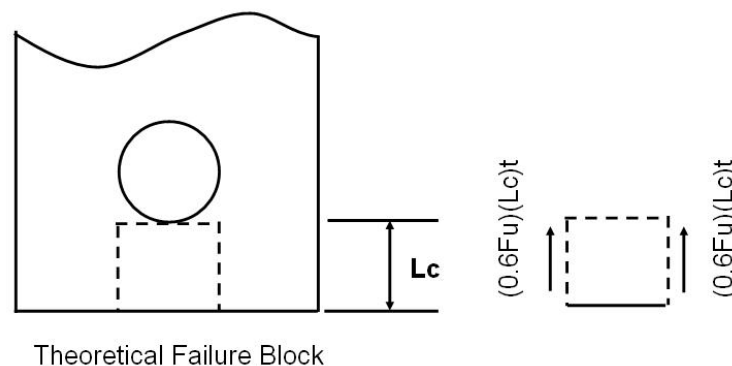
Figure 9-1 Theoretical Bearing Failure Mechanism

Therefore,

$$R_n = 2 \times (0.6F_u)L_c t = 1.2L_c tF_u \qquad (9\text{-}3)$$

At elevated temperature, the bearing failures were controlled by the same failure mechanism as at ambient temperature. This point was supported by the bearing failure occurred in single bolt connection tests shown in Chapter 6.

In Table 9-6, the measured dynamic ultimate strength of 3/8 inch Grade 50 steel at each temperature level was submitted into Eq. (9-1) to calculate bearing strength at that temperature and compared with corresponding test results. The dynamic ultimate strength from high deformation rate coupon tests were chose because both the tested connection and coupon failed in similar amount of time. That indicates similar strain rate existed on connection's bearing failure paths and coupon's reduced section. The measured clear end distance and plate thickness were used instead of their nominal values. It is found that Eq. (9-1) gives conservative estimation of bearing strength in the whole temperature range with about the same amount of safety margin.

Figure 9-2 and Figure 9-3 show the ratio of tested bearing capacity to ultimate strength at different temperature. In calculating $1.2(L_c)t$ and $1.5(L_c)t$, nominal values of $L_c$ and $t$ were used.

$$L_c = \begin{cases} 1.0d - 0.5(d + 1/16) = 13/32^{"} \\ 1.5d - 0.5(d + 1/16) = 27/32^{"} \end{cases}$$

$t = 3/8^{"}$

$d$ = nominal diameter of bolt, inch.
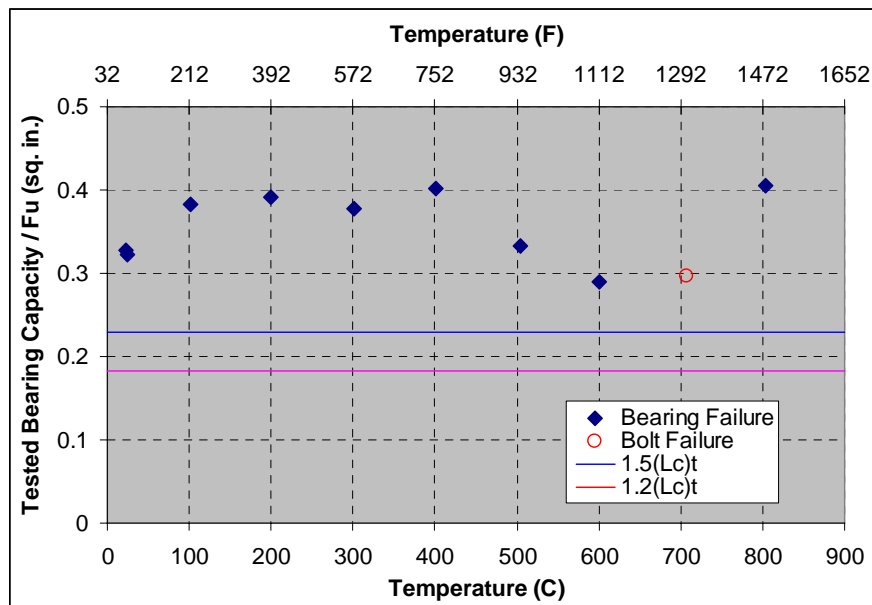


Figure 9-2 Ratio of Bearing Capacity (1.0d) to Ultimate Strength vs. Temperature

Table 9-6 Predicted Bearing Strength vs. Single Bolt Connection Test Results

| Test Name | Test Temperature (°F) | (°C) | Measured Lc (in) | Measured t (in) | Material Test Fu (ksi) | Bearing Strength, Eq. (9-1), (kip) | Load Capacity (kips) | Failure Mode |
|---|---|---|---|---|---|---|---|---|
| SC-T25-D10-1 | 72 | 22 | 0.410 | 0.365 | 78.56 | 14.11 | 25.8 | Bearing |
| SC-T25-D10-2 | 75 | 24 | 0.388 | 0.360 | 78.56 | 13.17 | 25.3 | Bearing |
| SC-T100-D10 | 214 | 101 | 0.493 | 0.365 | 72.78 | 15.72 | 27.9 | Bearing |
| SC-T200-D10 | 392 | 200 | 0.472 | 0.366 | 74.86 | 15.52 | 29.3 | Bearing |
| SC-T300-D10 | 574 | 301 | 0.420 | 0.363 | 80.07 | 14.65 | 30.2 | Bearing |
| SC-T400-D10 | 754 | 401 | 0.508 | 0.363 | 74.07 | 16.39 | 29.7 | Bearing |
| SC-T500-D10 | 939 | 504 | 0.476 | 0.365 | 60.80 | 12.68 | 20.2 | Bearing |
| SC-T600-D10 | 1112 | 600 | 0.401 | 0.386 | 35.57 | 6.61 | 10.3 | Bearing |
| SC-T700-D10 | 1305 | 707 | 0.488 | 0.364 | 18.53 | 3.95 | 5.5 | Shear |
| SC-T800-D10 | 1479 | 804 | 0.474 | 0.364 | 9.36 | 1.94 | 3.8 | Bearing |
| SC-T25-D15-1 | 75 | 24 | 0.843 | 0.368 | 78.56 | 29.25 | 40.8 | Bearing |
| SC-T25-D15-2 | 77 | 25 | 0.894 | 0.366 | 78.56 | 30.85 | 42.8 | Bearing |
| SC-T100-D15 | 216 | 102 | 0.902 | 0.363 | 72.78 | 28.60 | 42.8 | Bearing |
| SC-T200-D15 | 390 | 199 | 0.906 | 0.365 | 74.86 | 29.71 | 43.7 | Bearing |
| SC-T300-D15 | 574 | 301 | 0.850 | 0.369 | 80.07 | 30.14 | 46.4 | Bearing |
| SC-T400-D15 | 752 | 400 | 0.924 | 0.367 | 74.07 | 30.14 | 39.0 | Shear |
| SC-T500-D15 | 934 | 501 | 0.911 | 0.364 | 60.80 | 24.19 | 23.6 | Shear |
| SC-T600-D15- | 1112 | 600 | 0.848 | 0.365 | 35.57 | 13.21 | 11.9 | Shear |
| SC-T600-D15- | 1116 | 602 | 0.860 | 0.365 | 35.57 | 13.40 | 8.6 | Shear |
| SC-T700-D15 | 1294 | 701 | 0.905 | 0.362 | 18.53 | 7.28 | 6.0 | Shear |
| SC-T800-D15 | 1481 | 805 | 0.906 | 0.362 | 9.36 | 3.68 | 4.9 | Shear |
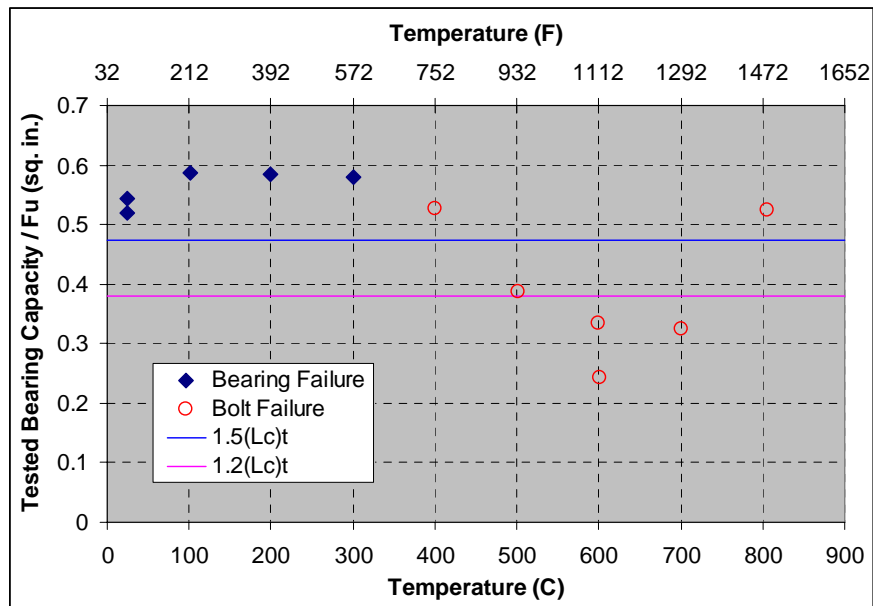
Figure 9-3 Ratio of Bearing Capacity (1.5d) to Ultimate Strength vs. Temperature

The design formula offers conservative results of bearing capacity of bolt hole with 1.0d end distance. For 1.5d end distance, design formula provided a better estimation. This could be explained by the difference between theoretical and practical failure path. When the plate of steel has good ductility, the failure paths are as shown in the left of Figure 9-4. The practical failure path is longer than the theoretical one. The absolute difference is between zero and 0.5d. The smaller the end distance, the larger percentage the error is. However in AISC Steel Construction Manual, the minimum end distance (from center of bolt hole to edge) for 7/8 inch diameter bolt is 1.5 inch, which is greater than 1.5d. It is still acceptable to use this formula. The right part in Figure 9-5 shows the failure path when steel is in its brittle temperature range, 200˚F to 600˚F. The bearing failure paths have a flare angle, which increases the length difference between theoretical

167

and practical failure paths. Therefore in this temperature range, the design formula predicts a more conservative value.
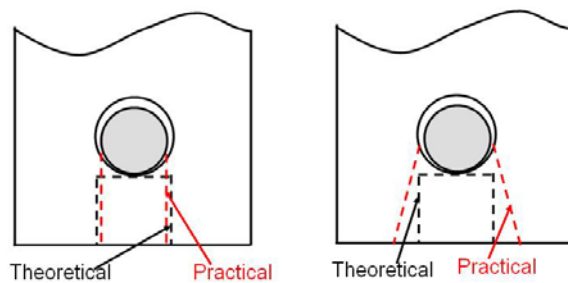


Figure 9-4 Theoretical and Practical Bearing Paths
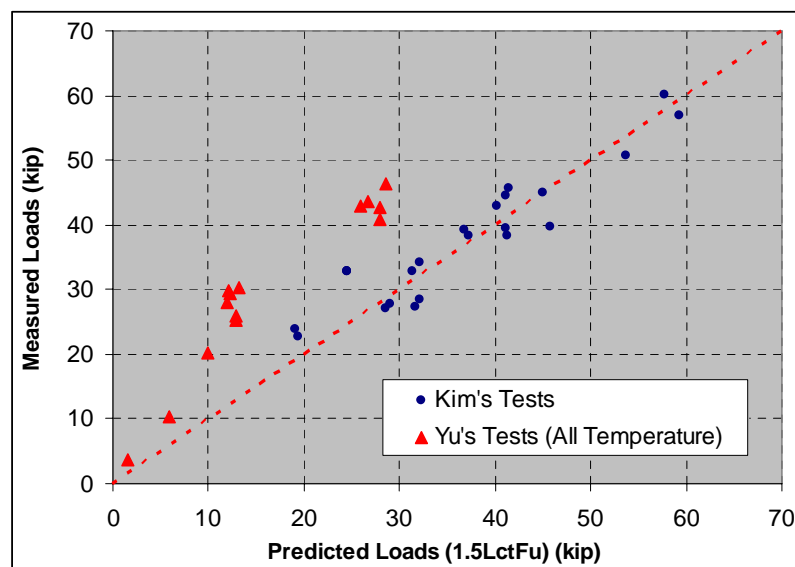


Figure 9-5 Compare of Measured and Predicted Bearing Strength at Ultimate (Kim and Yura, 1996)

Figure 9-5 compares present test results with Kim's test results. It is shown that Kim's results agree with predicted values better than present test results. The reason could be the clamping force in bolt. Kim removed the nut from bolt to avoid any influence from clamping force, while Yu had bolt nut snug tight. Local bearing deformation near bolt hole results in plate thickness increase and

168

generate tension force in bolt. Even though the current design formula, Eq. (9-1) and Eq. (9-2), gave conservative results; it is still acceptable to use it to determine bearing strength at elevated temperatures with the ultimate strength of steel at the same temperature.

### 9.5.2 Block Shear Failure

In the AISC Steel Construction Manual (13$^{th}$ Edition), the block shear is specified as:

$$R_n = 0.6F_u A_{nv} + U_{bs}F_u A_{nt} \leq 0.6F_y A_{gv} + U_{bs}F_u A_{nt} \qquad (9\text{-}4)$$

$A_{gv}$ = Gross area subject to shear, in$^2$.

$A_{nt}$ = Net area subject to tension, in$^2$.

$A_{nv}$ = Net area subject to shear, in$^2$.

$U_{bs}$ = Tension stress distribution factor, which is 1.0 when tension stress is uniform and 0.5 when tension stress is non-uniform.

Figure 9-6 compares the predicted block shear load with test results. Eq. (9-4) gives conservative predictions at all the temperature levels except 700˚C, compared to constant temperature test results. The safety margin varies from 25.5% to 7.9%. For constant load tests, Eq. (9-4) is conservative at 75 kips and 60 kips but slightly unsafe at 33 kips.

Table 9-7 gives the comparison of block shear capacity that is predicted by Eq. (9-4) and the test results. Net shear area and net tension were calculated with measured dimensions, but not according to AISC manual specification and nominal dimensions. The dynamic ultimate strength from high deformation rate coupon tests were chosen since the loading and deformation rates of the coupon tests closely matched the connection rates.

169
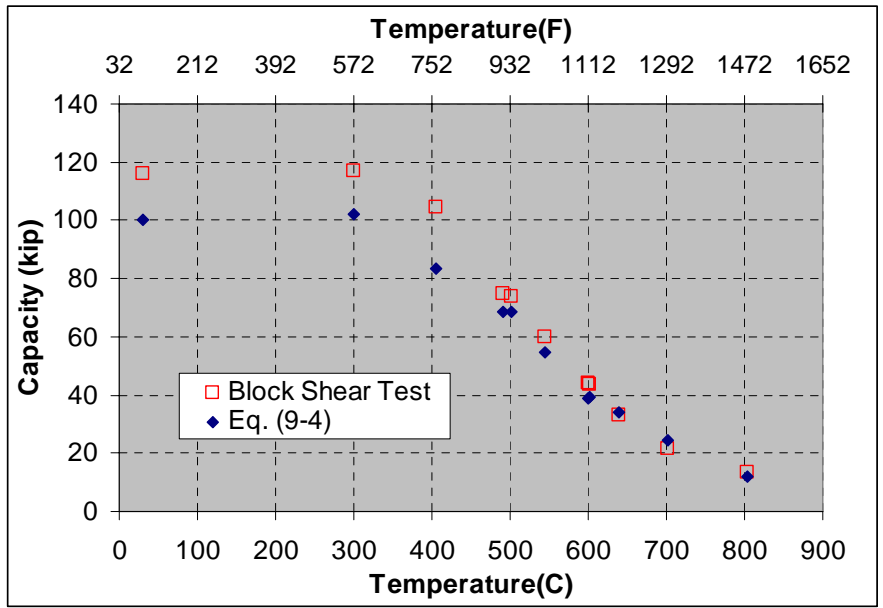
Figure 9-6 Predicted Block Shear Load vs. Test Results

Table 9-7 Predicted Block Shear Strength vs. Twin Bolt Connection Test Results

| Test Name | Temperature | | Measured Clear End Distance Lc (in) | Measured Clear Space Between Holes Lb (in) | Measured Plate Thickness t (in) | Measured Ultimate Strength (ksi) | Eq. (9-4) (kip) | Tested Capacity (kip) | Ratio of Tested capacity to Eq. (9-4) |
| | ˚C | ˚F | | | | | | | |
|---|---|---|---|---|---|---|---|---|---|
| Ambient | 30.0 | 86.0 | (1.395) | (1.031) | (0.500) | 74.19 | 100.34 | 116.0 | 1.156 |
| TC-T300-CT | 299.6 | 571.2 | 1.404 | 1.076 | 0.516 | 73.59 | 102.34 | 116.8 | 1.141 |
| TC-T400-CT | 405.4 | 761.7 | 1.398 | 1.038 | 0.523 | 60.36 | 83.45 | 104.7 | 1.255 |
| TC-T500-CT | 502.3 | 936.1 | 1.406 | 1.057 | 0.530 | 48.32 | 68.49 | 73.9 | 1.079 |
| TC-T600-CT- | 600.5 | 1112.9 | 1.391 | 1.035 | 0.529 | 27.93* | 38.90 | 44.2 | 1.136 |
| TC-T600-CT- | 600.9 | 1113.6 | 1.440 | 1.044 | 0.524 | 27.93* | 39.41 | 43.6 | 1.106 |
| TC-T700-CT | 701.9 | 1295.4 | 1.421 | 1.050 | 0.533 | 17.21 | 24.59 | 21.4 | 0.870 |
| TC-T800-CT | 804.3 | 1479.8 | 1.411 | 1.049 | 0.531 | 8.41 | 11.92 | 13.3 | 1.116 |
| TC-L75-CL | 491.6 | 916.9 | 1.383 | 1.033 | 0.523 | 49.88* | 68.42 | 75.0 | 1.096 |
| TC-L60-CL | 544.9 | 1012.8 | 1.383 | 1.043 | 0.530 | 39.30* | 54.88 | 60.0 | 1.093 |
| TC-L33-CL | 639.5 | 1183.2 | 1.401 | 1.057 | 0.534 | 23.77* | 33.88 | 33.0 | 0.974 |

1. Ultimate strength denoted by * was obtained by linear interpellation and dimensions in ( ) were nominal design value.

2. Ultimate strength was from high loading rate coupon tests.

3. $A_{nv} = 2L_c t$, $A_{nt} = L_b t$.

171

**9.6 Design Example**

**9.6.1 Forces in Connection**

In Chapter 8, a typical floor beam in a high rise hotel building was analyzed with Finite Element Method in order to determine the forces in its connections at elevated temperatures. Both non-composite and composite cases will be used for connection safety check in this part. AISC Steel Construction Manual (13$^{th}$ Edition) specifies the load reduction under fire condition as,

$$[0.9 \, or \, 1.2]D + 0.5L$$

$D$ = nominal dead load.

$L$ = nominal occupancy live load.

Based on this load combination, the forces at the end of composite beam were calculated as shown in Table 9-8.

Table 9-8 Composite Beam End Forces at Elevated Temperature

| Temperature ˚C (˚F) | Shear Force (kip) | Axial Force (kip) | Temperature ˚C (˚F) | Shear Force (kip) | Axial Force (kip) |
|---|---|---|---|---|---|
| 30 (86) | 26.1 | 2.1 | 500 (932) | 26.1 | -176.2 |
| 100 (212) | 26.1 | -52.9 | 600 (1112) | 26.1 | -121.7 |
| 200 (392) | 26.1 | -128.4 | 700 (1292) | 26.1 | -75.2 |
| 300 (572) | 26.1 | -190.5 | 800 (1472) | 26.1 | -51.9 |
| 400 (752) | 26.1 | -204.2 | | | |

Note: Negative is compression and positive is tension.

The axial force here is the total force on composite section. According to the equivalent area ratio, the axial force on the steel beam section could calculated as,

$$F_{steel} = \frac{A_s}{A_{con,eq} + A_s} F$$

$F_{steel}$ = axial force in steel beam

172

$A_s$ = steel beam cross section area

$A_{con,eq}$ = equivalent concrete cross section area

$F$ = total axial force in composite beam

Here

$$\frac{A_s}{A_{con,eq} + A_s} = 0.149$$

Table 9-9 Steel Beam End Forces at Elevated Temperature

| Temperature ˚C (˚F) | Shear Force (kip) | Axial Force (kip) | Temperature ˚C (˚F) | Shear Force (kip) | Axial Force (kip) |
|---|---|---|---|---|---|
| 30 (86) | 26.1 | 7.7 | 500 (932) | 26.1 | 17.2 |
| 100 (212) | 26.1 | -27.0 | 600 (1112) | 26.1 | 42.5 |
| 200 (392) | 26.1 | -62.9 | 700 (1292) | 26.1 | 57.9 |
| 300 (572) | 26.1 | -4.6 | 800 (1472) | 26.1 | 63.9 |
| 400 (752) | 26.1 | 1.4 | | | |

Note: Negative is compression and positive is tension.

## 9.6.2 Connection Design

Figure 9-7 shows the connection design of W18 × 35 floor beams. Four ASTM A325 bolts with one inch diameter and standard holes were used. At ambient temperature, there is vertical shear force on the connection only. At elevated temperature, both vertical shear force and horizontal force exist simultaneously on the connection. Block shear capacity, bearing capacity and bolt shear capacity need to be verified.

## 9.6.2.1 Ambient Temperature

Single shear capacity of 1 inch A325 bolt is:

(AISC manual, assume threads is included in shear plane)

$$\Phi_v r_n = 28.3 kips$$

Shear capacity of 4 bolts is:

$$\Phi R_n = 4 \times 28.3 = 113.2 kips$$

Block shear capacity of beam web is:

$$R_n = 0.6 F_u A_{nv} + U_{bs} F_u A_{nt} < 0.6 F_y A_{gv} + U_{bs} F_u A_{nt}$$

$$A_{nt} = 0.281 in^2, A_{nv} = 1.969 in^2, A_{gv} = 3.150 in^2$$

$$\Phi R_n = 0.75 \times 95.1 = 71.3 kips$$

With the design load combination under normal condition, the shear force in connection is:

$$V_{max} = 40.9 kips$$

This shear force is only 57% of beam web's block shear capacity and 36% of bolts' shear capacity. The connection design is quite conservative.
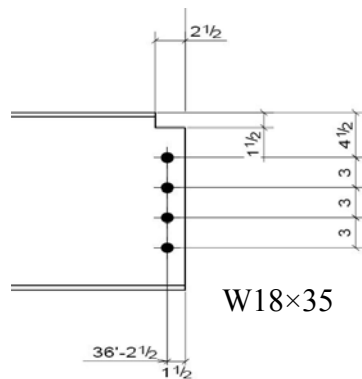


Figure 9-7 Connection Dimensions

### 9.6.2.2 Elevated Temperature

- **Block Shear Capacity:**

    From Eq. (9-4)

    $$R_n = 0.6 F_u A_{nv} + U_{bs} F_u A_{nt} < 0.6 F_y A_{gv} + U_{bs} F_u A_{nt}$$

    $F_u$ is the ultimate strength at checking temperature.

There are two possible block shear failure modes. One is under horizontal tensile force and the other is under the combination of horizontal tensile and vertical shear forces.

Under horizontal tensile force, the block shear failure path is shown in Figure 9-8. The net tension area, net shear area, and gross shear area are shown below:

$$A_{nt} = 1.688in^2, A_{nv} = 0.563in^2, A_{gv} = 0.9in^2$$
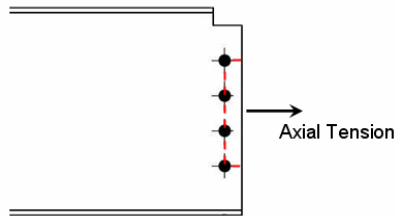


Figure 9-8 Block Shear Paths under Axial Tension Force

Under the combination of horizontal and vertical force, the block shear failure path is shown in the right of Figure 9-8.
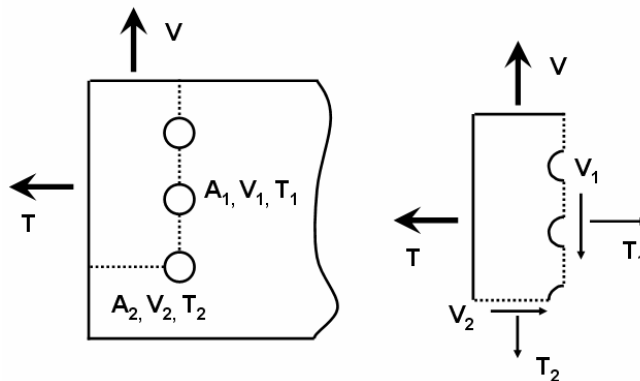


Figure 9-9 Block Shear under Orthogonal Forces

T and V are forces on the block at two orthogonal directions, as shown in Figure 9-9. Let the net area of two failure paths be $A_1$ and $A_2$. Net area $A_1$ carries

shear force $V_1$ and tension force $T_1$; net area $A_2$ carries shear force $V_2$ and tension force $T_2$.

$$V = V_1 + T_2 \tag{9-5}$$

$$T = V_2 + T_1 \tag{9-6}$$

Based on AISC block shear design formula,

$$R_n = 0.6 A_{nv} F_u + A_{nt} F_u \tag{9-7}$$

Block shear capacity consists of shear capacity on net shear area $0.6 A_{nv} F_u$ and tensile capacity on net tensile area $A_{nt} F_u$. The ratio of shear capacity and tensile capacity is $0.6 A_{nv} / A_{nt}$. Therefore it is reasonable to assume that both $V$ and $T$ be distributed on their shear and tension paths by the ratio of $0.6 A_{nv}$ to $A_{nt}$. The factor of 0.6 comes from the Von Mises theory, which has shear strength equal to $\sqrt{3}/3 (= 0.577 \approx 0.6)$ time tensile strength. Therefore,

$$\frac{V_1}{T_2} = \frac{(\sqrt{3}/3)A_1}{A_2} \tag{9-8}$$

$$\frac{T_1}{V_2} = \frac{A_1}{(\sqrt{3}/3)A_2} \tag{9-9}$$

Submit (9-8) and (9-9) into (9-5) and (9-6), then:

$$V_1 = \frac{(\sqrt{3}/3)A_1}{(\sqrt{3}/3)A_1 + A_2} V \tag{9-10}$$

$$T_2 = \frac{A_2}{(\sqrt{3}/3)A_1 + A_2} V \tag{9-11}$$

$$T_1 = \frac{A_1}{A_1 + (\sqrt{3}/3) A_2} T \tag{9-12}$$

$$V_2 = \frac{(\sqrt{3}/3)A_2}{A_1 + (\sqrt{3}/3)A_2} T \tag{9-13}$$

176

Assume that tension and shear forces distribute evenly across net area $A_1$ and $A_2$.
Then

$$\sigma_1 = \frac{T_1}{A_1} = \frac{1}{A_1 + (\sqrt{3}/3)A_2}T \tag{9-14}$$

$$\tau_1 = \frac{V_1}{A_1} = \frac{(\sqrt{3}/3)}{(\sqrt{3}/3)A_1 + A_2}V \tag{9-15}$$

$$\sigma_2 = \frac{T_2}{A_2} = \frac{1}{(\sqrt{3}/3)A_1 + A_2}V \tag{9-16}$$

$$\tau_2 = \frac{V_2}{A_2} = \frac{(\sqrt{3}/3)}{A_1 + (\sqrt{3}/3)A_2}T \tag{9-17}$$

According the Von Mises failure theory,

$$\sqrt{\sigma_1^2 + 3\tau_1^2} \le F_u \tag{9-18}$$

$$\sqrt{\sigma_2^2 + 3\tau_2^2} \le F_u \tag{9-19}$$

Take square of (9-18), (9-19) and sum both sides, then

$$\sigma_1^2 + \sigma_2^2 + 3\tau_1^2 + 3\tau_2^2 \le 2F_u^2 \tag{9-20}$$

Submit (9-14) to (9-17) into (9-20), then

$$B^2T^2 + C^2V^2 \le F_u^2 \tag{9-21}$$

Where

$$B = \frac{1}{A_1 + (\sqrt{3}/3)A_2}$$

$$C = \frac{1}{(\sqrt{3}/3)A_1 + A_2}$$

Considering the strength reduction factor $\Phi$, (9-21) is modified as,

$$B^2T^2 + C^2V^2 \le (\Phi F_u)^2 \tag{9-22}$$

Check for consistence with block shear capacity design formula; say T is 0, then

177

$$B^2T^2 + C^2V^2 = B^2T^2 \leq F_u^2$$

$$CV = \frac{V}{(\sqrt{3}/3)A_1 + A_2} \leq F_u$$

$$V \leq (\sqrt{3}/3)A_1 F_u + A_2 F_u \approx 0.6 A_1 F_u + A_2 F_u$$

Therefore (9-21) agrees with current block shear design formula (9-7) when there is only force in one direction.

- **Bolts Strength:**

    Bolt strength at elevated temperature is determined by strength reduction factor of A325 bolt. Bolt shear capacity needed be verified against the vector sum of vertical shear force and horizontal force.

- **Bearing Capacity:**

    From Eq. (9-1)

    $$R_n = 1.2 L_c t F_u \leq 2.4 dt F_u$$

    $F_u$ is the ultimate strength at checking temperature.

    However, the direction of force is not perpendicular to the edge of steel plate at elevated temperature, as shown in Figure 9-10. The length difference between two shear failure paths is:

    $$\Delta = \tan(\alpha)(d + 1/16") \tag{9-23}$$

    $d$ is the nominal diameter of bolt;

    It is assumed that the length difference between shear paths does not affect the bearing capacity. The average shear path length $L_c'$ is used in calculating bearing capacity.

    $$R_n = 1.2 L_c' t F_u \tag{9-24}$$

$$L_c^{'} = \frac{L_e}{\cos(\alpha)} - \frac{(d + 1/16")}{2} \qquad (9\text{-}25)$$

$$F = \sqrt{T^2 + V^2} \qquad (9\text{-}26)$$

$$\cos(\alpha) = \frac{T}{F} \qquad (9\text{-}27)$$
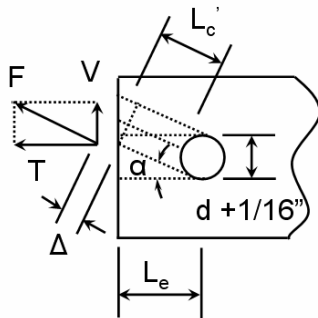


Figure 9-10 Bearing Failure with Force Not Perpendicular to Plate Edge

Table 9-10 gives the composite beam connection capacity at elevated temperatures and compares with connection forces. Because the horizontal force points towards middle of the beam, bearing capacity shall be verified against bearing strength limit. Web's block shear capacity shall be verified against vertical shear force. Bolts shear capacity be verified against the vector sum of vertical shear force and horizontal force. It was found that at 600°C, bolts would fail in shear. At 700°C and 800°C, both bolts and beam web would fail.

Table 9-11 gives the non-composite beam connection capacity at elevated temperatures and compares with connection forces. Since the axial force is pointing away from the middle span of the beam, bearing capacity was calculated and found controlling the capacity of beam web in horizontal direction. At 600°C, bolts shear failure would happen. At 700°C and 800°C, bolt shear failure, beam web block shear in the vertical direction, and beam web bearing failure in the horizontal direction will all occur.

179

### 9.6.2.3 Improvement of Connection Design

- **Bolt Shear Capacity**

It was found that in both non-composite and composite beams, bolt shear failure first happens at 600˚C. Therefore, bolt strength needs to be increased.

1. Increasing the number of bolts will help but the option is limited by the height of beam web. In this example, one more bolt can be added to improve bolt shear capacity by 25%.

2. Increasing the diameter of bolts is another option. Replacing the one inch diameter bolts with 1-1/8 inch or 1-1/4 inch bolts, the capacity will be increased by 27% or 56%. At the same time, this will reduce block shear capacity. Therefore, a check of block shear capacity is needed.

3. By excluding threads from shear plane, the shear capacity of bolts can be increased by 25%.

4. Changing the bolt's working condition from single shear to double shear can increase shear capacity by 100%.

Table 9-12 compares the shear load on bolts and original shear capacity. The required improvement is presented in percentage. It is found that none of the options can fulfill the task alone. For non-composite beam, it is almost impossible to make the bolt shear capacity high enough to carry the load at 800˚C. For composite beam, it is not hard to modify the bolt's design to carry the load from 600˚C to 800˚C by the combination of two of the above four options.

Table 9-10 Load and Capacity of Example Connection of Composite Beam at Elevated Temperature

| Connection Temperature | | Forces on Connection (kip) | | Shear Force on Bolts (kip) | Ultimate Strength Reduction Factor, Gr. 50 | Bearing Capacity (kip) $\Phi = 0.75$ | Block shear capacity (kip) $\Phi = 0.75$ | Bolt Strength Reduction Factor | Bolt shear capacity (kip) $\Phi = 0.75$ | Safety Status |
|---|---|---|---|---|---|---|---|---|---|---|
| ˚C | ˚F | Vertical | Horizontal | | | | | | | |
| 30 | 86 | 26.1 | 0.3 | 26.1 | 1.00 | 187.2 | 71.3 | 1.00 | 113.2 | OK |
| 100 | 212 | 26.1 | -7.9 | 27.3 | 0.91 | 170.4 | 64.9 | 0.96 | 108.7 | OK |
| 200 | 392 | 26.1 | -19.1 | 32.4 | 0.85 | 159.1 | 60.6 | 1.00 | 113.2 | OK |
| 300 | 572 | 26.1 | -28.4 | 38.6 | 0.70 | 131.0 | 50.0 | 1.00 | 113.2 | OK |
| 400 | 752 | 26.1 | -30.4 | 40.1 | 0.67 | 125.4 | 47.8 | 0.61 | 69.1 | OK |
| 500 | 932 | 26.1 | -26.3 | 37.0 | 0.57 | 106.7 | 40.7 | 0.36 | 40.8 | OK |
| 600 | 1112 | 26.1 | -18.1 | 31.8 | 0.39 | 73.0 | 27.8 | 0.21 | 23.8 | N.G. |
| 700 | 1292 | 26.1 | -11.2 | 28.4 | 0.26 | 48.7 | 18.5 | 0.12 | 13.6 | N.G. |
| 800 | 1472 | 26.1 | -7.7 | 27.2 | 0.12 | 22.5 | 8.6 | 0.10 | 11.3 | N.G. |

181

Table 9-11 Load and Capacity of Example Connection of Non-Composite Beam at Elevated Temperature

| Connection Temperature | | Forces on Connection (kip) | | Shear Force on Bolts (kip) | Ultimate Strength, Gr. 50 Steel | | Block shear capacity $\Phi = 0.75$ | | Bolt Strength Reduction Factor | Bolt shear capacity (kip) $\Phi = 0.75$ | Bearing Capacity, Eq. (9-23) (kip) $\Phi = 0.75$ | Safety Status |
|---|---|---|---|---|---|---|---|---|---|---|---|---|
| °C | °F | Ver. V | Hor. T | | Reduction Factor | $(\Phi F_u)^2$ (ksi$^2$) | Hor. Eq. (9-4) (kip) | Hor. & Ver. Eq. (9-22) (ksi$^2$)* | | | | |
| 30 | 86 | 26.1 | 7.7 | 27.2 | 1.00 | 2377 | 98.8 | 349 | 1.00 | 113.2 | 83.7 | OK |
| 100 | 212 | 26.1 | -27.0 | 37.6 | 0.91 | 1968 | 89.9 | 461** | 0.96 | 108.7 | 170.4** | OK |
| 200 | 392 | 26.1 | -62.9 | 68.1 | 0.85 | 1717 | 83.9 | 1002** | 1.00 | 113.2 | 159.1** | OK |
| 300 | 572 | 26.1 | -4.6 | 26.5 | 0.70 | 1165 | 69.1 | 342** | 1.00 | 113.2 | 131.0** | OK |
| 400 | 752 | 26.1 | 1.4 | 26.1 | 0.67 | 1067 | 66.2 | 339 | 0.61 | 69.1 | 323.0 | OK |
| 500 | 932 | 26.1 | 17.2 | 31.3 | 0.57 | 772 | 56.3 | 388 | 0.36 | 40.8 | 22.0 | OK |
| 600 | 1112 | 26.1 | 42.5 | 49.9 | 0.39 | 361 | 38.5 | 641 | 0.21 | 23.8 | 8.4 | N.G. |
| 700 | 1292 | 26.1 | 57.9 | 63.5 | 0.26 | 161 | 25.7 | 900 | 0.12 | 13.6 | 5.1 | N.G. |
| 800 | 1472 | 26.1 | 63.9 | 69.0 | 0.12 | 34 | 11.9 | 1023 | 0.10 | 11.3 | 2.3 | N.G. |

* For checking block shear capacity under horizontal and vertical forces, submit horizontal and vertical forces into Eq. (9-22) and compared with the square of ultimate strength at that temperature.

** When T is compression force, there is no need to check block shear capacity with Eq. (9-22) and bearing with Eq. (9-23). The bearing capacity is checked against deformation limit $2.4dtF_u$.

Table 9-12 Shear Load on Bolts and Required Improvement

| Temperature (˚C) | Non-composite Beam | | |
| --- | --- | --- | --- |
| | Shear Load on Bolts (kip) | Bolt Shear Capacity (kip) | Required Improvement (%) |
| 600 | 49.9 | 23.8 | 110 |
| 700 | 63.5 | 13.6 | 367 |
| 800 | 69.0 | 11.3 | 511 |
| Temperature (˚C) | Composite Beam | | |
| | Shear Load on Bolts (kip) | Bolt Shear Capacity (kip) | Required Improvement (%) |
| 600 | 31.8 | 23.8 | 34 |
| 700 | 28.4 | 13.6 | 109 |
| 800 | 27.2 | 11.3 | 141 |

- **Block Shear and Bearing Capacity**

Block shear and bearing capacity of beam web can be increased by increasing the end distance of bolt hole. This is an efficient way to increase bearing capacity, while it is not true for increasing block shear capacity. As long as the spacing between bolts does not change, block shear failure paths could not be increased much. Therefore, locally increasing beam web thickness near the connection is a better way to improve block shear capacity of beam web. This could be done by welding patch steel plate to beam web.

# Chapter 10
# Conclusions and Future Work

## 10.1 Summary of Work

- Shear capacity of A325 and A490 bolts at temperatures up to 800˚C (1500˚F) was obtained and strength reduction factors was put forward;

- Residual shear capacity of A325 and A490 bolts after exposure to temperatures up to 800˚C (1500˚F) was achieved and strength reduction factors were developed;

- Slip load capacity of fully tightened A490 bolt connection after exposure to temperatures up to 800˚C (1500˚F) was tested and strength reduction factors were developed;

- The bearing capacity of bolted connections at elevated temperatures was determined and correlated with the measured tensile strength of the material;

- The block shear capacity at elevated temperatures of a connection was measured and correlated with the measured properties of the steel;

- A typical floor beam was analyzed at elevated temperature and forces in connections were determined. Connection strength was confirmed at elevated temperature and failure of connections at 600˚C was highlighted.

## 10.2 Conclusions

The behavior of A325 and A490 bolts from ambient temperature to 800˚C can be divided into three ranges. Below 300˚C (572˚F), the strength of both bolts does not change much. From 300˚C (572˚F) to 700˚C (1292˚F), both bolts lose their strength dramatically with temperature. The strength of A490 bolt drops linearly by about 80% within this temperature range. A325 bolt has the same

percentage of original strength as the A490 bolt at 300°C (572°F) and 700°C (1292°F). However, A325 bolt loses its strength even faster than linearity in this range. From 700°C (1292°F) to 800°C (1472°F), the strength of both A325 and A490 bolts does not drop any further.However A325 bolt loses its strength even faster than linearity in this range. From 700°C (1292°F) to 800°C (1472°F), the strength of both A325 and A490 bolts does not drop future.

Material properties of Grade 50 structural steels change with temperature adjustment. As temperature rises from ambient temperature to 300°C (572°F), the yielding plateau gradually disappears from the stress strain curve. Steel enters the hardening range right after proportional limit. From 300°C (572°F) to 400°C (752°F), steels have lower ductility and slightly increased ultimate strength. Beyond 400°C (752°F), the difference between yielding strength (defined by 0.2% rule) and ultimate strength become less and less as temperature rises. Steels reach ultimate strength at relatively low strain level. As temperatures rise, the creep and relaxation of steel becomes more significant. Therefore strain rate has significant effects on the behavior of steel at temperatures beyond 400°C (752°F). For the two different heats of Grade 50 structural steels tested, their ultimate strength behavior from ambient temperature to 800°C (1472°F) can be divided into two ranges. Below 300°C (572°F), ultimate strength of both Grade 50 steels does not change much; from 300°C (572°F) to 800°C (1472°F), both steels lose their ultimate strength almost linearly with temperature by about 89% at 800°C (1472°F). The yield strength of both steels change almost linearly, when temperature rise from ambient temperature to 800°C (1472°F).

The shear strength estimated from hardness tests on the bolts after a fire gave a very good estimate of the post fire shear strength of a bolt. This simple test can be used to determine whether bolts need to be replaced after a fire. In addition, the rate of cooling of bolts from elevated temperatures including quenching in

185

water did not affect their post fire strength. Post fire residual strength of A325 and A490 bolts was determined by the relationship of the maximum temperature $T_{max}$, that they were exposed to, and tempering temperature $T_{temper}$ during manufacture. When $T_{max}$ is lower than $T_{temper}$, residual strength is equal to original strength. When $T_{max}$ is higher than $T_{temper}$, both bolts suffer strength loss. The residual strength changes linearly with $T_{max}$ beyond tempering temperature. The tested A325 bolt was tempered at 400°C (752°F), while A490 bolt was tempered at 500°C (932°F). After being exposed to 800°C (1472°F), both bolts have about 50% original strength left.

Slip load capacity of fully tightened A490 bolt connection changes with the maximum temperature that the connection has been exposed to. When the maximum temperature is below 400°C (752°F), connection slip load capacity is significantly increased up to about 50% of its original capacity. However, from 400°C (752°F) to 500°C (932°F), connection slip load capacity drop dramatically from 150% to 50% of its original capacity. From 500°C (932°F) to 800°C (1472°F), connection slip capacity drops slowly with the maximum exposed temperature to about 10% of its original capacity at 800°C (1472°F).

Design methods for determining the strength of bolted connections in a fire was developed. They include the limit states of bolt shear, bearing or tear out of the connection material and block shear failure of connection material. The material strength at elevated temperature provided could be used in the standard strength calculations to estimate the strength of the connections during a fire. Connections whose strength was governed by plate failure at room temperature may be controlled by bolt shear at higher temperatures due to the difference in the strength reduction with increasing temperature for the bolts and the connected material.

186

**10.3 Future Work**

- A325 and A490 bolts from different manufacturers and heats have different alloy element contents, which may affect their strength at elevated temperature. More test results are needed to determine if the shear strength reduction factors generated in this study can be applied to all A325 and A490 bolts;

- Bearing capacity of bolt hole with different length shear paths need be investigated. When catenary effects plays an important role in affecting beams behavior at elevated temperatures, beam connections have vertical shear force and horizontal tension force simultaneously, as shown in Figure 10-1. This may produce a bearing failure along the inclined paths shown in the figure. This need to be examined in future experimental studies.
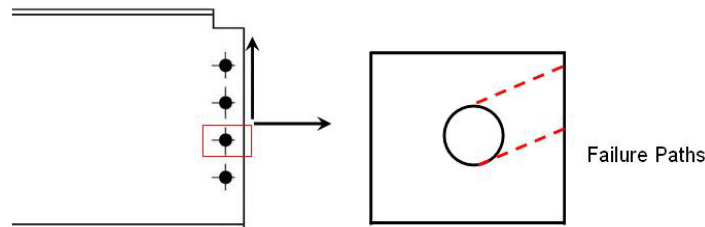


Figure 10-1 Bearing Failure with Different Length Shear Paths

- Full scale floor beam test at elevated temperature with unprotected connections need to be performed on realistic span length, beam depths, and connections. The development of the forces from the deformation during a fire, including the initial development of compressive forces

followed by development of catenary forces at high temperatures, need to be measured for both non-composite and composite beams.

- Experimental studies on the properties of structural steels at elevated temperatures need be performed. Most of the data available today is from work in 1970's. Structural steels have changed with new manufacture technologies since then. Therefore, material tests on structural steels at elevated temperatures are needed.

# References

FEMA, World Trade Center Building Performance Study: Data Collection, Preliminary Observations, and Recommendations, FEMA 403, May 2002

NIST NCSTAR 1-6, Federal Building and Fire Safety Investigation of the World Trade Center Disaster, Structural Fire Response and Probable Collapse Sequence of World Trade Center Towers, NIST, September 2005

Ivan Burgess, Fire Resistance of Framed Buildings, Physics Education, September 2002

FEMA Technical Report Series, High-rise Building Fire, One Meridian Plaza, Philadelphia, Pennsylvania, February 23, 1991

FEMA Technical Report Series, Interstate Bank Building Fire
Los Angeles, California, May 4, 1988

Beitel, J.J. and Iwankiw, N.R., Historical Survey of Multi-story Building Collapse Due to Fire, Fire Protection Engineering, 2005

Dougal Drysdale, An Introduction to Fire Dynamics, Second Edition, Chichester (West Sussex); New York: Wiley, c1985

Caracas Tower Floor Beams Deflected but Did Not Collapse, Engineering News Record, November 15, 2004

http://enr.ecnext.com/coms2/gi_0271-8849/Caracas-Tower-Floor-Beams-Deflected.html

Fire in the Windsor Building, Madrid –Survey of the Fire Resistance and Residual Bearing Capacity of the Structure after the Fire, INTEMAC, NIT-2(05)

Cardington Fire Test Report, The Behaviour of Multi-storey Steel Framed Building Subject to Fire Attack, Experimental Data, British Steel, Swinden Technology Center, 1998

NIST NCSTAR 1-6B, Federal Building and Fire Safety Investigation of the World Trade Center Disaster, Fire Resistance Tests of Floor Truss System, NIST, September 2005

T.C.H. Liu, M.K. Fahad, J.M. Davies, Experimental Investigation of Behavior of Axially Restraint Steel Beams in Fire, Journal of Constructional Steel Research, 58 (2002) 1211-1230

Y.Z. Yin, Y.C. Wang, A Numerical Study of Large Deflection Behavior of Restrained Steel Beams at Elevated Temperatures, Journal of Constructional Steel Research, 60 (2004) 1029-1047

Y.Z. Yin, Y.C. Wang, Analysis of Catenary Action in Steel Beams Using a Simplified Hand Calculation Method, Part 1: Theory and Validation for Uniform Temperature Distribution, Journal of Constructional Steel Research, 61 (2005) 183-211

Peter Moss, Andy Buchanan, Jenny Seputro, Clayton Wastney and Richard Welsh, Effect of Support Conditions on the Fire Behavior of Steel and Composite Beams, Second International Workshop of Structures in Fire, March 2002

Liu TCH, Davies JM, Performance of Steel Beams at Elevated Temperatures under the Effect of Axial Restraints, Steel Composite Structures 2001; 1(4), 427-40

S. Lamont, Barbara Lane, Graeme Flint, Asif Usmani, Behavior of Structures in Fire and Real Design – A Case Study, Journal of Fire Protection Engineering, Vol. 16, February 2006
S. Lamont, Asif Usmani, Key events in the structural response of a composite steel frame structure in fire, Fire and Materials, Vol. 28, Issue 2-4, 2004. Pages 281-297

ASTM A325-04, Standard Specification for Structural Bolts, Steel, Heat Treated, 120/105 ksi Minimum Tensile Strength

ASTM E119-00a, Standard Test Methods for Fire Tests of Building Construction and Materials

A.Y. Elghazouli and B.A. Izzuddin, Analytical Assessment of the Structural Performance of Composite Floors Subject to Compartment Fires, Fire Safety Journal, 36 (2001) 769-793

Martin Gillie, Asif Usmani, Michael Rotter, Mark O'Connor, Modelling of Heated Composite Floor Slabs with Reference to the Cardington Experiments, Fire Safety Journal, 36 (2001), 745-767

A.S. Usmani, N.J.K.Cameron, Limit Capacity of Laterally Restrained Reinforced Concrete Floor Slabs in Fire, Cement & Concrete Composites, 26 (2004) 127-140

Zhaohui Huang, Ian W. Burgess, Roger J. Plank, Fire Resistance of Composite Floors Subject to Compartment Fire, Journal of Constructional Steel Research, 60 (2004) 339-360

C.G. Bailey, Efficient Arrangement of Reinforcement for membrance Behavior of Composite Floor Slabs in Fire Conditions, Journal of Constructional Steel Research, 59 (2003) 931-949

B.R. Kirby, R. R. Preston, High Temperature Properties of Hot-rolled, Structural Steels for Use in Fire Engineering Design Studies, Fire Safety Journal, 13 (1988) 27-37
ASTM, A490-04, Standard Specification for Structural Bolts, Alloy Steel, Heat Treated, 150 ksi Minimum Tensile Strength

B. R. Kirby, The Behavior of High-Strength Grade 8.8 Bolts in Fire, Journal of Construction Steel Research 33(1995) 3-38

Jyri Outinen, Jyrki Kesti, Pentti Makelainen, Fire Design Model for Structural Steel S355 Based Upon Transient State Tensile Test Results, Journal of Constructional Steel Research, Vol. 42, No3, pp. 161-169, 1997

Pentti Makelainen, Jyri Outinen, Jyrki Kesti, Fire Design Model for Structural Steel S420M Based Upon Transient State Tensile Test Results, Journal of Constructional Steel Research, Vol. 48, 1998, 47-57

Zhaohui Huang, Ian W. Burgess, Roger J. Plank, The Influence of Shear Connectors on the Behavior of Compsite Steel-framed Buildings in Fire, Journal of Constructional Steel Research, 51 (1999) 219-237

Outinen J, Makelainen P, Transient State Tensile Test Results of Structural Steels S235, S355 and S350GD + Z at Elevated Temperatures, TKK/Rakennetekniikan laitosjulkaisu 129, 38S. Espoo: 1995

G.M.E. Cooke, An Introduction to the Mechanical Properties of Structural Steels at Elevated Temperature, Fire Safety Journal, 13 (1988), 45-54

NIST NCSTAR 1-3, Federal Building and Fire Safety Investigation of the World Trade Center Disaster, Mechanical and Metallurgical Analysis of Structural Steel, NIST, September 2005

NIST NCSTAR 1-3D, Federal Building and Fire Safety Investigation of the World Trade Center Disaster, Mechanical Properties of Structural Steels, NIST, September 2005

AISC Steel Construction Manual (LRFD), 3rd Edition, 2001

AISC Steel Construction Manual, 13th Edition, 2005

Guo-Qiang Li, Shou-Chao Jiang, Ying-Zhi Yin, Kai Chen, Ming-Fei Li,
Experimental Studies on the Properties of Constructional Steel at Elevated
Temperatures, Journal of Structural Engineering, ASCE, December 2003

K.S. Al-Jabri, Component-Based Model of the Behavior of Flexible End-Plate
Connections at Elevated Temperatures, Composite Structures, 66 (2004) 215-
221

Al-Jabri KS, Burgess IW, Lennon T, Plank TJ, Behavior of Steel and
Composite Beam-to-Column Connections in Fire, Journal of Constructional
Steel Research, Vol. 46, (1998) 1-3

L. Simoes da Silva, Aldina Santiago, Paulo Vila Real, A Component Model
for the Behavior of Steel Joints at Elevated Temperatures, Journal of
Constructional Steel Research, Vol. 57, (2001) 1169-1195

Liu TCH, Finite Element Modeling of Behavior of Steel Beams and
Connections in Fire, Journal of Constructional Steel Research, Vol. 36, (1996)
181-199

E. Paul DeGarmo, Materials and Processes in Manufacturing, fifth edition,
Macmillan Publishing Co., Inc., 1979

George E. Linnert, Welding Metallurgy, Carbon and Alloy Elements, third edition, volume 1 fundamentals, American Welding Society, New York, 1965

R W K Honeycombe, Steels Microstructures and Properties, Metallurgy and Materials Science Series, 1981

Structural Fire Protection, ASCE Manuals and Reports on Engineering Practice No. 78, 1992

United States Steel, the Making, Shaping and Treating of Steel, ninth Edition, edited by Harold E. McGannon, Herbick & Held, 1970

Hyeong Jun Kim and Joseph A Yura, PMFSEL Report No. 96-1, The Effect of End Distance on The Bearing Strength of Bolted Connections, February, 1996

# VITA

Liang Yu was born in Changchun, China on October 6, 1975, the son of Youmin Yu and Ruizeng Zhang. After completing his work at High School of Northeast Normal University, Changchun, in 1994, he entered Tianjin University, China. He received the degree of Bachelor in Science in Tianjin University, China, in 1998. In September 1998, he entered the Graduate School at Tsinghua University. He received his degree of Master in Science in Department of Civil Engineering from Tsinghua University in 2001. In August 2000, he entered graduate school at The University of Texas at Austin for his Ph.D study.


Permanent Address:

Room 501, Building 2, Area 52, The First Automobile Group Company

Changchun, Jilin Province,

China, PR


This dissertation was typed by the author.